# Failure Rate Calculation Method for High Voltage Semiconductor Devices under Space Radiation Environments

| | |
|---|---|
| 著者 | Erdenebaatar Dashdondog |
| その他のタイトル | 高耐圧パワー半導体素子の宇宙放射線環境下故障率の計算手法に関する研究 |
| 学位授与年度 | 平成29年度 |
| 学位授与番号 | 17104甲工第445号 |
| URL | http://hdl.handle.net/10228/00006913 |

Academic year 2017 DISSERTATION

# Failure Rate Calculation Method for High Voltage Semiconductor Devices under Space Radiation Environments

**Erdenebaatar Dashdondog**

*A dissertation submitted for in partial fulfilment of the requirements*

*for the degree of Doctor of Philosophy in Engineering*



Department of Electrical Engineering and Electronics,

Graduate School of Engineering,

Kyushu Institute of Technology,

Kitakyushu, Fukuoka, Japan

Dissertation Committee

Professor. Kazuhiro Toyoda

Professor. Mengu Cho

Professor. Kei-ichi Okuyama

Professor. Ichiro Omura

**Acknowledgement**

First of all, I would like to say thank to my lovely parents for grown up and driven me for this good life and opportunity to being individual human being. Thanks my little sister for taking care of our parents during period of my study here in Japan.

I would like to deeply appreciate to my supervisor Professor Ichiro Omura. He has helped and instructed to me for this research and achievement. Without his vise advices I wouldn't come here. His word made me to think about technology development of my country many time on many points. I believe that those points will become real results in Mongolia. This is the biggest luck of my life to meet him as his student. There is word that "One day's teacher is thousand days virtue". His three years supervising to me will be the all my life's virtue.

Also I would like to say thank to my Professor Cho Mengu. I had participated for three satellites projects, HORYU-4, BIRDS-1 and SPATIUM, as a member of Electric Power System team under his leading. His generous treatment gives me lot of knowledge and thinking about top level manager and great future of my life. I have learned a lot from him.

I thanks for Professor Toyoda for his great guidance and helpful advice. I was happy for to be his student in last semester of my study.

I would like to appreciate to Miyo Iwahori san for supported and helped me since first day I came in Japan until today. Her help was huge for my private daily and campus life in Japan. I was lucky to meet her during my study.

Also I would like to thank for assistant professor Masui Hirokazu and LASEINE colleagues for the helping and advice Mongolian very first "Mazaalai" satellite of BIRDS project.

I also deeply appreciate Harada Shohei san, Takahara Satoru san, Shiba Yuji san, Sudo Masaki san, Kenta Nakashima san for helping me lot for my research and daily life at Kyutech. They have become my good friends.

I thank for all of my friends and SEIC students at Kyutech; T.Turtogtokh, D.Amartuvshin, B.Battuvshin, U.Tuguldur, B.Bolortuya, S.Purevdorj, Dmytro Faizullin, Sidi Ahmed Bendoukha, Rafael Rodriguez Leon and all other members of BIRDS-1, HORYU-4 and SPATIUM projects. They had been making my life happy in Campus.

I would like to express my respect to Japanese helpful friendly people and Japanese government. I studied here in Japan by scholarship from Japanese Government (MEXT) through The United Nations Office for Outer Space Affairs' PNST project. I have studied

at Kyushu Institute of Technology for last three years. These three years were turning point of my life to better direction. I hope what I have learnt here leads to me to do lots of things for my country's future. I will continue my study and academic life back in Mongolia. All of people above have deepest respect from me. Any of my success is also theirs.

## Abstract

Space industry market and manufacturing have been increased for last decades. Furthermore, this trend seems will being increased. In order to practically use large size of manned and unmanned spacecraft for space missions, the total power generation of that will soon reach to range of Megawatts. Consequence of power demand increasing leads to the harness weight increasing of spacecraft in order to decrease power loss on harness. Harness mass is approximately 8% of spacecraft dry mass. Relation between harness mass and power demand of spacecraft was studied. For instance if the bus voltage increase by 100V, then harness mass reduction would be 75% of initial mass. Hence it seems that bus voltage increase will be the requirement for future space platforms. By using high voltage in bus system of spacecraft, there is a risk to destruct that power device due to the energetic particle penetration from the space. The well-known studies have been studied this failure which basically named “single event burn out for power devices and other electronics. In order to mitigate that risk, evaluate reliability then failure rate should be investigated against space radiation environment. The proton flux is the majority of energetic particle flux at low earth orbit. Therefore this thesis initially proposes and discusses method for space proton induced failure rate on high power device. The proposed method could be developed to be able to calculate failure rate of any power device under space radiation in various altitude. We selected low earth condition as basic example study for this thesis. Besides, high energetic particles can be the reason of power device failure in both terrestrial and space.

In Chapter 1 of this thesis, satellite and space industry development trend which leads to the high power usage of next generation spacecraft was presented. Due to that trend, there will be appeared several aspect of spacecraft especially on the electrical power subsystem. The basic structure of electrical power subsystem was discussed as well.

In Chapter 2 of this thesis, high voltage power semiconductor devices were basically presented. The electrical power subsystem of spacecraft works at DC voltage. A power management and distribution unit is the main part of energy controlling and conditioning in the electrical power system. The high voltage power devices are the main component of that power management distribution unit. Therefore high power semiconductor device will be the key component of the next generation spacecraft’s electrical power system.

In Chapter 3 of this thesis, the cosmic ray induced failure and its mechanism were

presented. This chapter includes two sections. First is that understanding about cosmic rays and its aspect in low earth orbit. Second is that semiconductor devices failure mechanism which induced by energetic particles. Proton silicon nuclear interaction, charge multiplication avalanche phenomena in the silicon device especially for power devices were explained as well.

In Chapter 4 of this thesis, proposed method to calculate failure rate that induced by cosmic ray was presented. The proposed method in this study is expressed as formula and consists of three sections. First, T-CAD simulation, its result gives a threshold charge value for the device destruction, at various applied voltages case, which is triggered by energetic proton from space. The amount of threshold charge depends on applied voltage for high power device. Second, there is a probability of charge generation in silicon due to proton penetration. This probability function's variation depends on the thickness of device and incident energy of proton. This function was defined before at library. Third consideration on this study is space proton flux data at low earth orbit which has been provided by astrophysics studies, assumed energy range of proton flux is 1MeV to 200GeV. Simulated device model was 3.3 kV PiN diode. At the end of this chapter ionization particle model of T-CAD simulation were briefly discussed.

In chapter 5 of this thesis, calculated result by proposed was discussed. T-CAD simulation result, Proton flux function fitting result, proton induced failure cross section and failure rate calculation results were included this chapter. Shielding function obtained from literature. As seeing result aluminum shielding could not be proper protection against proton flux. Comparing results at FIT=1(one failure in $10^9$hours) that typically used for power device's allowed failure rate for commercial application, space applications power semiconductor devices failure rate was higher than terrestrial failure rate several magnitude. For instance in case of an application voltage of 3.3kV diode should be approximately 1.5kV for space application.

This thesis concluded in Chapter 6. Conclusion were basically that we established method that consists of Destruction charge values from T-cad simulation, proton flux data and probability of energy deposition due to proton-silicon interaction from literature. From the result we can see that failure rate is apparently higher than terrestrial region case (assumed terrestrial FIT=1). By using Single Event burnout cross section $\sigma(V)$, that we obtained can be used for any proton flux of environment. PiN diode model can be changed by any other power semiconductor devices. Proposed method can contribute to mitigate failure for high power devices' usage and predict space application's MW range of power systems reliability in future.

In this study, T-CAD simulation electric field, that can affected by proton hitting position in silicon, was fixed at highest field of position. Crystal degradation due to space radiation was not considered as well.

# 1. INTRODUCTION

**Research Vision** is to contribute for accounting of increase of high power devices' reliability in the future space applications.

**Purpose of research** is to develop failure rate calculation method for all kind of power devices in various space environments.

**Goal of thesis research** is to demonstrate that proposed method can give derating value and failure rate of the high voltage device at the low earth orbit environment.

This thesis discusses the universal calculation method for space proton induced failure rate of a high power device. High energy particles can be the reason of power device failure in both terrestrial and space. In order to know failure of power devices, T-CAD simulation result gives a threshold charge value for the device destruction which is triggered by energetic proton from space. The amount of threshold charge depends on the applied voltage for high power devices. The probability of charge generation in silicon due to proton penetration is considered as a study. This probability function variation less depends on the thickness of the device and strongly affected by the incident energy of proton which studied before. Last consideration in this study is PiN diode model's single event upset cross section and failure rate, which was calculated by the proposed method in Low earth orbit environment condition. Following subtitle talk about rationale and importance of this study. The main application of this study is big space platforms in future.

## 1.1. Satellite and Space industry

Space industry brings up to economic activities related to fabricating elements that travel into Earth's orbit or beyond, bearing them to those regions, and linked services. The three major sectors of the space industry are: satellite manufacturing, support ground equipment manufacturing, and the launch industry. The satellite manufacturing sector is framed of satellite and their subsystem makers. [**1**].

The space industry started to make grow after World War II, as rockets and then satellites introduced into military armouries, and later establish civilian applications. It holds back significant links to the governments. In particular, the launch industry features a substantial government involvement, with some launch platforms (like the space shuttle) being controlled by governments. In late years, however, private spacefaring is becoming realistic, and even major government agencies, such as NASA and JAXA, have started relying on privately worked launch services. Some future developments of the space industry that are progressively being regarded include new services such as space tourism and deep space missions. The 2015 Space Report estimates that in 2014 total global space activity was $330 Billion [**2**].

### 1.2. High Power for Satellite Power System

Space industry market and manufacturing have been increased for the last decades. Furthermore, this trend seems will be increased as well [**3**]. In order to implement large-scale space platforms, such as space station, big satellites, power generation will soon reach to the level of Megawatt. Total power is gradually increasing as shown in the last twenty years its trend as we can see Fig. 1-1 [**4**].

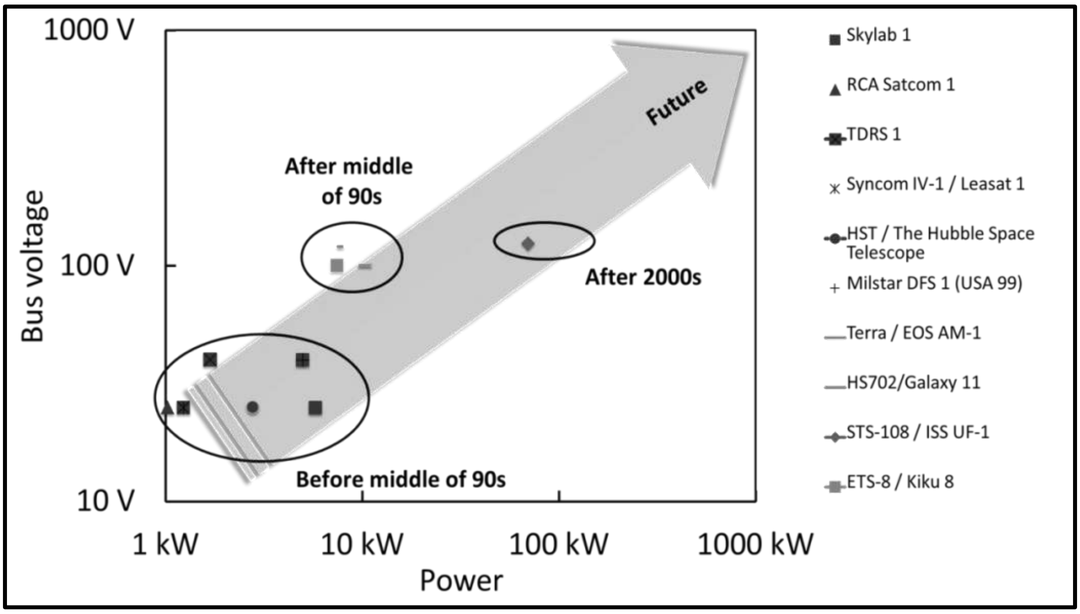


Fig. 1-1 Total power increasing trend last twenty years

Consequence of power increasing in space platform is harness mass increases. Relation between harness mass and power of satellite was studied as shown in Fig. 1-2 [**5**]. When the total power of spacecraft is increase, then power loss also will increase. There are three feasible solutions to reduce power loss. First is to use short cable, second is to use thicker cable and third is use of higher voltage. Most suitable solution to reduce power loss is to use higher voltage for the Electrical Power System of satellite; other two solutions make a mass increase for application which leads to the budget issue of space technology. We can confirm it as that power loss during transmission is proportional to cable length over multiple of voltage square and cable cross section. The Eq. 1-1 shows relation between power loss and applied voltage, if bus voltage increases then power loss will be decreased.

$$\frac{\Delta P}{P} = \frac{\rho I^2}{VI} = \frac{\rho I}{V} = \frac{\rho P}{V^{\ 2}} = \frac{\sigma l P}{sV^{\ 2}}$$

Eq. 1-1 Relation between Power loss and applied Voltage

$P_L$ : Load power consumption

$P$ : Cable resistance

$\sigma$ : Cable electrical resistivity

$l$ : Cable length

$S$ : Cross-sectional area

$P=VI$ : Generated power

$\Delta P=\rho I^2$ : Cable loss

Hence power of spacecraft leads to use of high voltage system by relation of Eq. 1-2. On the other hand if power usage reaches to MW range then applied voltage should be reached KV range.

$$V \propto \sqrt{P}$$

Eq. 1-2 Relation between Bus voltage and Total Power

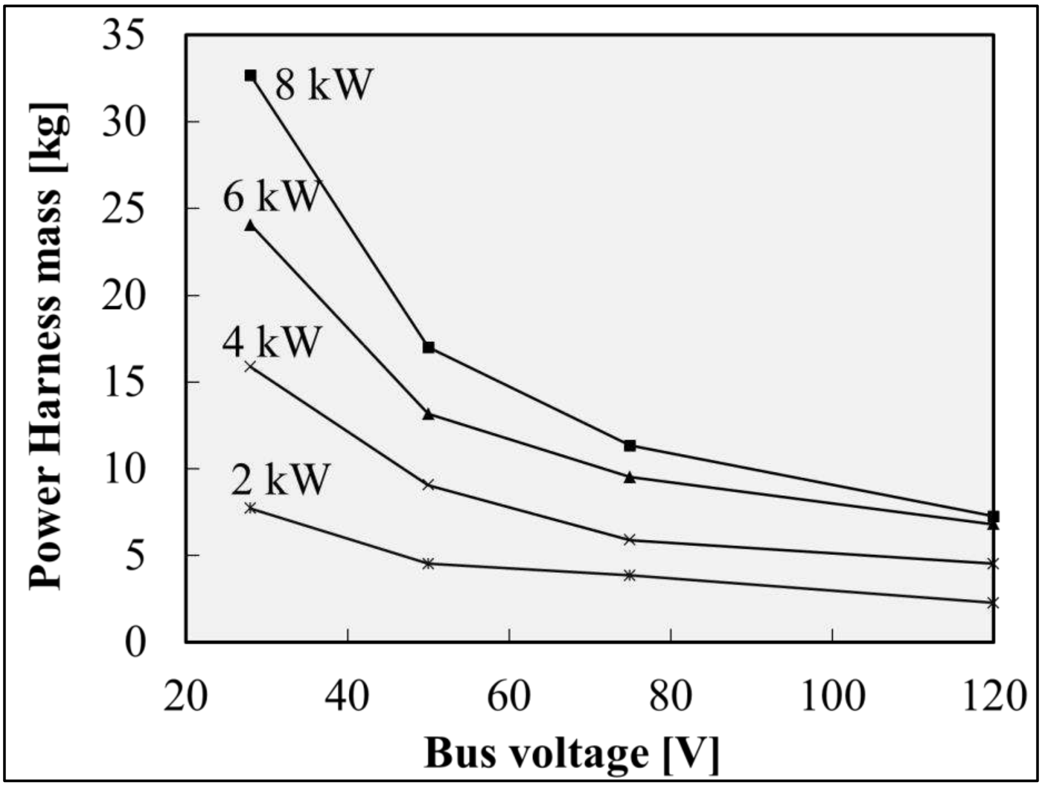


Fig. 1-2 Relation between harness mass and power of satellite

The main idea of research is based on needs of high power demand on future space applications. It calls for high voltage generation and transmission since minimize the energy loss during power transmission and the cable mass. High voltage usage can be the mitigation of harness mass increase. Satellite electric power system size (power level) is verbalized by payload characteristics. Typical power levels and mass of today's satellites range between 100 and 1000W and 250 kg or less for small satellites, between1 and10 kW and on the order of 1000–5000 kg for conventional large satellites. However, due to present lessening space budgets, mission developers are pushing strongly toward cheaper, small-satellite designs capable of launch on smaller, cheaper, and more easily deployed vehicles [**5**].

### 1.3. Electrical Power Subsystem

A spacecraft Electrical Power Subsystem (Electrical Power System) is one of the bus system compounds, which takes responsible for power generation and control, energy storage, and power distribution. Fig.1-3 shows the functional block diagram of Electrical Power Subsystem. The basic typical functions of Electrical Power Subsystem can be listed as below [**6**]:

- Supply continuous power to the loads during the mission lifetime.
- Control and distribute electrical power to the spacecraft.
- Fulfil the loads average and peak power requirements.
- Provide regulated voltage bus to the loads.
- Protect the spacecraft against any failures within Electrical Power Subsystem.

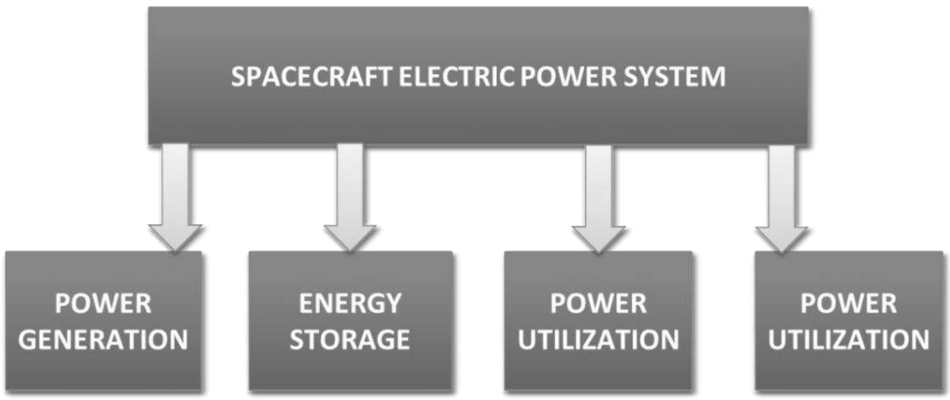


Fig. 1-3 The functional block diagram of Electrical Power Subsystem

In the space missions, power requirements, mass, cost and lifetime are the key parameters of Electrical Power Subsystem. Historically, power requirements of spacecraft started from several watts. In future, this will reach several kilowatts to megawatts as for big satellites and space platforms such as international space station. The previous data of different Spacecraft shows that, the Electrical Power Subsystem mass is 20-30% of the all mass of spacecraft ( [**6**], [**7**]). Mission cost estimation and model which mentioned in [**6**], the Electrical Power Subsystem total cost can be estimated as ~23% of the total spacecraft bus cost. The designed Electrical Power Subsystem lifetime depends on the required mission lifetime and environment. The estimated lifetime is in the range of few hours to more than 10 years as big space platforms.

Researchers and designers are trying to find out way to optimize Electrical Power Subsystem performance, by minimizing mass, volume and cost.The Electrical Power Subsystem is typically has two main architectures of the connection between its compounding parts, Direct Energy Transfer and Peak Power Tracking. Direct Energy Transfer architecture is less complex in the design; the power generated will be distributed directly to applications. Development of space technology makes Electrical Power System design challenges for future small and big spacecraft are similar in some behaviour. In the case of small satellites, the purpose is to increase Electrical Power System total power for reducing total satellite weight and volume to make it that increase payload capability and use of smaller, cheaper launch vehicles. In the case of big spacecraft, the important challenge is to increase Electrical Power System total power to enable enough power supply when maintaining acceptable spacecraft mass and volume to make it possible to use of existing launchers. Fig. 1-4 shows an illustration for basic architecture of Electrical Power System, which comply with both basic designs.

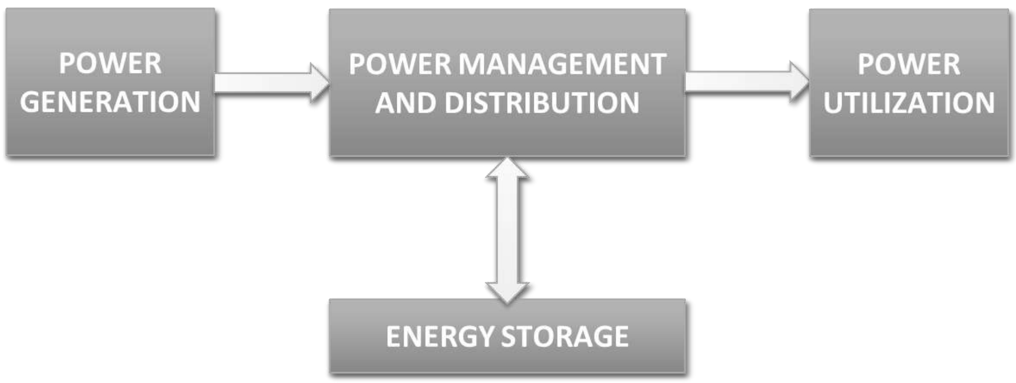


Fig. 1-4 Basic architecture of Electrical Power System

It is shows that the exceeding generated electric power than the load using will be stored in the energy storage element, on the contrary, in case of high consumption, the power will be flown to the load from power generator and energy storage element such as battery. In the usual application, this aspect is main function of Power management and distribution unit. This energy flowing controller Power management and distribution unit is consisted of power devices as a key components such as PiN diode, IGBT and MOSFET etc. Power management and distribution unit of electrical power system of spacecraft was conceptually developed since 1990's [**8**]. Basic idea of this concept is to reduce mass and volume as much as possible due to the reason as we mentioned before. In order to execute this idea to reality, basic components of power management and distribution unit such as semiconductor power devices are should work in high power range. In the next subchapter we will briefly talk about semiconductor power devices.

## 2. POWER SEMICONDUCTOR DEVICES

As before mentioned main part of Electrical Power System of spacecraft is Power Management Distribution. Main components of this part are Power Semiconductor Devices such as Power diodes, Thyristors, MOSFET and IGBT. What are semiconductor power devices? This is a semiconductor device used as a switch or rectifier in power electronics; power management distribution unit is an example which includes power converters and rectifiers. Such a device is also called a power device or, when used in an integrated circuit, a power IC. Basic one of possible classification of Power Semiconductor Devices is shown in Fig. 2-1. It consists of two parts. First is two terminal devices which includes diodes and its operation depends only applied power on its terminals. Those terminals are called anode and cathode. Second are three terminal devices which depend on applied power on terminals and also controlling signal on driven terminal. Also there are four terminal power devices developed recently.

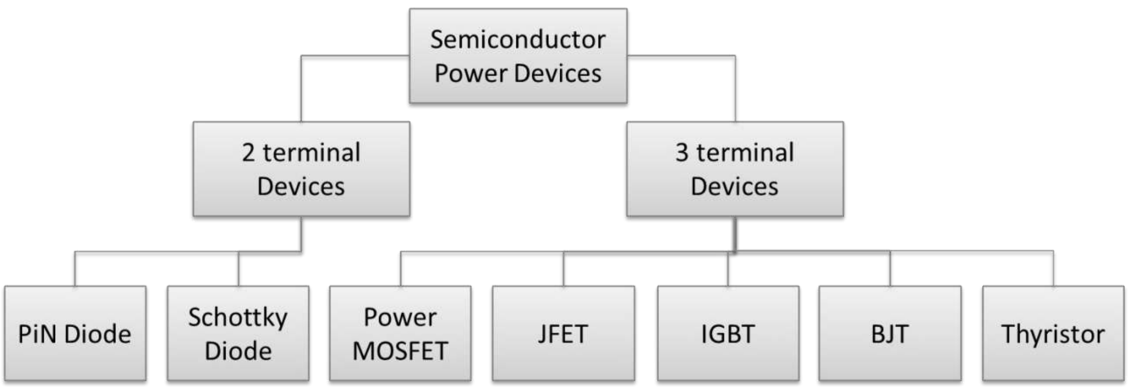


Fig. 2-1 Basic classification of Power Semiconductor Devices

Nowadays, power devices usage is everywhere in technology. These are the components which are for control energy flowing through any equipment. The main application of power devices are home applications, motor drives and low voltage inverters, converters so on in low voltage range, electric vehicle, electric train, renewable energy specially for wind turbine drive and even for space platforms such as communication satellite in a high voltage range [**9**]. In this dissertation, high voltage device will be the main focus. In the next subchapters we will discuss about MOSFET, IGBT and Power diodes whereas these are the main components of power management and distribution unit. In the component level, designing challenge to reduce volume and mass still exists, but in space application reliability is highest priority especially for big space platforms. [**8**]

### 2.1. IGBT and MOSFET

The metal–oxide–semiconductor field-effect transistor (MOSFET) and insulated-gate bipolar transistor (IGBT) are a three-terminal power semiconductor device primarily used as an electronic switch which, as these were developed, came to combine high efficiency and fast switching. These two types of transistor can basically represent three terminals of power devices. In the Fig. 2-2 shows that comparison of those two types of devices internal structure.

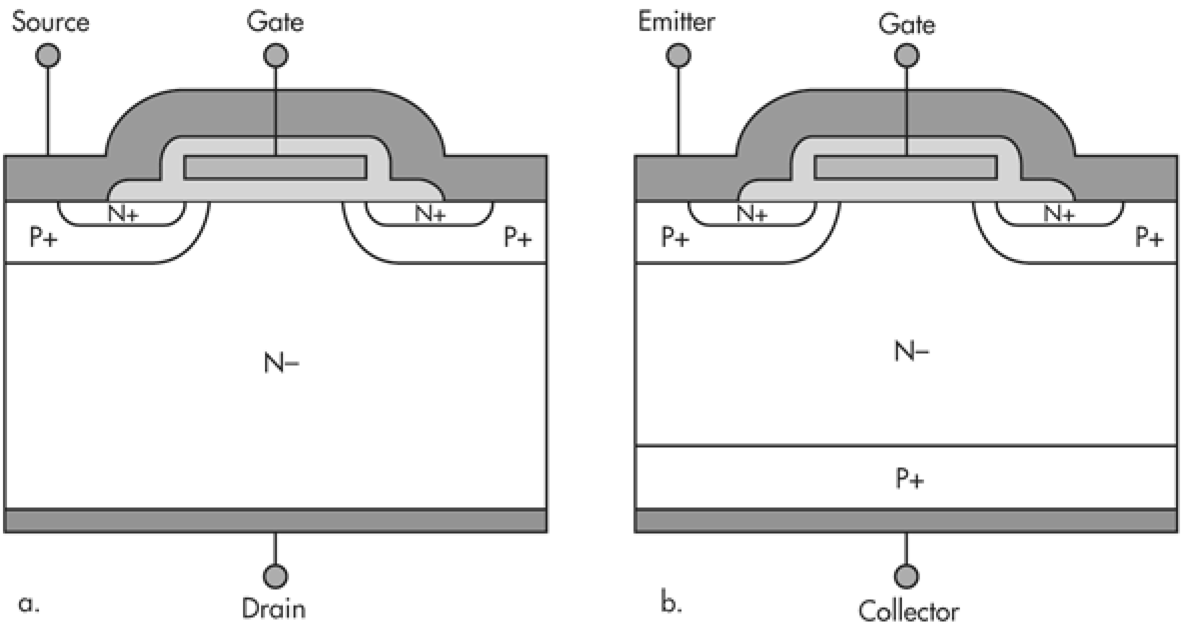


Fig. 2-2 IGBT and MOSFET internal structure comparison a) MOSFET b) IGBT

The IGBT has better performance than MOSFET at high switching frequency range.

But at low switching frequency range, the MOSFET has the less power loss and lower operating junction temperature [**10**]. There is operational performance limitation on MOSFET, between specified voltage rate and on-state resistance as said “Silicon limit”. By using different material than silicon such as Silicon-Carbide, the limitation range may increase. However Silicon material will be the majority material of manufacturing of power devices due to the manufacturing and material costs even though there are lots of researches have been done by companies and institutes. This is a reason that we focused on Silicon material in this study.

On the other hand IGBT has a low operational power loss even at higher operational voltage. Due to this reason various applications, in the range of 1 kHz to 100 kHz frequency, 1kVA to 10MVA power and voltage of 600V - 4.5kV, will use suitable one of silicon IGBT, Silicon Carbide MOSFET [**9**]. This range of power is actually our target rated power of space platforms.

### 2.2. PiN Diode

A PiN diode is a diode with a wide, un-doped intrinsic region between p-n semiconductor regions. This wide intrinsic region is a main difference PiN diode from ordinary PN diodes. The p-type and n-type regions are usually highly due to its purpose of ohmic contacts. The Fig. 2-3 shows that the basic internal structure of PiN diode. The PiN diode is suitable for attenuators, fast switches, photo detectors, and high voltage power electronics applications.


Fig. 2-3 Basic PiN diode internal structure

The PIN diode consists of three layers of semiconductor material as we mentioned before. The typical P and N regions and between them is a layer of intrinsic material which has a very low concentration of doping. It could be one of N-type or P-type, but with a concentration of the order of 13^13 cm^-3 which makes it a resistivity of the order of one kilo ohm cm. The high-frequency resistance is inversely proportional to the DC bias current through the diode. The PIN diode acts as a variable resistor. This high-frequency resistance may vary for big interval. The thickness of the intrinsic layer is generally from 10 to 300 micrometres. The P and N-type regions are heavily doped.

There are two ways in which the PIN diode can be manufactured. First one is to fabricate it in a planar structure, and other one is to make it as mesa structure. The planar structure fabrication is that an epitaxial film is grown onto the substrate material and the P+ region is made by one of the diffusion or ion implantation. The mesa structure is method that layers grown onto the substrate. These layers have the impurity incorporated. In this way it is possible to control the thickness of the layers and the level of impurity more accurately and a very thin intrinsic layer is possible to manufacture as required. The advantage of the mesa structure is that it provides a reduced level of fringing capacitance and inductance.

## 3. COSMIC RAY INDUCED FAILURE AND ITS MECHANISM ON DEVICES

The well-known studies have been shown that the cosmic ray penetration in semiconductor device is the failure which basically named “single event upset” (SEU) [**11**]. The failure induces by space proton is the one of problem; however we can generate high voltage in space. As studies shown, high power device failure due to space particles occurs in both space and terrestrial [**12**] [**13**] [**14**].

The reliability of high power device for space application have to be evaluated somehow, in order to mitigate issues of its. In space most of failures of electronic devices are occurred due to the single event upsets through cosmic rays. In the next subchapters, cosmic ray and failure mechanisms will be explained.

Cosmic Ray

There is still not certain scientific description for terms of cosmic ray. Sometimes it is named Space radiation. As known, cosmic rays come from outer space was discovered in 1913. Customary, cosmic ray is energetic particles that composed of protons, electrons, and fully ionized nuclei, which come from outer space. Nowadays, cosmic rays basically divide to four sections [**15**]:

Primary Cosmic rays: It consists of Galactic particles which enter to Solar system and some of them to earth. It called Galactic Cosmic Rays

Solar Cosmic rays: It is originated by phenomena on the Sun which called solar wind.

Secondary cosmic rays: When cosmic rays enter to the earth atmosphere, it becomes shower of secondary particles due to its hitting with atmosphere molecules.

Terrestrial cosmic rays: Particles which comes to the earth surface. More than 99% of particles are non-primary cosmic rays particles. Most of them third to seventh generation cascade of initial particles.

However, we will focus on space radiation environment. In the near-Earth environment first and second classification of particles are basically discussed. In additionally there are trapped particles in the near-Earth environment.

There is a continuous flux of Galactic Cosmic Ray ions. Although the flux is low, a few particles per area of $cm^2$ and per time of $s^{-1}$, Galactic Cosmic Rays include energetic heavy ions which can deposit significant amounts of energy in sensitive materials and it may cause problems to spacecraft's electronics and manned missions in space [**16**].

Second huge source of Cosmic ray is the Sun. It has eleven years of periodical activation cycle as shown in Fig. 3-1. As for solar particles, the Earth's magnetic field acts a varying degree of geomagnetic shielding for near Earth environment.

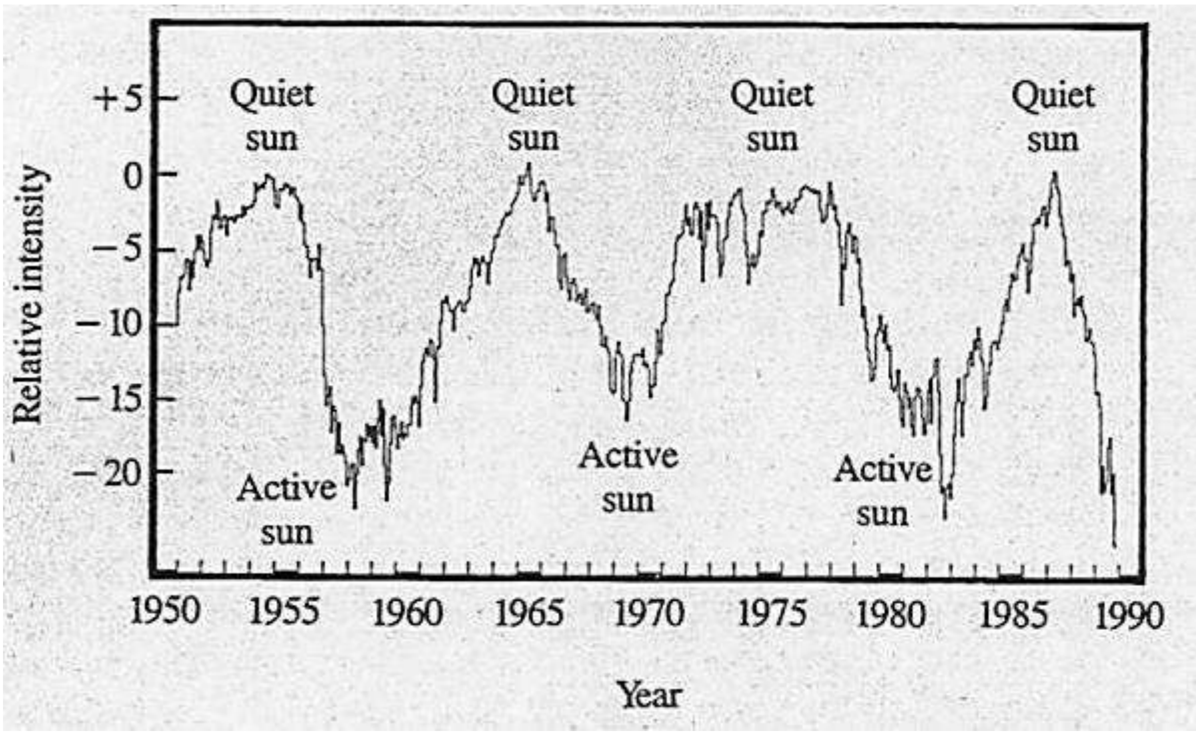


Fig. 3-1Cosmic Ray flux at Terrestrial altitudes [**15**]

A number of significant events related to solar cycles may have been reason for several spacecraft operational anomalies. Thus, radiation protection is significant issue for big space platforms operations, for deep space missions such as to Mars, or for a landing on the Moon. For these several reasons, considerable importance has been appeared in last decades concerning the prediction data of solar proton fluencies [**16**].

### 3.1.1. Flux, Cross Section

In term of Flux, to calculate proton caused error which basically called single event error, is important understanding. Current density should be considered as well. “Integrals of the product of flux with corresponding cross sections yield the number of interactions of interest per cubic centimeter or per gram of material. Particle-material interactions, as opposed to particle-particle interactions, are of overwhelming interest. The latter interactions occur, such as high energy gamma reactions that produce an electron and positron” as mentioned in [**17**]. However, they have negligible bearing this dissertation. Particles have movement of omnidirectional. Particle flux at position **r** in spherical coordinates is shown in Fig. 3-2.

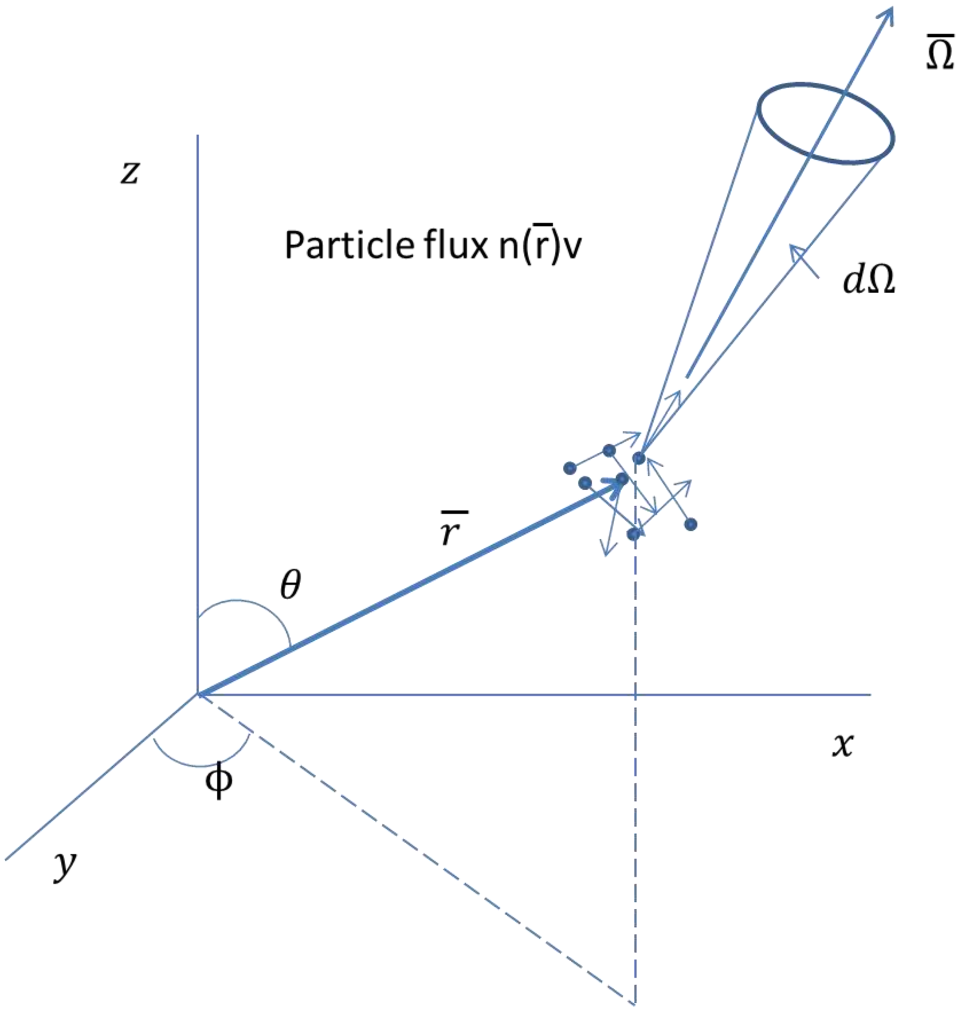


Fig. 3-2 Particle flux at position r in spherical coordinates

If we define *n(**r**) by* mathematical expression as it is a particle density. It can be expressed that as shown in Eq. 3-1. At around **r**, particles with Omni directionally travelling velocity is $v\mathbf{\Omega}$, for $d\Omega$, velocity becomes $v$.

$$n(\mathbf{r}) = \int n(r,\mathbf{\Omega})d\Omega = \int_0^{2\pi} d\phi \int_0^{\pi} n(\mathbf{r},\mathbf{\Omega}) sin\theta d\theta$$

Eq. 3-1 Particle density

Where:

**r** – Radius position vector

**Ω** – Directional unit vector

Here we should mention about cross section which is the important term for particles physics. Basically, an interaction cross section is written as letter $\sigma$. When the particle with $v$ of velocity travels in the medium for 1 second, it interacts with the medium and that makes cylindrical shape as shown in Fig 3-3. This interacted shape's length is defined by velocity of particle and here is the $\sigma$ as cross sectional area of interaction. We can consider that particle interacts with every single atom in that cylindrical volume. Here, $N$ is the number of atoms per cubic centimetre in that cylindrical volume (particles/cm$^3$). Hence, $N\sigma v$ will be the number of interactions by an incident particle per one second in the path volume.

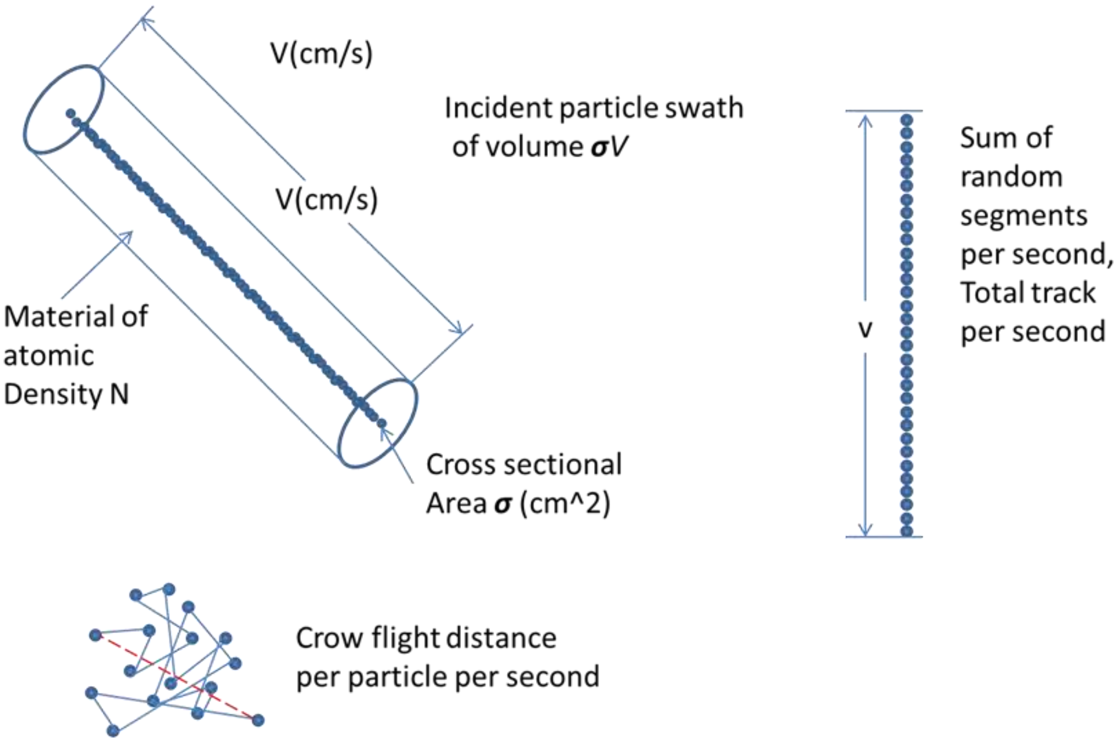


Fig. 3-3 Interacts with the medium and that makes cylindrical shape

On the other hand $N = \rho N_0/M$ or $\rho N_0/A$, here $\rho$ is material density and $N_0$ is Avogadro's number. $A$ is materials mass number when targets are nuclei; $M$ is the molecular weight when targets are atoms or molecules. Yields in Eq. 3-2 are defined as number of interactions per cubic centimetre which occur at **r,** characterized by corresponding cross section.

$$N\sigma v n(\boldsymbol{r}) = \frac{n(\mathbf{r})v}{\lambda} = \frac{\phi(\mathbf{r})}{\lambda}$$

Eq. 3-2 Interactions at **r**

If there is needs to define interaction computing, probability of interaction should be considered as well. This probability is defined by terms of Cross section. As shown in Fig. 3-4. It can be simply explained by this manner which shown in figure. Particles beam (Intensity of $I$ particles/cm$^2$) is normally incidence on the $A$ area of thin slab which has $\Delta x$ of thickness. The material type of slab can be any which includes molecules or nuclei etc. Those interacting area with beam normal incidence is assumed circular. All of target should be normal to the beam which defined as $\sigma$(cm$^2$).

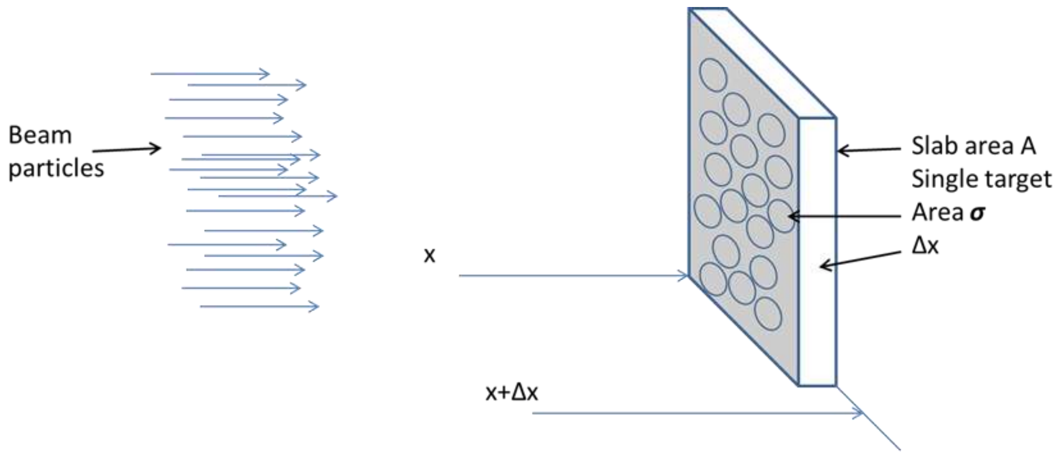


Fig. 3-4 Particles beam on the thin target material.

If we consider that beam is the function of *I(x)* along to the x direction. Slab becomes attenuator. Total number of targets per cubic centimeter is *N*. Total number of targets in the slab is $A\Delta xN$. Here $A$ is the slab area, $\Delta x$ is the thickness of the slap and multiple of these are the total volume of the slab. From here total target area becomes $A\Delta xN\sigma$. Attenuation defined by ratio of total target area and slap area. Thus beam intensity difference just after slab becomes that as Eq. 3-3. [**17**]

$$I(x+\Delta x) = I(x) - I(x)\frac{A\Delta x N\sigma}{A}$$

Eq. 3-3 Beam intensity difference after and before slap

From here we can derive $\lambda$ which is called the mean free path as shown in Eq. 3-4. It means $\lambda$ is mean distance between two collisions by particle and material atom.

$$\frac{1}{N\sigma} = \lambda$$

Eq. 3-4 Mean free path

Here are dimensions that $A(\mathrm{cm}^2), N(\mathrm{cm}^{-3}), \sigma(\mathrm{cm}^2), \lambda(\mathrm{cm})$, $N\sigma(\mathrm{cm}^{-1})$. Even though $\sigma$ is the interaction probability per centimeter square area, unit is $\mathrm{cm}^2$. Cross section can be varied that depends on what kind of method considered for collision. For example mechanical collision electromagnetic collision or quantum collisions are different. In our calculation, proton flux is the main particles, for this reason electromagnetic collision is considered.

### 3.1.2. Proton flux at earth environment

90% of those cosmic rays consist of protons in low Earth orbit (below an altitude of 2000km) [**15**]. For that reason this study assumed proton flux as a main consideration. (Neutron flux is dominated in terrestrial; in spite of space proton flux is higher than other space particles [**18**]). Further Protons of Cosmic rays will be called Proton flux in this dissertation.

Proton flux in near earth environment majorly consists of solar protons and trapped protons. The Earth's trapped particle radiation belts were discovered at the beginning of the space technological development and were immediately noticed as considerable problems to space missions. Consequently, NASA has developed several models which enable to predict population of trapped protons and other particles, such as model AP-8 and AE-8 since 1970. But results say that reality of trapped particles modeling is much complex than expected. Nowadays many models developed, however they are still limited in spatial or temporal coverage. Therefore dynamic and complete model is still required to be developed for trapped radiation belt of near earth environment.

The motions of charged particles entering the magnetosphere from the solar wind and undergoing acceleration, or resulting from the decay of neutrons produced by cosmic ray interactions with the neutral atmosphere, are dominated by the magnetic field of magnetosphere. The motion of these energetic charged particles consists of three components as shown in Fig. 3-5 [**16**]:

Gyration about magnetic field lines;

Movement of the gyration centre up and down magnetic field lines;

Slow longitudinal drift of the guiding centre path around the earth, westward for ions and eastward for electrons.

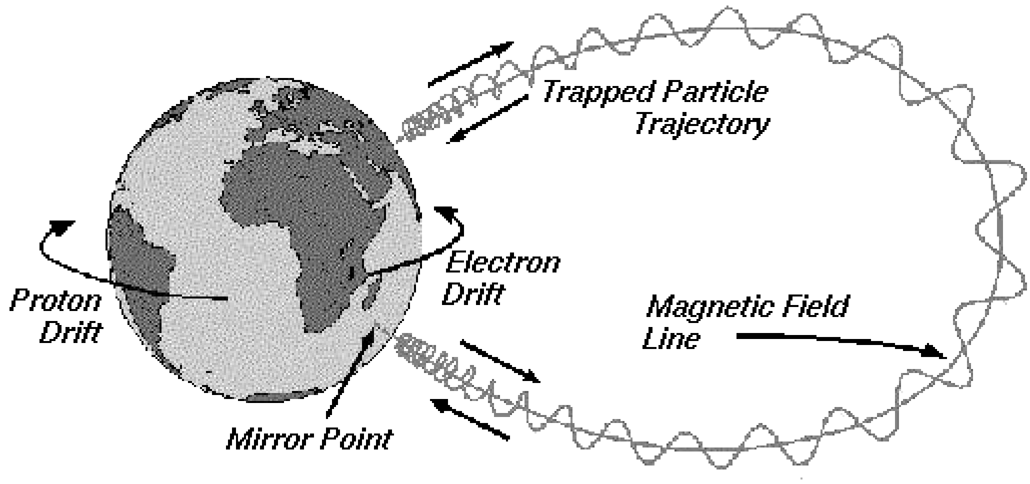


Fig. 3-5 The motion of energetic charged particles in magnetosphere [**16**]

The result of trajectories lies on toroidal surfaces, called drift shells, centered on the center of Earth's dipole. Particles limited to a drift shell can remain there for long times, up to several years for protons at altitudes of thousands kilometers, hence the term is called "trapped particles". The population of charged particles stably trapped by the Earth's magnetic field consists mainly of protons with energies between 100 keV and several hundred MeV.

A Solar protons are generated when protons emitted by the Sun during a solar flare accompanied by a coronal mass ejection it become very high energies of particles. After that Protons are guided by the deep space magnetic field lines as shown in Fig. 3-6.

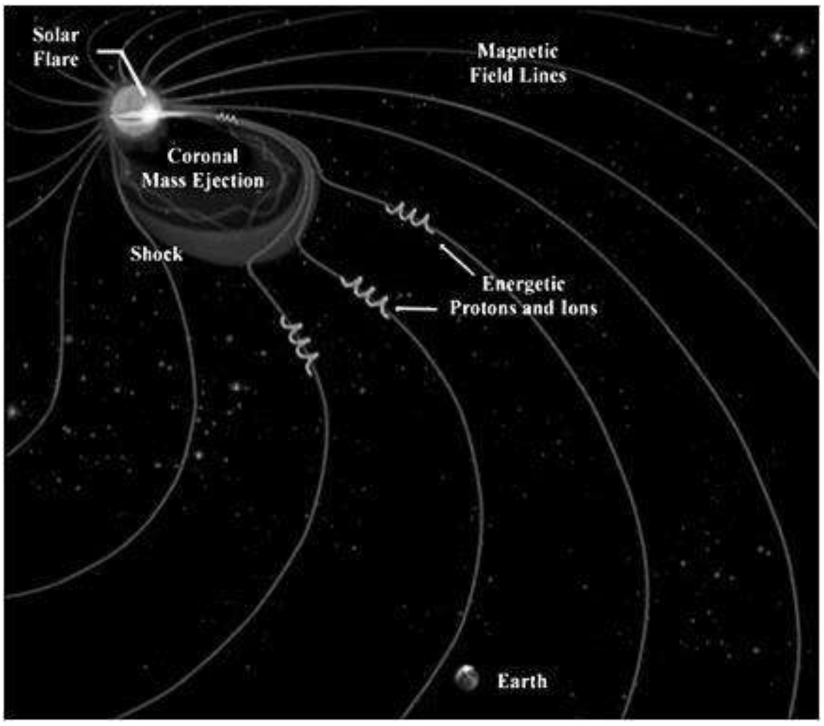


Fig. 3-6 Solar energetic protons emitted by the Sun and guided by magnetic field line [**19**]

Energetic proton flux can be reason of electrical charging of spacecraft to amount that can damage spacecraft components. This charging aspect is critical at high voltage application on spacecraft, especially for High voltage solar panel application. Earth is largely protected by its magnetic field, or magnetosphere. However, the closer a spacecraft near to the Polar Regions, these are been exposure higher radiation than other regions. In further subchapter, damage and failure which caused by proton will be discussed.

### 3.2. Mechanism and failure in Devices

One of the most difficult problems facing electronics of space application is that effect of charged particles. When these particles pass through a material, it loses its energy by ionizing volume material, generating electron-hole pairs along the path of the particle. The interaction of electrons, protons, and heavy ions with electronic devices leads to two different types of problems as shown in Fig. 3-7. The first one is total dose degradation, which the cumulative effect of many particles is passing through an electronic device cause parameter degradation and functional failure, and it will not be discussed here. Another one problem, single particles passing through electronic device may cause several of effects, generally known as single event errors or phenomena (SEP) [**20**].

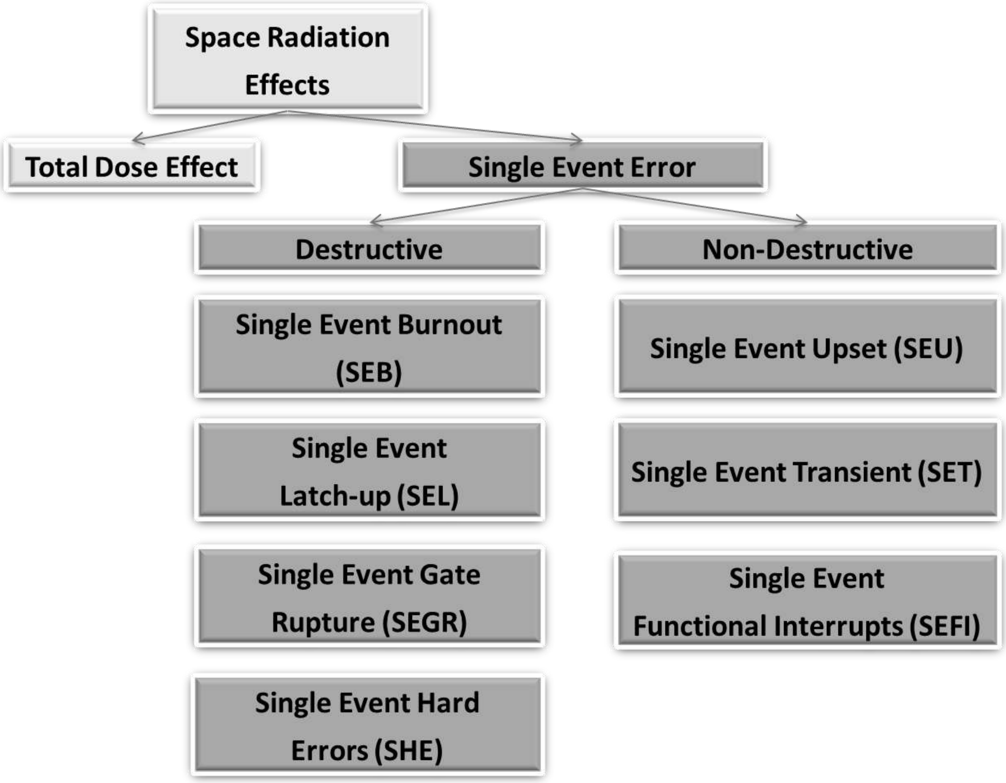


Fig. 3-7 Classification of Space radiation effects in electronics

The single event errors are classified in hard errors and soft errors. Hard errors are non-recoverable errors which named destructive error. Soft errors may be recovered by a reset, a power cycle or simply a rewrite of the information which named non-destructive error.

Single event errors due to protons are a significant problem in the electronic circuitry of earth-orbiting spacecraft. A nuclear reaction initiated by a proton can produce sufficient ionization for a single event error.

### 3.2.1. Proton-Silicon interaction

In this section basic physics understanding about proton induced failure phenomena in silicon will be briefly described. The cause of failure is proton flux. Why only proton flux was considered here is described in chapter 3.1.1. When an energetic proton penetrates silicon, several types of interactions may happen. For example, protons can scatter from the Silicon atoms as type of elastic, inelastic scattering can be happened, which can then recoil, or they can ionize the atom by hitting molecules, leading to the generation of charge inside material. The nuclear interaction makes a mechanism due to an energetic ionizing particle or non-ionizing neutron can deposit a large amount of energy in to the device material that has tiny dimensions. Ionizing is usually made by secondary recoiled heavy ions track. But these interactions inside silicon by energetic proton have some probability for those interactions occurrence. The incident proton interacts with the nuclei of the material then heavy particles and scattered protons are generated after this collision. As a result, scattered heavy particles transfer amount of energy to the Silicon. On the other hand, it can be said proton deposits energy to the silicon. Most of the energy deposition takes the form of ionization loss along the way of the charged secondary recoils coming out from the affected atoms or molecules and along the path of the recoiling residual nuclear fragment that as shown in Fig. 3-8. Generated charge due to that ionization is the reason of single event errors which mentioned previously. Basically those ionizing process generates extra charge inside semiconductor device which nearly proportional to the deposited energy by high energetic proton. Pair generation energy depends on the medium band gap energy. The energy $W$ required to create an h-e pair in a semiconductor by a charged mass particle traversing the medium depends on the band gap energy $E_g$ of the material and hence, although only slightly, on the temperature. The measurements of this quantity show a nearly linear dependence on the band gap energy, and the linear fit to the data obtained for different materials gives as shown in Eq. 3-5.

$$W(E_g) = 1.76\ eV + \ E_g * 1.84eV$$

Eq. 3-5 Required energy to generate one hole-electron pair

The probability of proton-induced failures and the dependence of cross section on proton energy can be investigated both experimentally and theoretically.

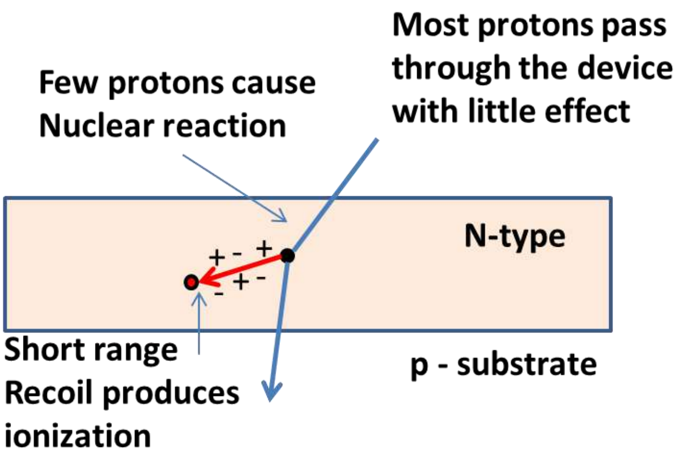


Fig. 3-8 Ionization made by secondary recoils due to proton induced nuclear reaction.

To measure this energy transfer from proton to silicon we use some terms of understanding. These are terms of linear energy transfer (LET) and stopping power. These are almost same meaning; the stopping power includes meaning of LET. The basic unit for linear energy transfer and stopping power is same as ($\frac{MeV}{m^{-1}} or \ \frac{MeV\ cm^2}{mg}$). As before mentioned that particles loss its energy by nuclear, electrical material and density caused retracting when these penetrate to the material. In this study, we interest ionization phenomena inside silicon by proton induced.

Firstly, linear energy transfer is the average energy deposition of the particle per unit track length; it means how much energy deposits to the material and it purely generates hole-electron pairs in the unit length of the material. Linear energy transfer is the positive quantity and basically it represents energy which makes ionization in the material. Linear Energy Transfer which is expressed by Eq. 3-6.

$$L_{\Delta} = \frac{dE_{\Delta}}{dx}$$

Eq. 3-6 Linear Energy Transfer

This $L_{\Delta}$ and yield of energy deposition with distance travelled depends on the material properties. Here $E_{\Delta}$ is the energy of particle and $x$ is the distance travelled. Basically, Linear Energy transfer is varied depending on incident particles' kinetic energy. Linear Energy transfer of material depends on the atomic density (atomic number so on) as well as incident particles' energy. In other words, Linear Energy transfer is described by terms of atomic density thickness, rather than geometrical size of the length. In our calculation, for defining of the heavy ion model ionization in the T-CAD is used term of Linear Energy Transfer.

The term of stopping power is wider understanding than LET and that represents total energy loss of the particle per unit length path in the volume material by both elastic and inelastic collisions (another names are linear stopping power and mass stopping power). Here, linear stopping power also includes term of LET in the some case. Other words, term of stopping power includes two compounds terms which are nuclear and electronic stopping power. The stopping power represents total energy loss of energetic particle when it penetrates to the materials. The $s_{sp}$ can be described as the total quantity of stopping power, which described in Eq. 3-7 and Eq. 3-8. Here $\rho$ is the density of the material and $\rho x$ is the density-thickness.

$$S_l = -\frac{dE}{dx}$$

Eq. 3-7 Linear stopping power

$$S_m = -\frac{dE}{d(\rho x)} = -\frac{1}{\rho}\frac{dE}{dx} = \frac{S_l}{\rho}$$

Eq. 3-8 mass stopping power

Then the total energy losses of energetic particles rates $S_t$ can be defined sum of all interactions results. Basically LET and stopping power are identical unless energetic secondary particles may escape the material. LET is considered for the electromagnetic interaction in the material which means almost all energy transfer makes ionization. Charged particles such as proton can give energy to the atom even though it just passes closely. Stopping power consists of several interaction influences for its total value is mostly in the range of keV to few MeV as shown in Fig. 3-9 [**21**]. In our calculation proton flux energy range is up to 200 GeV corresponding literature data.

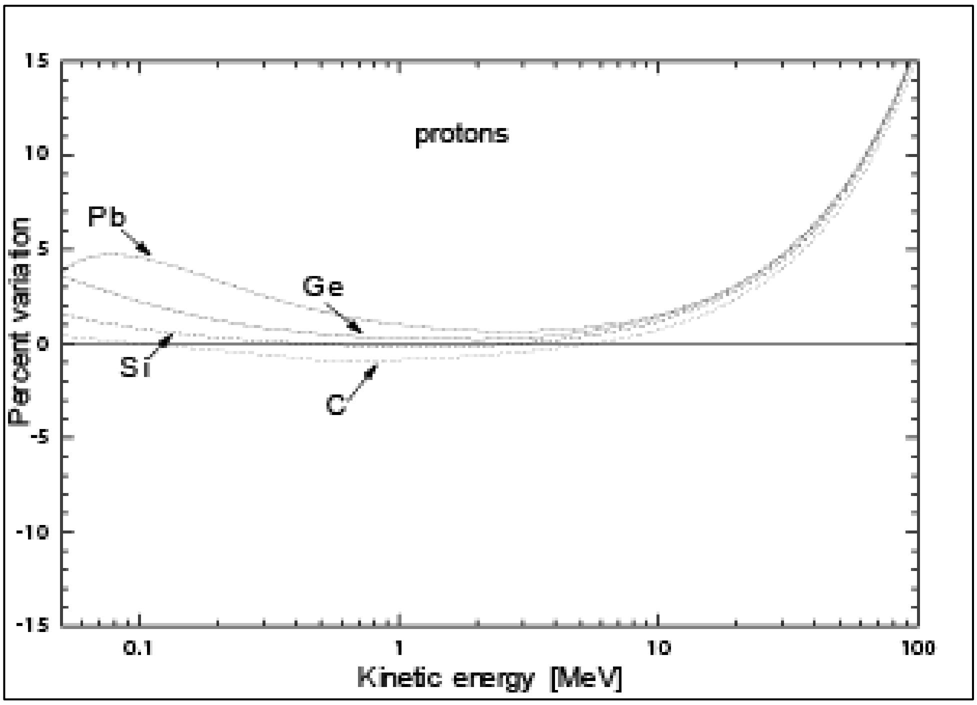


Fig. 3-9 Stopping power of the proton variation respects to the incident energy up to 100 MeV [**21**]

Then we should consider high energy range of proton flux affect rather than keV energy of range of proton flux. When the high energy range of proton penetrates to the material, electromagnetic stopping power will be dominated as shown in Fig. 3-10 [**22**]. Here we can see the $s_{sp}$ is majorly compound by electronic stopping power. Thus we used LET for our calculation and considering worst case, all energy were assumed to generate hole-electron pairs.

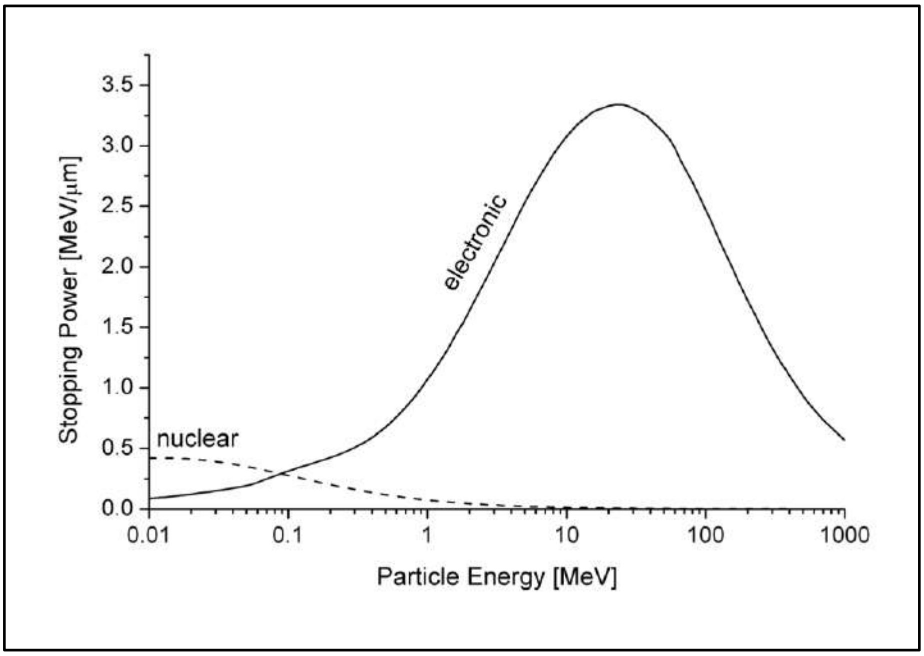


Fig. 3-10 Stopping power type corresponding to energy of incident particles [**22**]

### 3.2.2. Semiconductor devices failure due to cosmic ray

#### 3.2.2.1. Integrated circuits failure by cosmic ray

Huge amount of hole-electron pairs are generated due to this ionization loss. If such a nuclear event happens within or near the sensitive part of electronic elements such as large scal integrated circuits and power devices. The large scale integrated memory device and sufficient charge is generated, the result can switch logic state of the memory bit. The change of information stored at some location in memory has physical damage which cannot be seen by observer, to the device is usually caused by single event soft error. Energetic protons have been shown to induce soft errors in a number of Large Scale Integrated dynamic and static RAM devices, the trend of development of electronic components goes towards to usage of smaller, faster and more sensitive detectors in any field of application. Small size of modern devices minimized to improve power consumption and processing speed; a single particle can have a critical effect and even cause non-recoverable damage to an electronic device. As a consequence, these devices are more sensitive to radiation effects than older components. It makes needs to understand and protect for spacecraft systems against space proton effects. In traditional space applications, larger components were used. For this reason single particles could only affect a limited volume of the device, hence only cumulative damage occurred from multiple particle affect could lead to malfunction of the devices as shown in Fig. 3-11 [**23**].

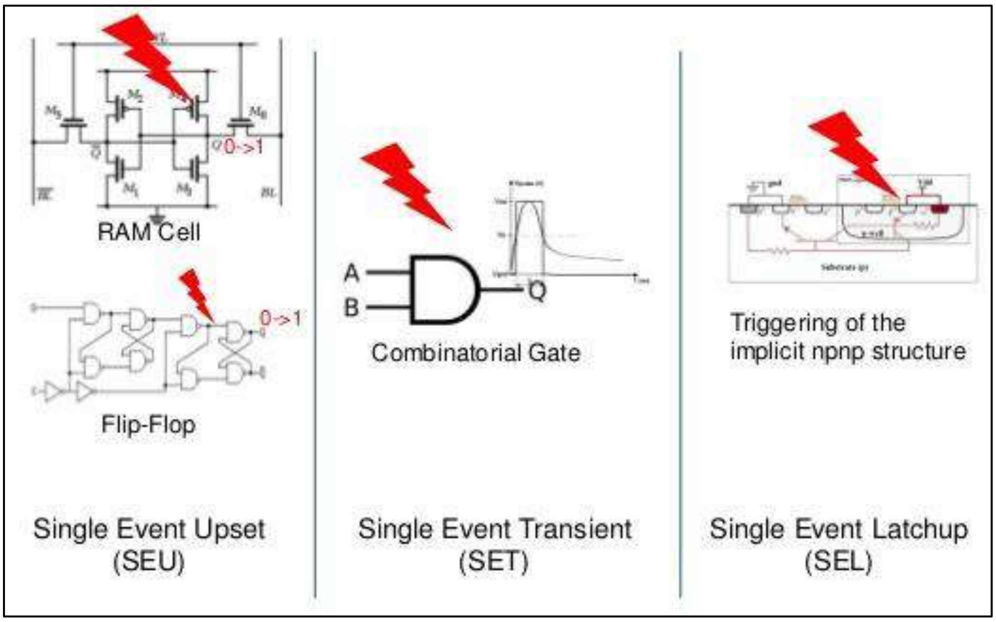


Fig. 3-11 Single event errors for low voltage electronics [**23**]

#### 3.2.2.2. Power devices failure by cosmic ray

Power devices for instance IGBTs, MOSFETs, and diodes in space application at high altitude and sea level systems are incompetent to wrecker single event burnout due to energetic particles. Single Event Burnout was initially observed in power MOSFETs, and the error was related to the regenerative feedback mechanism when energetic particles hit the device. Charge carrier multiplication process was the main reason of the failure. After that single event burn out in bipolar transistors, observed this is similar to failure mechanism of power MOSFETs. Recent studies have been related to accounting of Single Event Burn out in power transistors. Subsequently, power diode incompetent to Single Event Burnout was started to study. The Single Event Burnout mechanism is somehow similar to the other power devices. In this study, we discuss the Single Event

Burn out conditions in power diodes (PiN diode). Basic structure of power devices are similar that consists of P-N junction and semiconductor materials as shown in Fig 3-12. However we will briefly mention about power transistors failure as well in further.

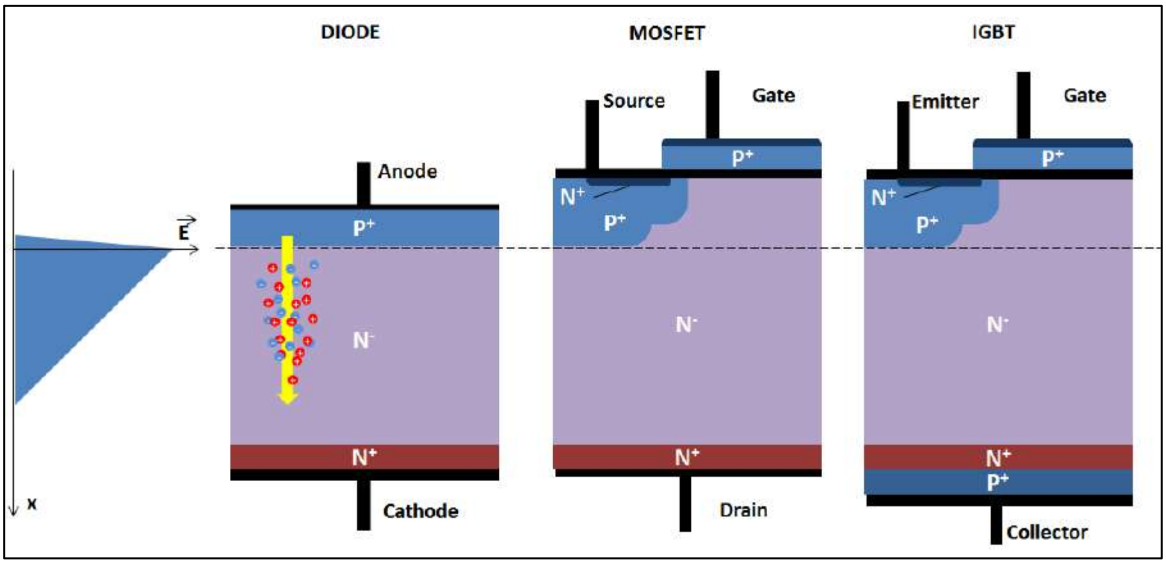


Fig. 3-12 Structural similarity of power devices

When high energetic particle hits power transistor, hole-electron pair will be generated along its track. And these charges will be flow both direction by electric field; current is flown.

When the charge flows to ground via the body, the voltage drop in the body resistance may turn on the parasitic bipolar transistor that is an integral part of double diffused MOS (DMOS) power transistors. If this current flows from positive to ground, there will be voltage drop inside transistor, and it will turn on parasitic bipolar transistor automatically. That parasitic bipolar transistor or thyristor is typically inside power transistors as shown in Fig.3-13 and Fig.3-14 [**24**]. If the applied voltage is continuously applied to the device quickly, at that time high currents and high voltages make second breakdown of the parasitic bipolar transistor or thyristor and can result in burnout of the device.

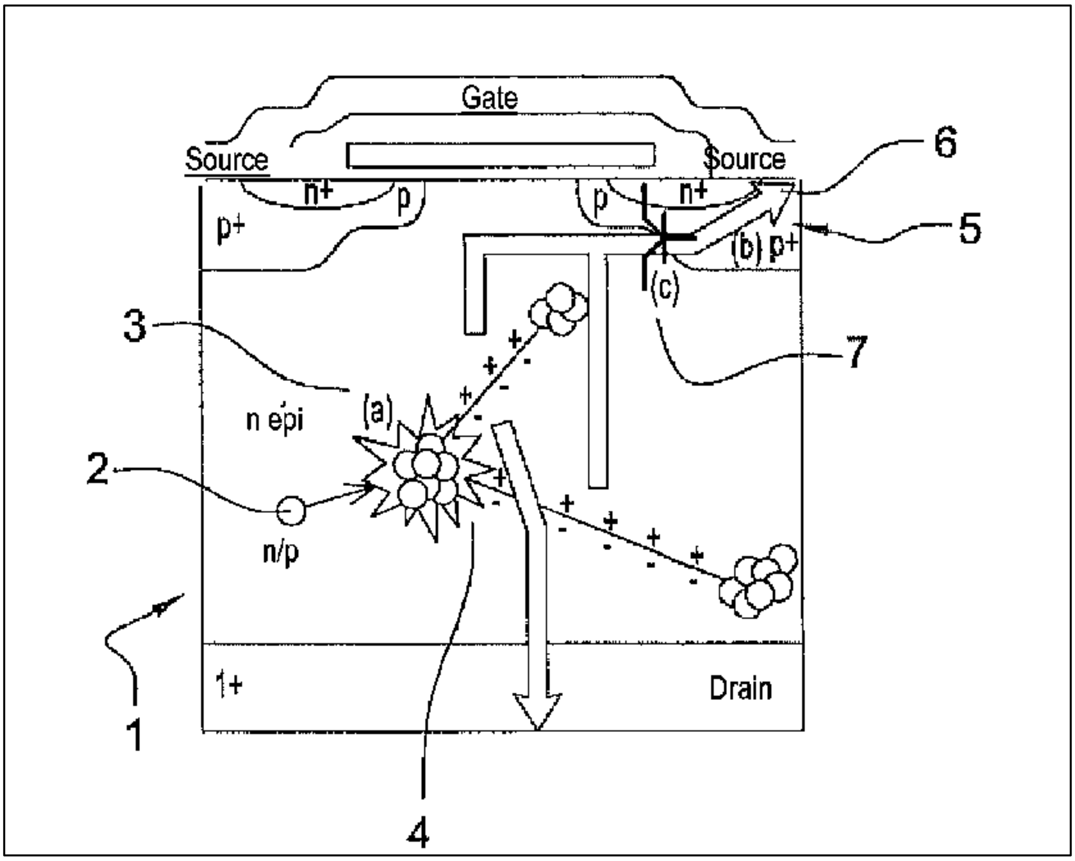


Fig. 3-13 A schematic representation of a power MOSFET transistor and a parasitic bipolar structure [**24**]

Here:

Power MOSFET body which hit by energetic particle

Energetic particles

Interaction of particle and materials atom

Secondary coils generates ionization which makes voltage drops

6- 7- parasitic bipolar transistor structure

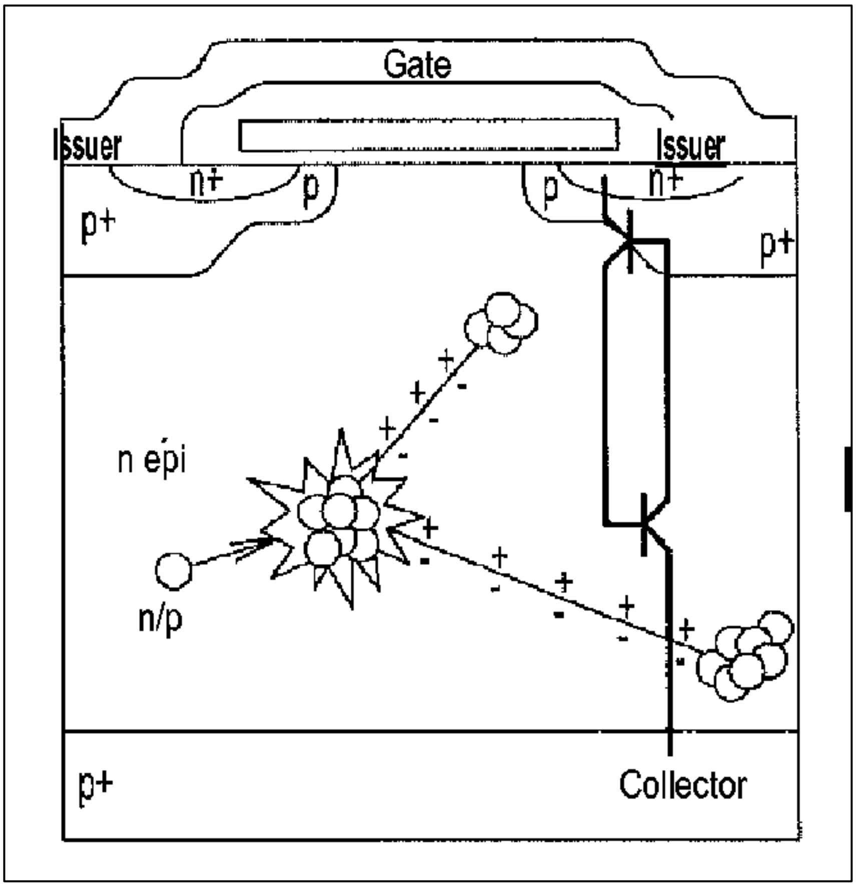


Fig. 3-14 A schematic representation of a parasitic thyristor in the IGBT components [**24**]

As a result of the base push-out phenomenon the failure mechanism was described based on the current induced avalanche model. For IGBT, single event burnout study is kind of newly developed. As mentioned before in this study we will discuss about power diode rather than other group of power devices such as power transistors and thyristors.

The reason for the single event error is often an internal gaining process for example due to a parasitic transistor or thyristor for the power devices. A lot of recent researches were observed that single event burnout can also be triggered by strong avalanche charge carrier multiplication alone.

This phenomena was watched in high-voltage power devices and in large area avalanche diodes, but has also been recognized for a long time in surface barrier detectors as a non-destructive phenomenon. The event of avalanche multiplication is contingent the start of event and its magnitude is exceedingly depending on the applied voltage to the power device. The power diodes failure is very low probabilistically occurred in the terrestrial area. Basically natural background of charged particles flux is not so high in the terrestrial area which can destroy power devices. However, still it has catastrophic possibility to destroy systems. But this failure rate is quite higher in the space environment as we mentioned before. It should be considered worst case ever of application systems every time. In order to investigate failure rate of power diode which triggered by avalanche phenomena, several experiments have been done by researchers. For well understanding about this phenomenon, let us take an example of power diode single event burn out process. The power device simulations have the disadvantage that the multiplication phenomenon is only triggered by nuclear reactions with the silicon atoms [**13**]. As shown in Fig. 3-15 diode has generated charge which flow through along to electric field distribution.

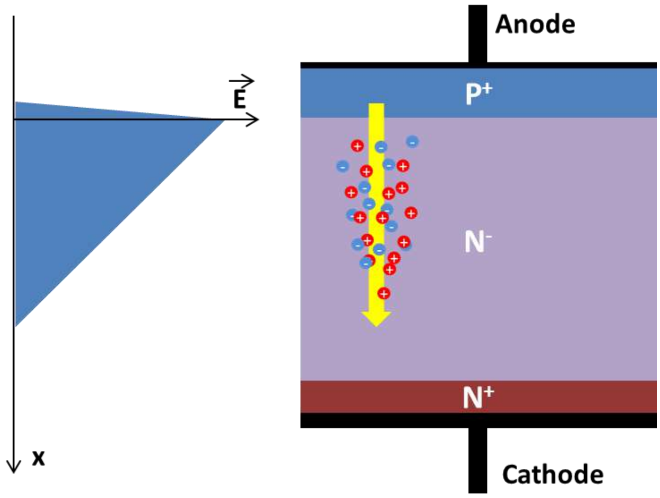


Fig. 3-15 PiN diode structure respect to electric field

Actual generated charge by energetic particle inside diode is not sufficient to make destruction. But there is a phenomenon which called avalanche charge carrier multiplication. This phenomenon explained in existing studies which tested 1700V power diode under exposure of energetic particle flux and result was that as shown in Fig. 3-16 [**25**]. Here yellow colored part represents direct ionized charges by energetic particle, and pink colored part represents multiplied charge under avalanche phenomenon. At the voltage of 1060V, power was destructed. Hence we can see that avalanched failure rate is much less than break down voltage of the power diode. In detail, other study shows that avalanched charge carrier respect to temporal and spatial evaluations as shown in Fig. 3-17 [**12**].

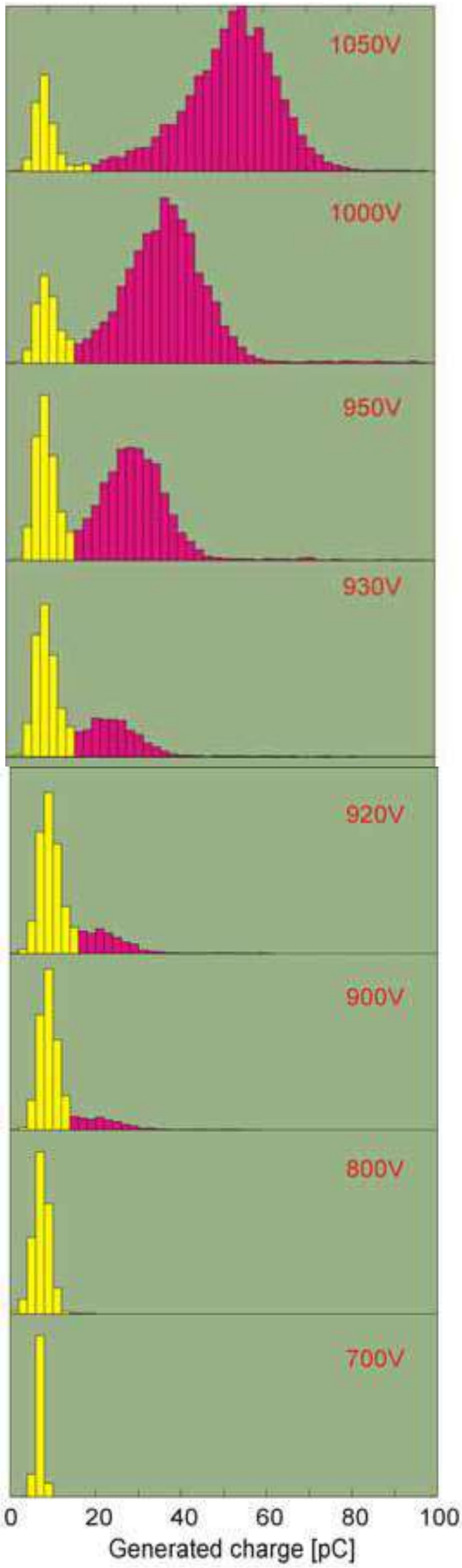


Fig. 3-16 Generated charge and multiplied charge histogram respect to the voltage [**25**]

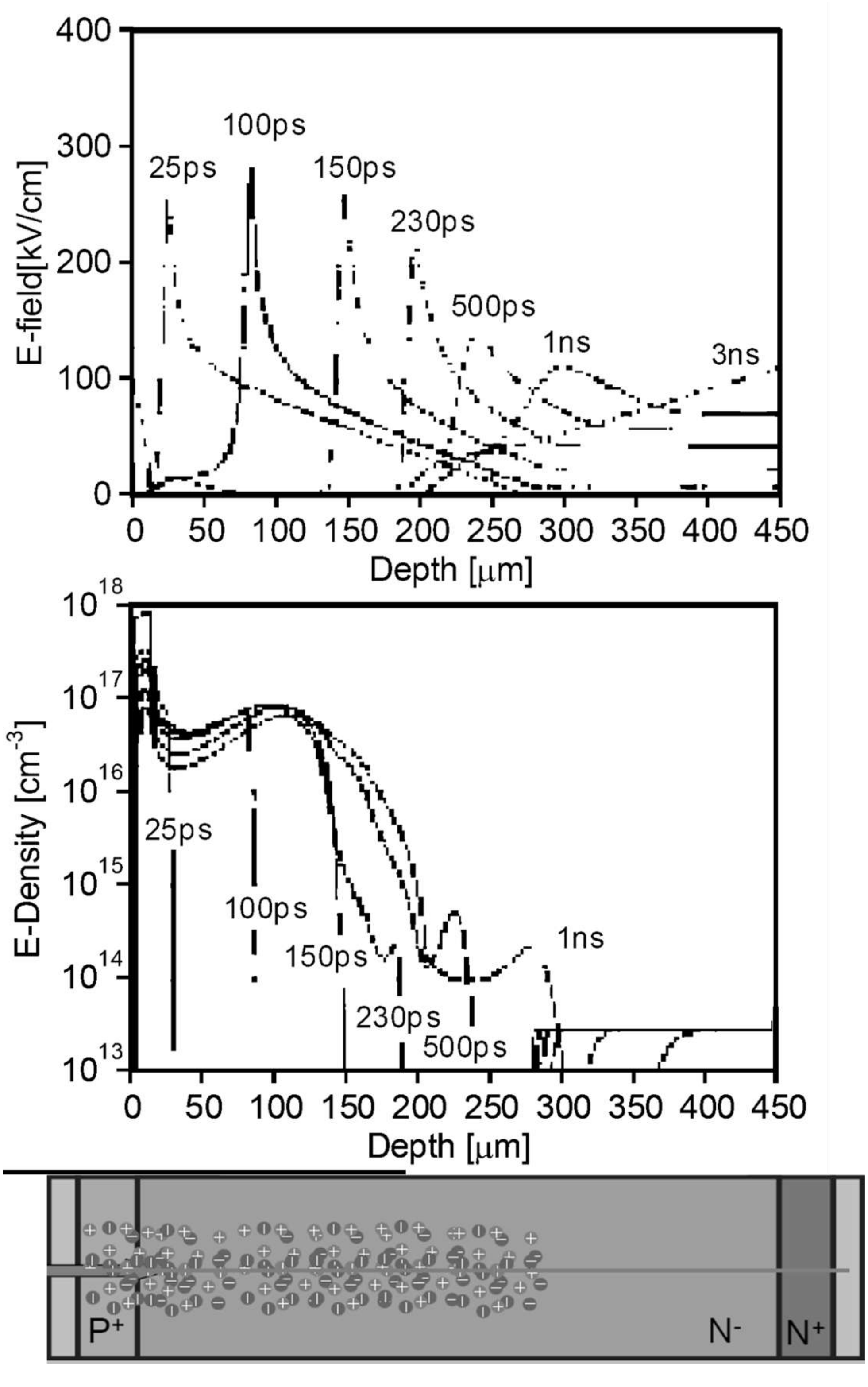


Fig. 3-17 Electric field and Current density variation respect spatial and temporal distribution. [**12**]

(Model 4k Diode, Nbase=450 µm, Applied voltage 1800V, *LET*=1.2 MeV/µm, Ion: $C^{12}$ 17MeV.)

## 4. PROPOSED METHOD TO CALCULATION OF FAILURE RATE

In our study, we proposed that failure rate calculation of power devices' main formula which based on Single Event burnout cross section and Space proton flux function. Difference from single event burn out cross section of small power semiconductor devices, the Single event burnout cross section for high voltage power semiconductor changes that depending on applied voltage for device itself. Basic background information was given in previous chapters.

The cross section is calculated by two functions, one is the threshold charge to destruction $Q_{dest}(V)$ obtained by T-CAD simulation as shown in Eq. 4-1 and charge generation probability function $\Phi_{Ep}(Q)$ which was found from literature. By convoluting proton flux function with the Single Event burnout cross section function, the main failure rate calculation formula was derived as shown in Eq. 4-2.

$$\sigma(V) = \mathrm{A} * \int_{Q_{dest}(V)}^{Q_{max}} \Phi_{E_p}^{300}(Q)\,\partial Q$$

Eq. 4-1 Cross section respect to applied voltage for the power device

$$FR = \int_{E_p^{min}}^{E_p^{max}} A * \int_{Q_{dest}(V)}^{Q_{max}} \Phi_{E_p}^{300}(Q)\,\partial Q * F(E_p)\partial E_p$$

Eq. 4-2 Failure rate calculation formula which proposed as new

Here:

$FR$ - failure rate of device [$s^{-1}$]

$A$ - Device area [$m^2$]

$E_p$ - Incident energy of proton [MeV]

$E_p^{max}$ -Maximum incident energy of Proton [MeV]

$E_p^{min}$ - Minimum incident energy of Proton [MeV]

$Q$ -Generated charge inside silicon by deposited energy [C]

$Q_{max}$ - Maximum generated charge inside of silicon by deposited energy [C]

$Q_{dest}(V)$ -Threshold charge which can generate avalanche phenomena inside silicon due to deposited energy from proton [C]

$\Phi_{Ep}^{300}(Q)$ - Probability function of charge generation according to incident energy [$C^{-1}$]

*F (E_p)* - Space proton flux funtion, which consists three sections by energy range at Low Earth Orbit [$MeV^{-1}s^{-1}m^{-2}$]

*σ (V)*- Single Event Upset Cross section [$m^2$]

In order to establish our proposed formula, three sections were considered. First, T-CAD device simulation, 3.3kV PiN diode was chosen for device model. Hence, destruction charge value, which is generated by deposited energy of space proton, was obtained from simulation. Second, Space proton flux data according to energy range in Low Earth Orbit (LEO), was obtained from SPENVIS web based software from European Space Agency, Alpha Magnetic Spectrometer (AMS) [**18**]and PAMELA data [**26**]. Third, probability functions of energy deposition in device because consequently silicon-proton reaction and SEU cross section were studied before [**27**] [**28**] [**29**] [**30**], from here, probability functions of energy deposition corresponding to device's applied voltages were calculated. Last result was defined as SEU cross section and failure rate respect to the applied voltage for 3.3 kV PiN diode. Details will be explained in next section as shown in Fig. 4-1.

$$\textbf{Failure Rate} = \int_{E_p{}^{min}}^{E_p{}^{max}} A * \int_{\boxed{Q_{dest(V)}}}^{Q_{max}} \boxed{\Phi_{E_p}^{300}(Q)\partial Q} * \boxed{F(E_p)\partial E_p}$$

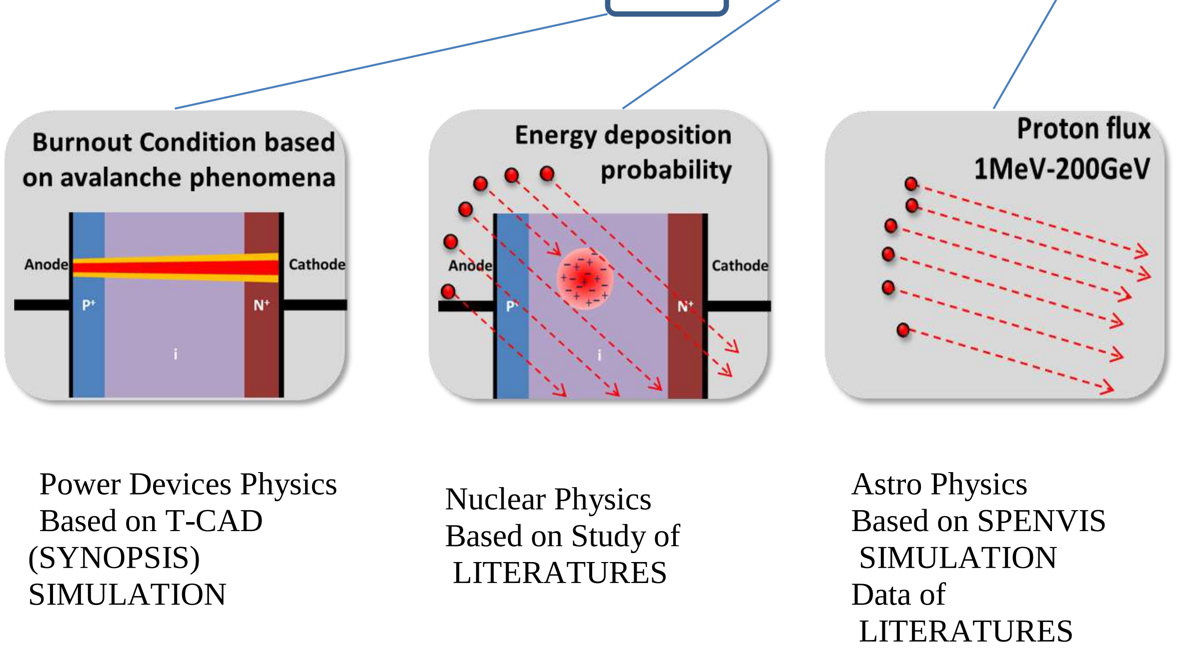


Fig. 4-1 Compounds of the Failure rate Formula

### 4.1. Proton flux data for formula

As mentioned before, majority of cosmic ray consists of proton in Low Earth Orbit [9]. Trapped proton flux, solar proton flux, and cosmic proton flux compound total space proton flux at Low Earth Orbit basically in range of up to energy of GeV. In this calculation, range was 1MeV-200GeV as shown Fig. 4-2. Proton flux data resources and its features is shown in Table 4-1.

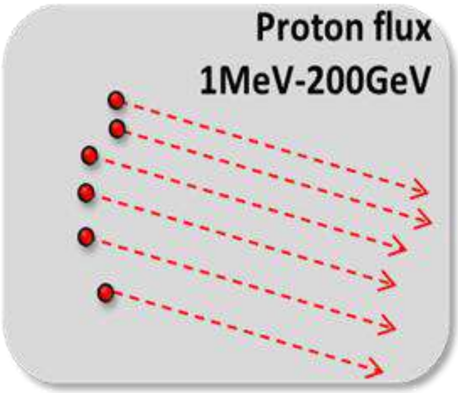


Fig. 4-2 Proton flux range at this calculation

Table 4-1Proton flux data resources and its features

| Source of data | 1. SPENVIS | 2. PAMELA | 3. AMS |
|---|---|---|---|
| Methods | Simulation | On orbit Experiment | On orbit Experiment |
| Considered Particles | Proton | Proton | Proton |
| Energy range | 1-400MeV | 1GeV-20GeV | 20GeV-200GeV |
| Altitudes | ~700km | ~610km | ~400km |

However proton flux density is not uniformly dispersed along the Low earth orbit, in the main formula, total space proton flux written as fitted function $F(E_p)$ which doesn't depend on orbital position. In calculation, shield material hasn't been considered in this section. But further for development of this research, shielding materials and hardening will be discussed. To find out precise data is still complicated and near consideration was taken in this study.

Entire energy range of considered proton flux divided three sections that was covered from 1Mev up to 200GeV. First 1MeV-400MeV proton flux data, which considered at 700 km altitude and its fitted function were taken from SPENVIS [**16**], here mission period assumed 2018-2019, that could clarify sun activation. SPENVIS is the web based software was developed by European Space Agency and is widely used space application studies. This web site has several models for predict cosmic ray distribution in the along to earth outer space. Basically space proton flux in the earth orbit consists of three kinds of resources. First one is Galactic proton flux that comes from deep space is predicted by CREME-96 Sol. Min (1977) model. Second one is solar proton flux that has two models which are CREME-96 (worst week) and ESP-PSYCHIC worst case event. Third one is the trapped proton flux that has a model AP-8 max. After combining these three of resources data, as shown in Fig. 4-3, majority of space proton is came from the sun. Fitted function in this section is considered by that total flux data for proton flux until 400MeV.

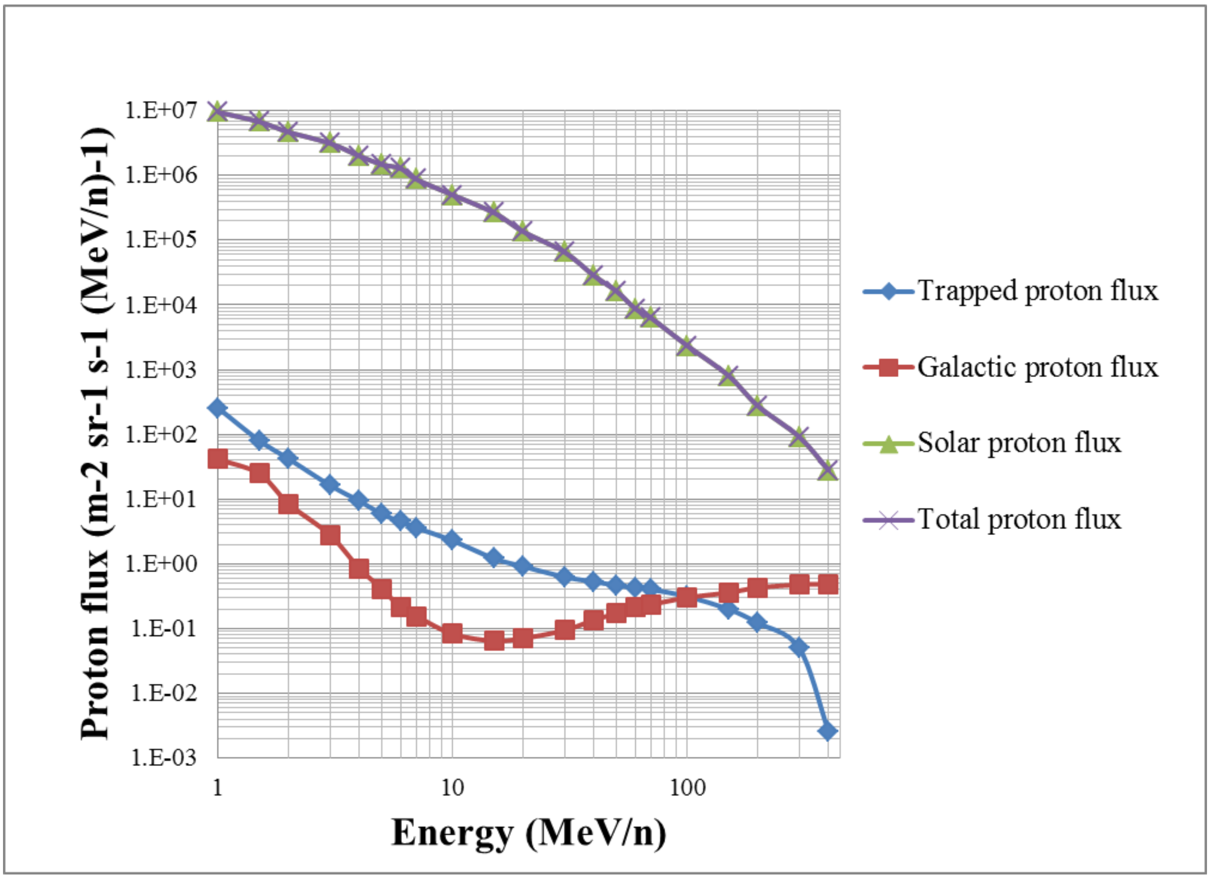


Fig. 4-3 Radiation sources data from SPENVIS (Differential flux ($Ep$)) [**16**]

Second 1GeV-20GeV proton flux data, which measured at around altitude of 350-610km were taken from PAMELA data source as shown in Fig. 4-4 [**26**]. PAMELA is the spacecraft mission payload for study about possible exotic cosmic ray source and its propagation reasons; mission time was 2006-2008. Proton is top set of data. Helium is the bottom set of data. All but one of the previous measurements comes from balloon-borne experiments. Previous data up to few hundred billion electron volts per nucleon were collected by magnetic spectrometer experiments, whereas higher-energy data come from calorimetric measurements. PAMELA data cover the energy range 1 GeV to 1.2 TeV (1 to 600 GeV per nucleon for He). The fluxes are expressed in terms of kinetic energy per nucleon, converted from the rigidity measured in the tracker and neglecting any contribution from less abundant deuterium (d/p ≃ 1%) (where d is deuterium) and 3He (3He/4He ≃ 10%). Therefore, pure proton and 4He samples are assumed. Error bars are statistical and indicate 1 SD; the gray shaded areas represent the estimated systematic uncertainty. E is kinetic energy per nucleon. (as explained in [**26**]).

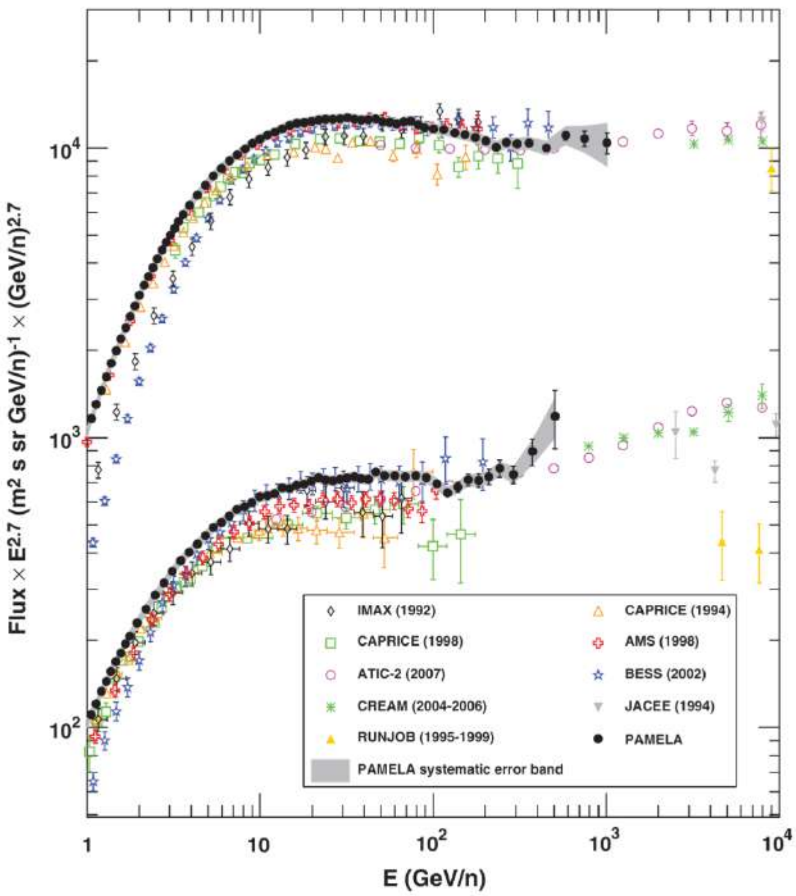


Fig. 4-4 Proton and helium absolute fluxes measured by PAMELA above 1 GeV per nucleon, compared with a few of the previous measurements [**26**].

From PAMELA data we have chosen proton flux until 20GeV and make a mathematical function for it through fitting data graph. However PAMELA data covers up to 1TeV energy of flux measurement, based on consideration of the influence of solar modulation, upper range of data from here is 20GeV in the beginning of the study.

At last 20GeV-200GeV proton flux data, which measured at altitude of International space station around 400 km and its fitted function were taken from AMS data source as shown in Fig. 4-5 [**18**]. AMS is a general purpose high energy particle physics detector in space. The permanent magnet, the silicon tracker, four planes of time of flight (TOF) scintillation counters, and the array of anticoincidence counters (ACCs), transition radiation detector (TRD), a ring imaging Cerenkov detector (RICH), and an electromagnetic calorimeter (ECAL) were the tools and equipment which used in this measurement. An accurate measurement of the electron and positron energy E and of the shower shape has been made by three-dimensional imaging capability of the 17 radiation length ECAL. The proton flux's precise measurement in primary cosmic rays is established based on 300 million of events. It has been covered with the rigidity (momentum/charge) from 1 GV to 1.8 TV. Due to our initial calculation capability, we have chosen upper limit of total proton flux by 200 GeV. Then from 20GeV to 200GeV energy range of proton flux data in Low earth Orbit was taken from AMS, corresponding around 400km altitude and its fitted function derived as well.

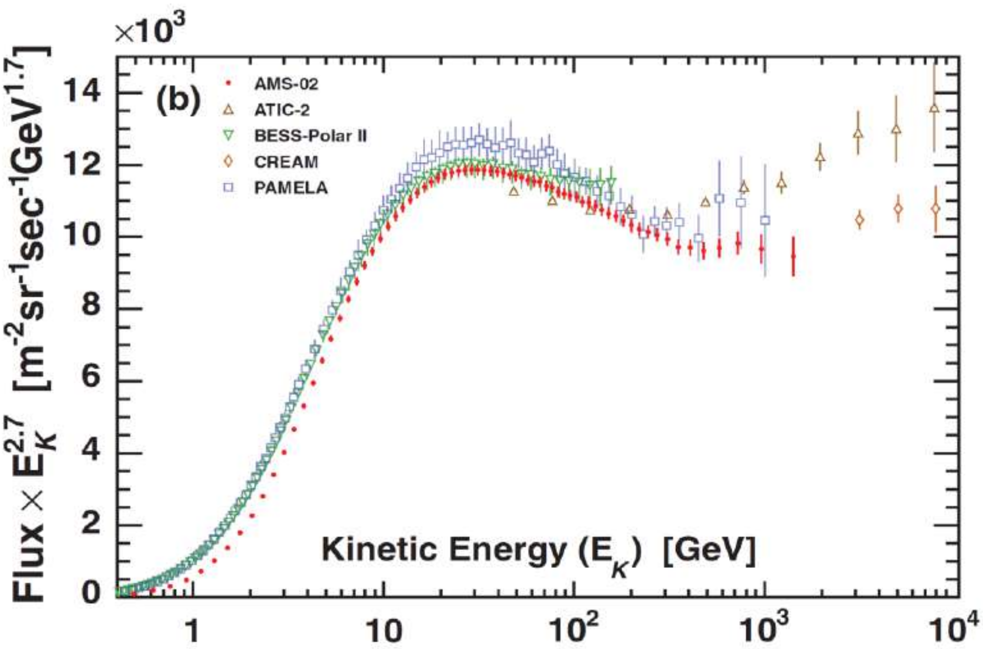


Fig. 4-5 The AMS measured proton flux as a function of kinetic energy $E_K$ as multiplied by $E^{2.7}_K$ compared with recent measurements [**18**]

These three set of data were used to fitting functions for calculation when early study. After that some our paper used PAMELA and STE-QUEST space missions' proton flux data [**26**] [**31**].

### 4.2. Energy deposition probability function

This section purpose is to derive probability function of charge generation $\Phi_{Ep}^{300}(Q)$ with depending energetic proton flux as shown in Fig. 4-6 .

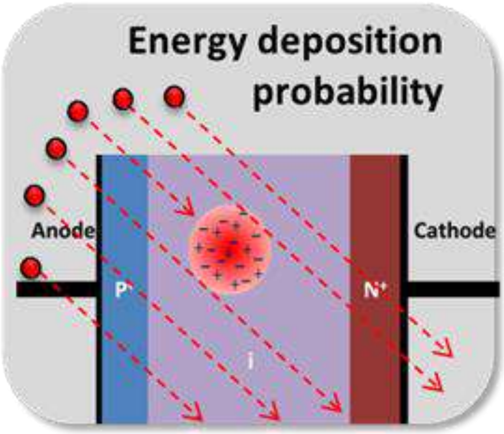


Fig. 4-6 Probability function of charge generation $\Phi_{Ep}^{300}(Q)$ by energetic proton.

We assumed that, deposited energies form protons to the silicon completely generate electron-hole pairs. On the other hand amount of generated charge linearly depends of deposited energy. Pair generation energy depends on the medium band gap energy. The energy $W(E_g)$ required to create an e-h pair in a semiconductor by a charged mass particle traversing the medium depends on the band gap energy $Eg$ of the material and hence, although only slightly, on the temperature. The measurements of this quantity show a nearly linear dependence on the band gap energy, and the linear fit to the data obtained for different materials gives Eq. 4-3.

$$W(Eg) = 1.76\text{ eV} + 1.84Eg\text{ eV}$$

Eq. 4-3 Required energy to generate a hole-electron pair in the silicon

The mean energy $W(Eg)$ to create an electron-hole pair has been calculated and measured in experiments including high energy charged particles. The mean energy $W(Eg)$ required to create an e-h pair in silicon is $W(Eg) \approx 3.68$ eV. The pair charge is $e=1.6*10^{-19}$ coulomb [**32**]. Hence coefficient $\alpha=2.33\times10^{13}$MeV/C, which shows relation between deposited energy and generated charge has been found.

In order to define proton cross section, literature study was used [**27**] [**28**]. In this that referenced paper, the modelling of proton single event phenomena cross-sections versus proton kinetic energies is based on the fact that secondary recoils induced by proton Silicon nuclear reactions are mainly responsible for the devices destruction. The proton energy loss in matter is too low (several keV/pm) to generate Single Event burnout directly. The secondary recoil energies, ranging from several keV to several MeV, are comparable to the energies lost by primary heavy ions crossing the devices. The referenced model, developed to define proton cross section in silicon, assumes that the semiconductor element will react similarly as long as the amount of energy $E_d$ is provided by a proton Silicon nuclear reaction or by an energetic heavy ion.

Basic idea of referenced paper is that proton cross section can be defined by heavy ion cross section which developed before in several studies. Using this study result, we can obtain proton energy deposition probability function $\Phi_{x,E_p}(E_d)$. The heavy ion $LET$ corresponds to exact energy deposition to the device $E_d$ (here $E_d$ = LET x device sensitive thickness). When the sensitivity of a component is well characterized as a function of incident heavy ion LET which depends on heavy ion cross section, the device's sensitivity can be expressed versus $E_d(\sigma_{IL}(E_d)$. Convoluting the probability function of $E_d$ from the secondary recoils $x$, $E_p$ $(E_d)$ with the heavy ion cross-section curve $\sigma_{IL}(E_d)$calculated for one incident proton energy $E_p$ gives the proton single event error cross section of the device at $E_p$ as shown in Eq. 4-4, Fig. 4-7.

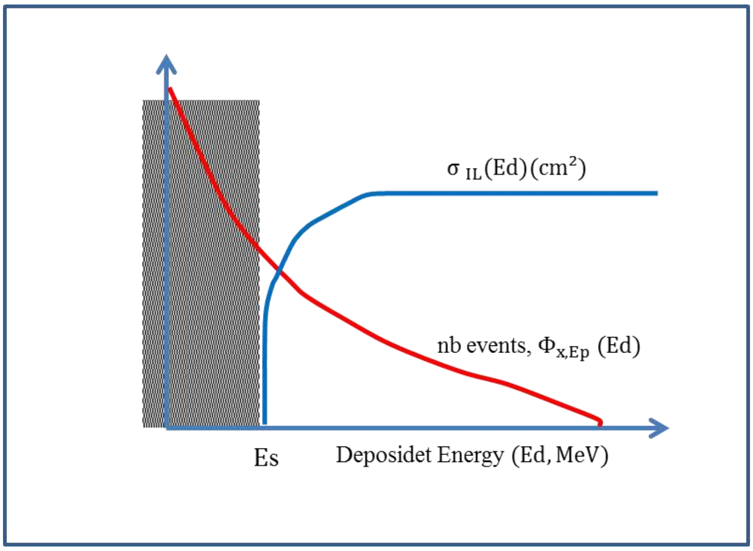


Fig. 4-7 $\Phi_{x,Ep}(E_d)$ and $\sigma(E_d)$ : the hatched area hides the part of $\Phi_{x,Ep}(E_d)$ which is not taken into account in the convolution

$$\sigma_p(E_p) = \int_{E_s}^{E_p} \sigma_{IL}(E_d)\Phi_{x,E_p}(E_d)\, dE_d$$

Eq. 4-4 Proton single event effect cross section of the device at $E_p$

The existing study defined probability function of energy deposition based on HETC calculation as shown in Eq. 4-5 [**27**] [**28**] [**29**] [**30**].

$$\Phi_{E_p}^{x}(E_d) = 10^{a_1(E_p^x)E_d + a_0(E_p^x)} + 10^{b_1(E_p^x)E_d + b_0(E_p^x)}$$

$$\Phi_{E_p}^{x}(E_d) = \Phi_1(E_d) + \Phi_2(E_d)$$

Eq. 4-5 Probability function of energy deposition based on HETC calculation

Here:

$E_d$ - Deposited energy [MeV]

$x$ - Sensitive thickness [μm]

$\Phi_1$ - Probability function for low energy deposition [$MeV^{-1}$]

$\Phi_2$ - Probability function for high energy deposition [$MeV^{-1}$]

$b_1$ - Parameter according to high energy deposition

$b_0$ - Parameter according to probability

Basically, we can say that energy deposition function consists of two decreasing exponential functions and $\Phi_1$ correspond to $E_d$ < 2 MeV energy of particles, $\Phi_2$ correspond to higher energy of particles [**27**]. In our calculation $\Phi_2$ is important, and then $\Phi_1$ omitted. Then we can have Eq. 4-6. If we define compound and shape of energy deposition probability by proton flux and silicon interactions, we can make $\Phi_{x,E_p}(E_d)$.

$$\Phi_{E_p}^{x}(E_d) = 10^{b_1(E_p^x)E_d + b_0(E_p^x)}$$

Eq. 4-6 Probability function of energy deposition from proton flux to silicon material

That neglecting is related to the method of evaluating deposited energy. Secondary protons were neglected in the total result for the all nuclear reaction cases. Their withdrawn energy after collision usually does not exceed 6 MeV that could be considered mean value. HETC is not appropriated to simulate intermediate and low proton energies such as less than 70 MeV.

As before mentioned $\Phi_1(E_d)$ represents the probability to deposit tiny amounts of energy less than 2MeV, while, $\Phi_2(E_d)$ represents the more practical assumable amounts.

Parameters $a_l$, $a_0$, $b_1$, $b_0$ provided by developed model in referenced paper depends strongly on the incident proton energies $E_p$ *(MeV)* and on the silicon thickness $x$ (µm). In order to prove that energy deposition probability function existence, this bidirectional parameter dependence is shown Fig. 4-8 for $b_1$, which represents the change of the slope corresponding high amounts of deposited energies. For insteance Fig. 4-7 shows that deposited energy spectrum at 6 µm thickness of silicon case, which represent energy deposition probability variate by incident energy.

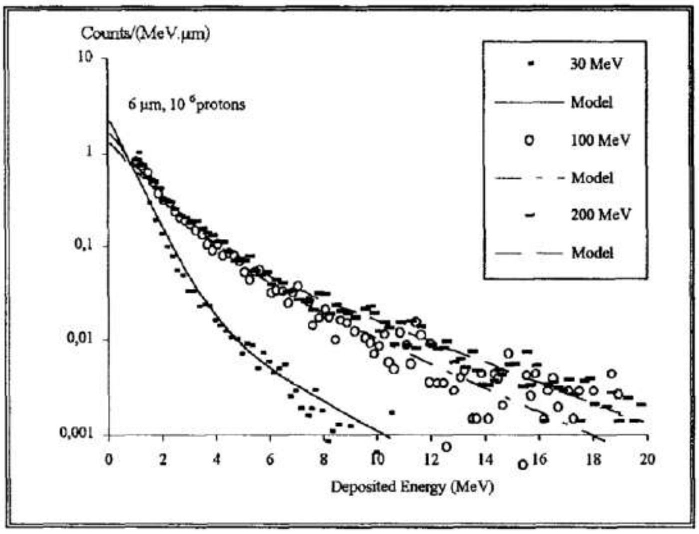


Eq. 4-7 Modeling of experimental $\mathbf{\Phi^{x}_{E_p}(E_d)}$ for various proton energies in 6 pm Si layer

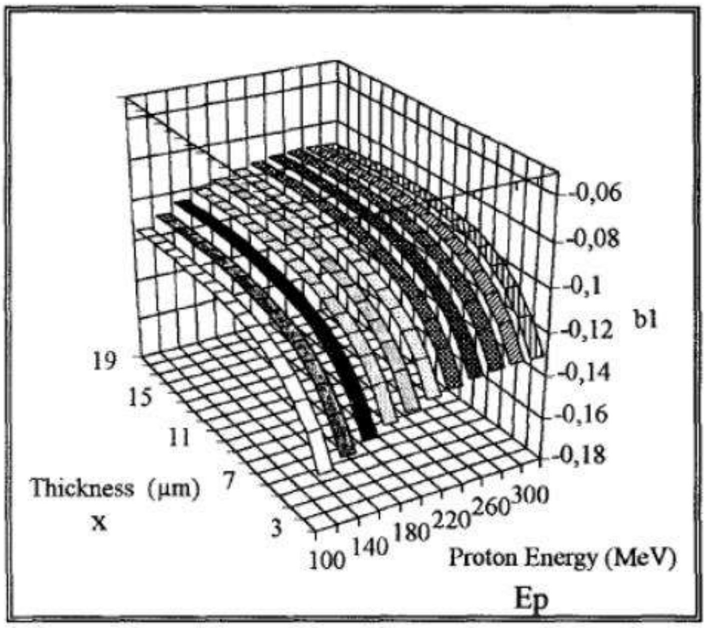


Fig. 4-8 Parametrization of $b_l$ $(E_p,x)$ [**28**]

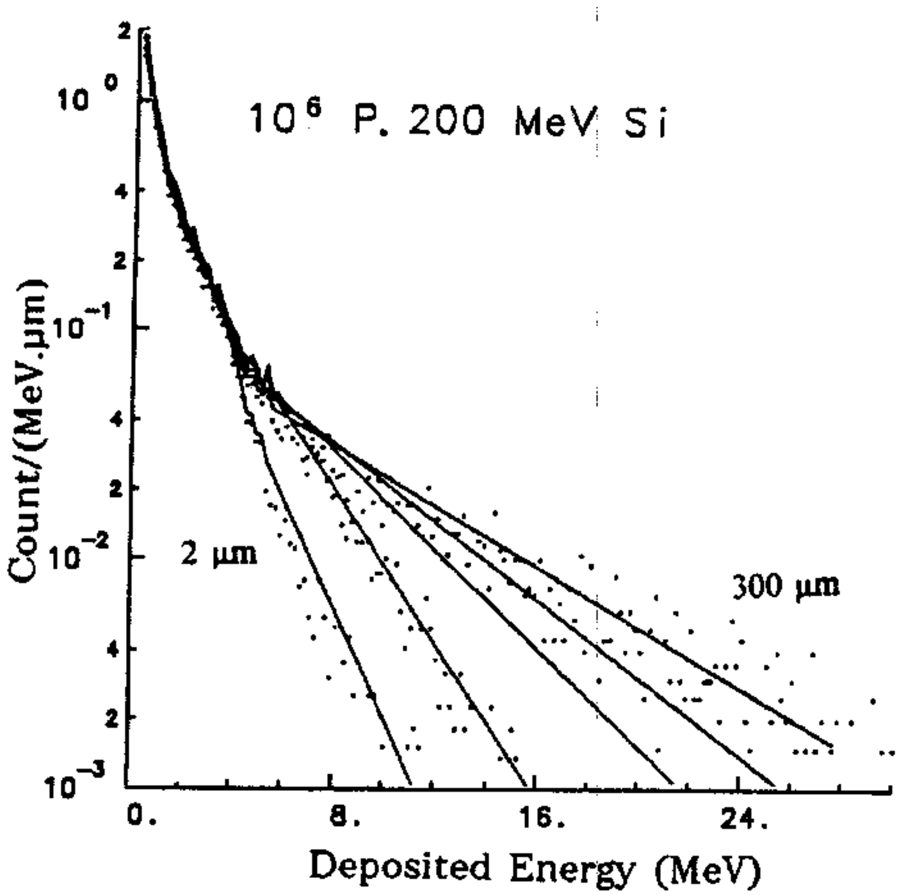


Fig. 4-9 Energy deposition probability function at various thickness of silicon under 200MeV energy of proton flux

Fig. 4-9 shows that same incident energy of proton flux gives different energy to silicon even though thickness of silicon is constant. These aspects proves bidirectional dependence of silicon's energy absorption function $\Phi_2$ which defined by two parameters.

In order to define $\Phi_2$, we need to Figure out $b_1$ and $b_0$. Parameters depend on sensitive thickness of silicon and incident energy of particles. Our model defined device thickness as around 350µm and on the other hand generally device thickness is around 300µm therefore sensitive thickness has been fixed on 300µm. Parameters $b_1$ and $b_2$ found from the paper as well [**27**].

Parameter $b_1$ at 19µm sensitive thickness defined at the paper [**28**]. By combining these data as shown in Table 4-2, fitted functions for $b_1$ and $b_0$ were obtained as shown in Fig. 4-10, Fig. 4-11.

Table 4-2 Fitting of $b_1$ and $b_0$

| Incident Energy (MeV) | $b_1$ (19um) | $b_1$ (300um) | $b_0$ (300um) | Fitted $b_1$ | Fitted $b_0$ |
|---|---|---|---|---|---|
| 100 | -0.107 | | | -0.077 | -4.481 |
| 120 | -0.105 | | | -0.076 | -4.480 |
| 140 | -0.102 | | | -0.073 | -4.477 |
| 160 | -0.1 | | | -0.072 | -4.476 |
| 180 | -0.097 | | | -0.070 | -4.474 |
| 200 | -0.095 | -0.068 | -4.472 | -0.068 | -4.472 |
| 220 | -0.094 | | | -0.068 | -4.472 |
| 240 | -0.092 | | | -0.066 | -4.470 |
| 260 | -0.09 | | | -0.065 | -4.469 |
| 280 | -0.09 | | | -0.065 | -4.469 |
| 300 | -0.09 | | | -0.065 | -4.469 |

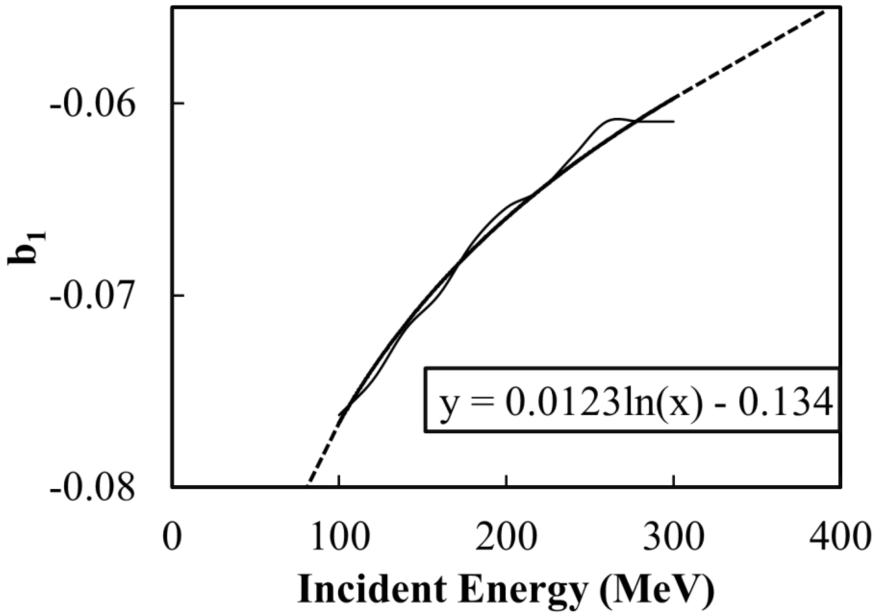


Fig. 4-10 Fitted b1 (at 300 µm Si).

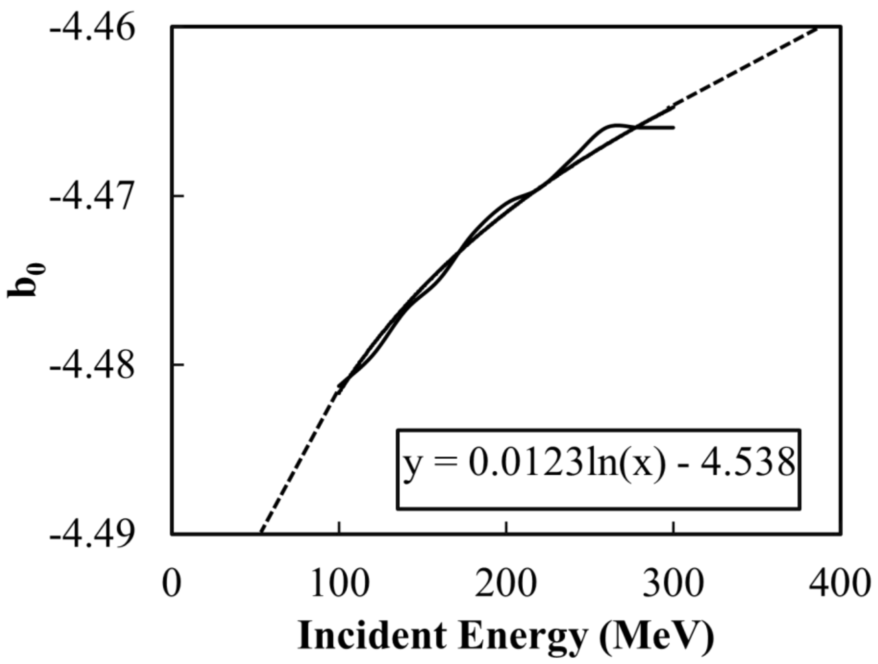


Fig. 4-11 Fitted b0 (at 300 µm Si).

Hence probability function of energy deposition $\Phi_{Ep}^{300}(E_d)$ has been defined at 300µm thickness as shown in Eq. 4-8. Here probability function defined by deposited energy, last purpose is to define probability function by generated charge. We used $\alpha$ coefficient for transition under the relation, $\Phi_{Ep}^{300}(E_d)$ to $\Phi_{Ep}^{300}(Q)$ as using expression $\Phi_{Ep}^{300}(E_d) = \Phi_{Ep}^{300}(\alpha\times Q)$. Probability function which defined by generated charge has been found as shown in Eq. 4-9.

$$\Phi_{E_p}^{300}(E_d) = 10^{b_1(E_p^x)E_d + b_0(E_p^x)}$$

Eq. 4-8 probability function of energy deposition $\Phi_{Ep}^{300}(Ed)$

$$E_d = \alpha Q_g$$

$$\Phi_{E_p}^{300}(\alpha Q) = 10^{b_1(E_p^x)\alpha Q_g + b_0(E_p^x)}$$

Eq. 4-9 Probability function which defined by generated charge

Using above relation we made transition from probability function of deposited energy $\Phi_{Ep}^{300}(E_d)$ to probability function of generated charge $\Phi_{Ep}^{300}(Q)$, and for simplicity we used same notation $\Phi_{Ep}^{300}$ for both functions.

### 4.3. T-CAD simulation to obtain charge generation in device

When high energetic particles penetrate a semiconductor device, they deposit their energy by the generation of hole–electron pairs. These charges can perturb the normal operation of the device. This chapter describes the models for T-CAD simulation to get critical charge which could lead to avalanche multiplication phenomenon. In chapter 3.2.2.2 we discussed about avalanche phenomena effect on the power diode. The deposited energy generates amount of charge that could be trigger of destruction which caused by avalanche phenomena as shown in Fig. 4-12.

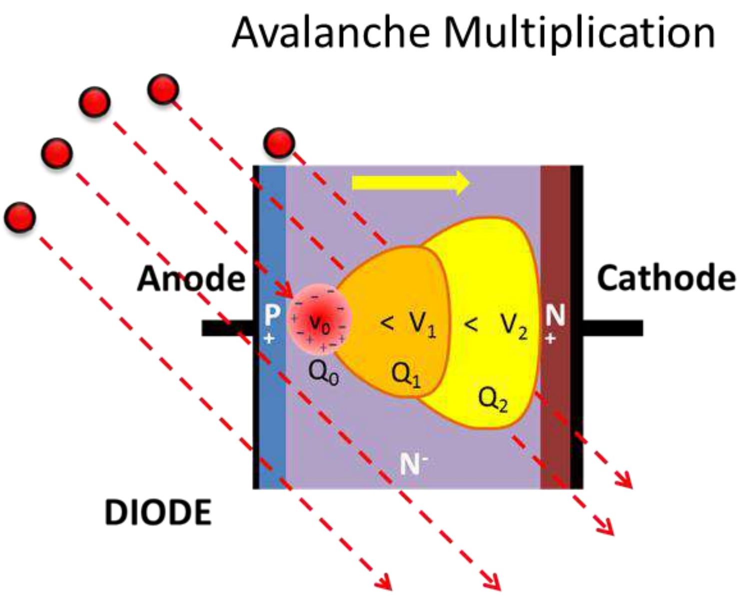


Fig. 4-12 Burnout Condition based on avalanche phenomena

Particles penetrate into the device and deposit energy, that generated charge by deposited energy expressed $Q$. Single Event Burnout failure occurs when the generated charge $Q$ exceed to a certain amount of charge, which causes avalanche phenomenon. We named it by threshold charge to destruction $Q_{dest}(V_{DC})$.

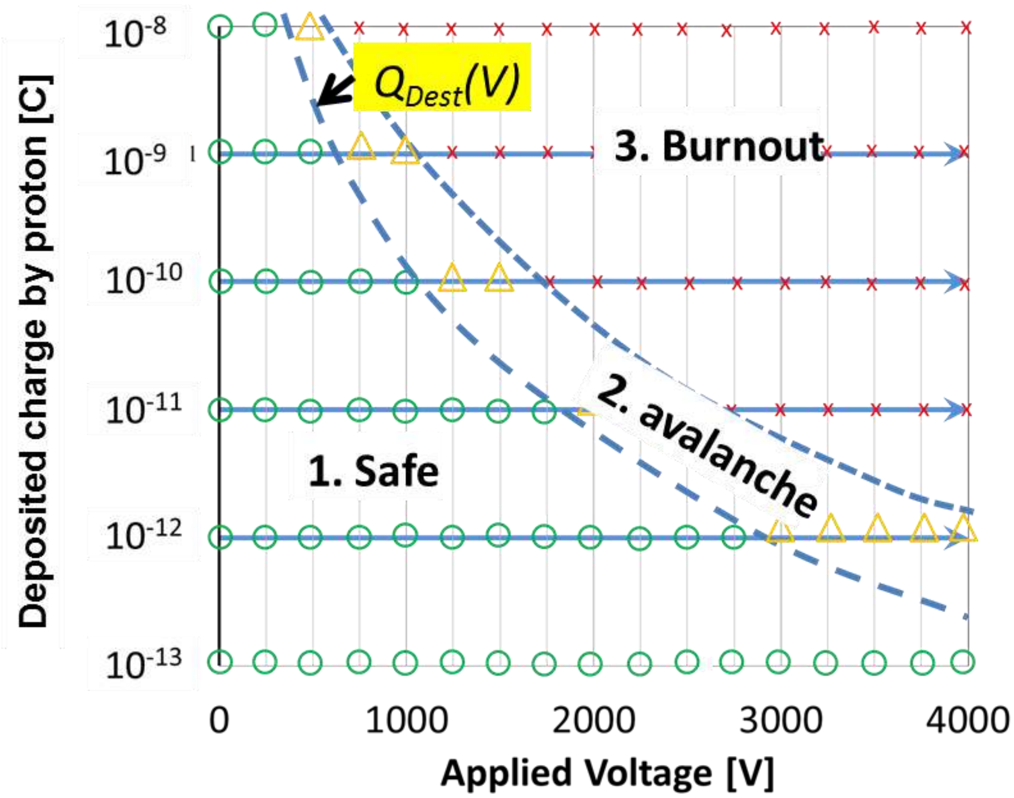


Fig. 4-13Function of threshold charge to destruction $Q_{dest}(V_{DC})$ respect to the applied voltage

Main purpose of this T-CAD simulation is to estimate function of threshold charge to destruction $Q_{dest}(V_{DC})$ respect to the applied voltage as shown in Fig. 4-13. Expected curve divides three zones which are illustrated safe zone, avalanche zone, burnout zone. $Q_{dest}(V_{DC})$ function defined by border line between safe zone and avalanche which depends on applied voltage. This was the expectation of result of simulation. Combination of charge and voltage need to be defined. Each point requires transient TCAD simulation for Avalanche phenomenon. More than 100 points needed to be simulated in order to mitigate problem of simulation time. To do that we selected PiN diode for simulation model for simplification of device structure and reduction of mesh number. PiN diode can represent other power devices as internal structure. Homogenous structure of diode makes it to be able to perform Cylindrical Simulations (Quasi-3D) instead of ordinary 3D simulation for reduction of simulation time as well.

#### 4.3.1. T-CAD simulation for charge generation function

In Combination of charge and voltage need to be defined Each point require transient TCAD simulation for Avalanche More than 100 points needed to be simulated Problem of simulation time

In order to evaluate generated charge $Q$ by energetic particle we used ionization particle model of T-CAD software. This model gives destruction function by generated charge inside semiconductor devices. When a particle penetrates a device structure, it loses energy and creates a trail of electron–hole pairs along its track. These additional electrons and holes cause the avalanche phenomena which leads to single event burnout. However, our study target is proton; it can make heavy ion as secondary recoils by hitting the Silicon atom with some probability. This probability function discussed in previous chapter. There may have misunderstood that seems like heavy ion relates to calculation formula. The calculation formula doesn't relate to the heavy ion. Heavy ion model has been used only for prediction of destruction charge generation value which leads to avalanche charge multiplication phenomenon. For modelling ionization particle in T-CAD important factors are:

- The energy and type of the particle.
- The angle of penetration of the particle.
- The relation between the lost energy and linear energy transfer (LET) and the number of pairs created.

The generation rate by the ionization particle is in most cases practiced in transient simulations. The number of hole–electron pairs generated before the initial time of the transient is added to the carrier densities at the beginning of the simulation.

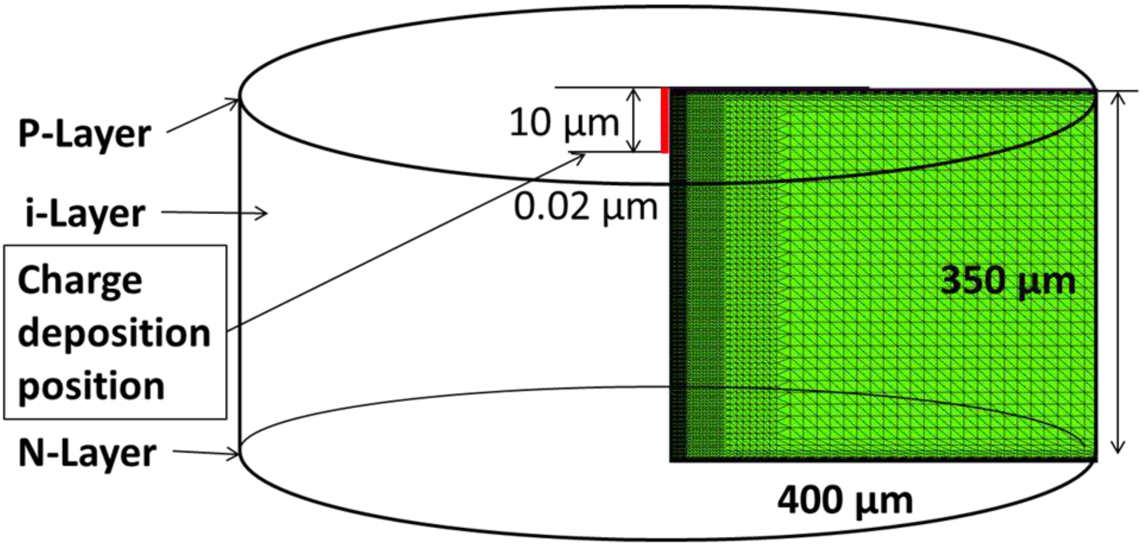


Fig. 4-14 Track of ionization particle penetration a semiconductor material; it is defined by a length and the transverse spatial influence is assumed to be symmetric about the track axis

`

A simple model for the heavy ion impinging process is shown in Fig 4-14. The generation rate caused by the heavy ion is computed by Eq. 4-10:

$$G(l,w,t) = G_{LET}(l)R(w,l)T(t)$$

Eq. 4-10 The generation rate

If $l < l$max ($l$max is the length of the track), and by $G(l,w,t) = 0$:

If $l >= l$max $*R(w)$ and $T(t)$ are functions describing the spatial and temporal variations of the generation rate. $G_{LET}(l)$ is the linear energy transfer generation density and its unit is pairs/cm$^3$.

$T(t)$ is defined as a Gaussian function as show in Eq. 4-11:

$$T(t) = \frac{2 \cdot \exp\left(-\left(\frac{t - t_0}{s_{hi}\sqrt{2}}^2\right)\right)}{\sqrt{2} \cdot s_{hi}\sqrt{\pi}\left(1 + \operatorname{erf}\left(\frac{t_0}{s_{hi}\sqrt{2}}\right)\right)}$$

Eq. 4-11 Gaussian function

Where the moment of the ionization particle penetration and $s_{hi}$ is the characteristic value of the Gaussian.

In the T-CAD simulation, 3.3 kV PiN diode model was chosen as energetic particle penetrated devices; because simple structure of PiN diode can basically represent other semiconductor power devices, as P-N junction structure and biasing. The transient simulation was performed on default value of most characteristics of model. We analysed $Q_{dest}(V_{DC})$ with 3.3-kV PiN diode in T-CAD simulation. A cylindrical structure with a 400 μm radius was used. Fig 4-15 and Fig 4-16 show that simulated diode model and meshing method of it. The structure consists of highly doped N-layer and P-layer, and lightly doped 350 μm N-base between these highly doped layers. Position of the energetic particle penetration is the centre axis of the cylindrical structure, and it is 10 μm deep from the boundary between P-layer and N-base toward N-base that path includes generated charge $Q$. The radial distribution of the generated charge was determined by a Gaussian distribution with a characteristics length of 0.02 μm.

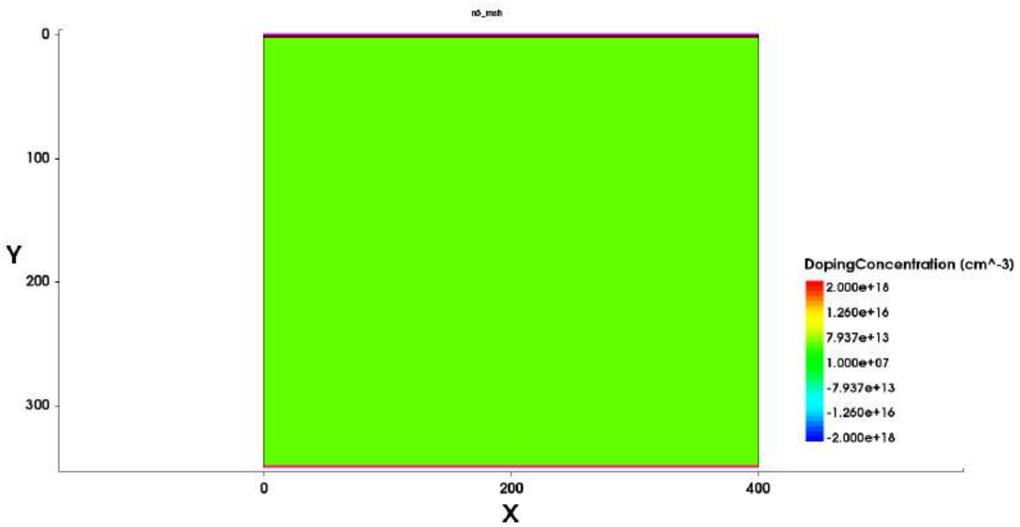


Fig. 4-15 Simulated diode model in TCAD

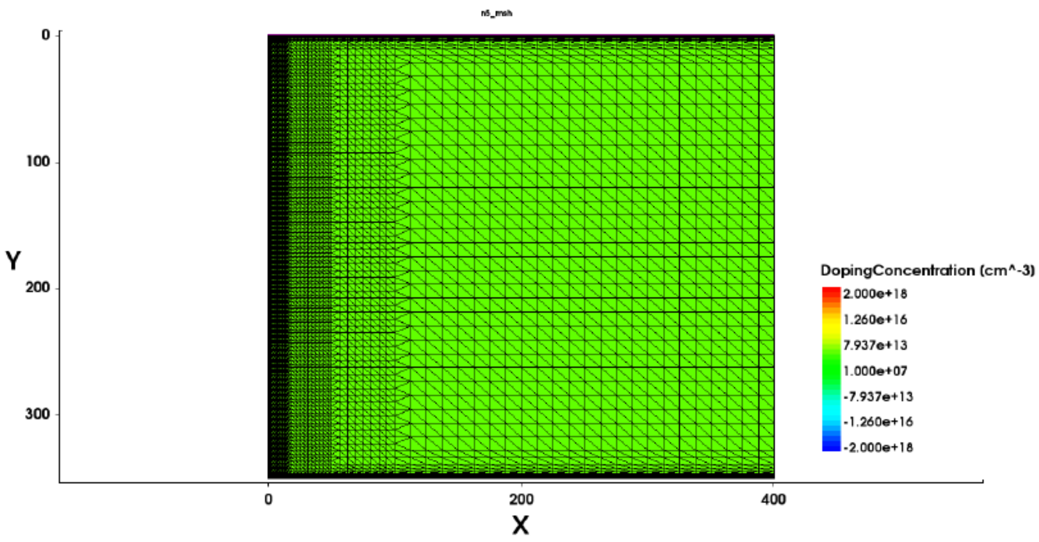


Fig. 4-16 Meshing method of simulated diode mode in TCAD

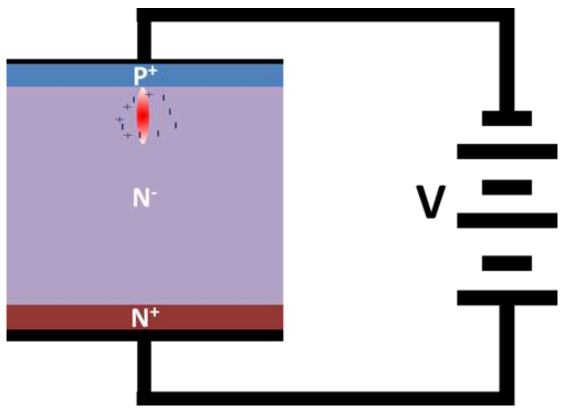


Fig. 4-17 Charge deposited 3.3 kV PiN diode model in T-CAD simulation.

As shown in Fig. 4-17, reverse biased diode, the charge generation as a function of applied voltage for different particle energy. When the generated charge $Q$ becomes larger than certain amount, then avalanche phenomenon starts. The value of generated charge $Q$ that triggers avalanche phenomenon starting was determined as the threshold charge to destruction $Q_{dest}(V_{DC})$, which has a function of the applied voltages. We obtained values of threshold charge to destruction $Q_{dest}(V_{DC})$ from three kinds of energy of particle cases (10 MeV, 50 MeV and 100 MeV).

The Fig. 4-18 shows Reverse bias Characteristics of 3.3kV PiN diode model for T-CAD simulation.

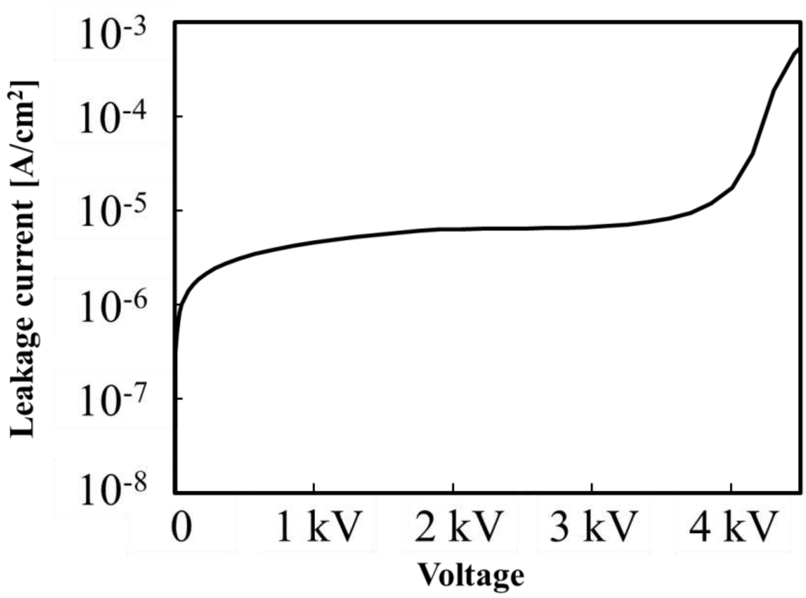


Fig. 4-18 Reverse bias Characteristics of 3.3kV PiN diode model for T-CAD simulation.

Purpose of simulation is to obtain destruction charge value prediction, which can be reason of SEU in device. When charged particles penetrate to the silicon, it generates amount electron-hole pairs, which can be trigger of avalanche phenomena in power device. It also strongly depends on applied voltage [**12**]. However heavy ion model were used for this simulation, it can gives properly destruction charge value function. Because avalanche phenomena can be occur as long as charge generates by any charged particles inside silicon. No matter ionization particle is either heavy ion or proton.

Defined PiN diode model with injected ionization particle is shown in Fig. 4-19 – Fig. 4-22. This is simultaneously with initial charge injected moment cases appearance. Initial charge injection distribution is respected by Gaussian distribution. The length of initial injected charge is chosen 10 µm. However in the reality ionization track can reach up to 350 um. It is assumed as diode thickness. We can see here that charge injection's starting point is almost in top boundary line of the diode. This boundary is corresponded to highest electric field region along to the diode body.

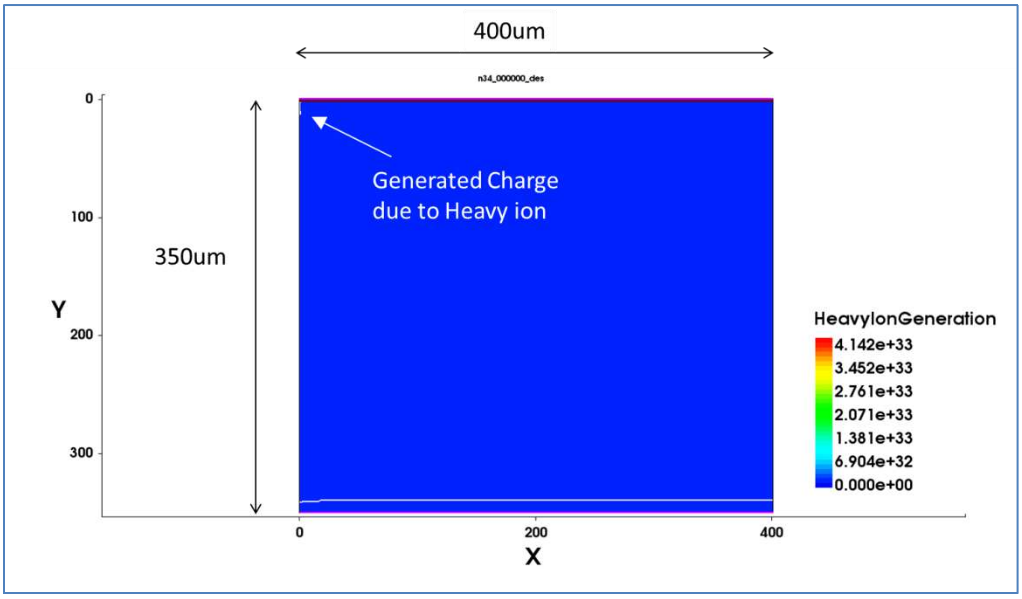


Fig. 4-19 Main model appearance of cylindrical model of PiN diode simulation on T-CAD

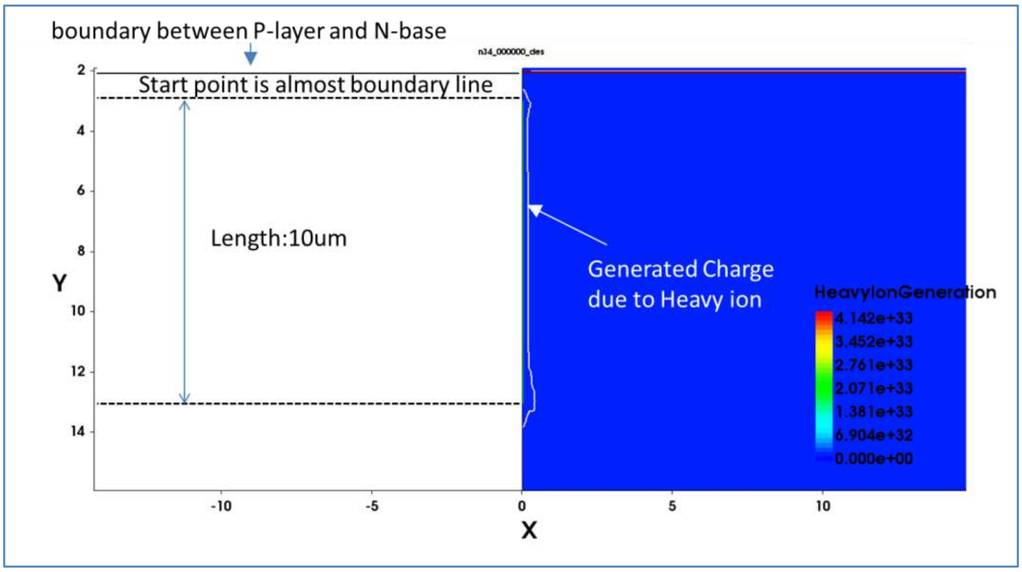


Fig. 4-20 Total length of ionization particle track is 10μm starting position is just below P-layer.

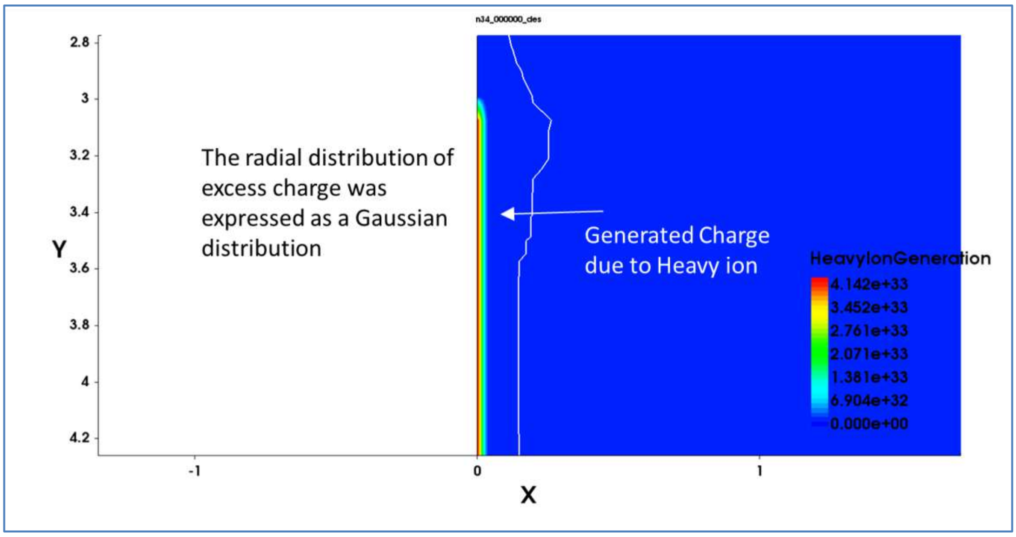


Fig. 4-21 The radial distribution of excess charge was not uniform it was expressed as a Gaussian distribution. Center of ionization particle injection is highest charge concentrated place.

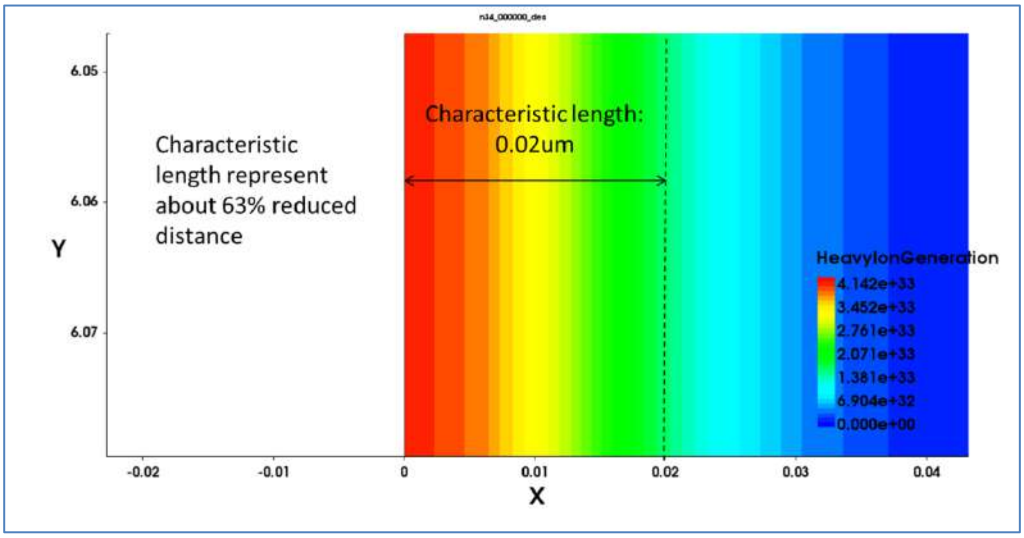


Fig. 4-22 Characteristic length represent about 63% reduced distance at Expanded width view

In order to have sufficient values to make function of destruction charge, we did several different input of simulations. Among them we have chosen 10 MeV, 50 MeV and 100 MeV energy of heavy injection simulation. Table 4-3 shows main input parameters of ionization particle model.

Table 4-3 Main input parameters of ionization particle model

| E (MeV) | LET (pairs/cm3) | Q(C) |
|---|---|---|
| 10 | $2.16\text{x}10^{20}$ | $4.35\ \text{x}10^{-13}$ |
| 50 | $1.08\ \text{x}10^{21}$ | $2.18\ \text{x}10^{-12}$ |
| 100 | $2.16\ \text{x}10^{21}$ | $4.35\ \text{x}10^{-12}$ |

Here LET represents the possible charge generation amount which means that how much charge can be generated by deposited energy from ionization particle. Calculation was made through Eq. 4-12 and Eq. 4-13.

$$Q = q \int_0^\infty LET \cdot e^{\left(\frac{r}{w_t}^2\right)} \cdot 2\,\pi hr\, dr$$

Eq. 4-12 Charge generation calculation equation

$$E = \alpha Q$$

Eq. 4-13 Deposited energy conversion to generated charge

Here:

q – Elementary charge [$1.6 \times 10^{-19}$ C]

r – Radius of ion track [cm]

h – Length of ion track [$10 \times 10^{-4}$cm]

$w_t$ – characteristic width of track [$2 \times 10^{-6}$cm]

E – Incident energy of ion

Hence, LET was calculated by Eq. 4-14

$$LET = \frac{Q}{q \cdot \pi h \cdot {w_t}^2}$$

Eq. 4-14 LET calculation formula for ionization particle model of T-CAD simulation.

After simulation values of charge generations by diverse energy of ionization particle case were obtained from simulation as described result section of this dissertation. Generated charge should obtained by integrating generated charges values from cathode current curves which shown in Fig. 4-23. Here we can see that current curve area, generated charge, relatively increased by applied voltage. Depending on initial injected charge, curve area is defined. At the same time it also depends on applied voltage. In this certain example, burn out occurred when applied voltage reaches 4kV. The main target to find out is the threshold charge value which can be trigger of single event burnout. Basically this phenomena duration is from several hundred picoseconds to several decades of nanoseconds.

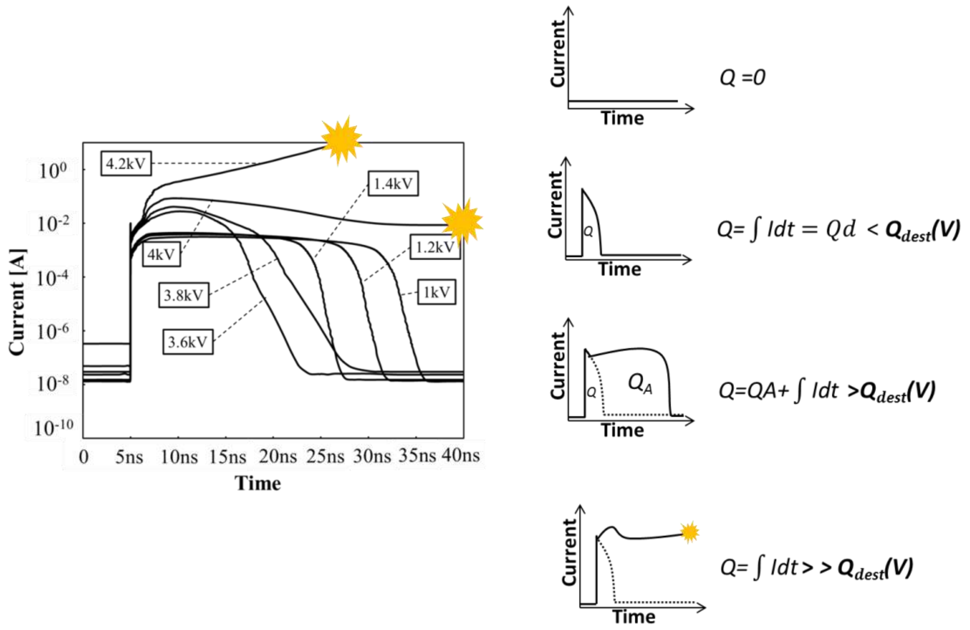


Fig. 4-23 Current waveform through PiN diode after charge depositing to inside the device.

The current generated by avalanched charge has aspects that either continues or stoppable. There is threshold charge value for destruction. Hence we can say that burnout condition is depends on how much charge generated by deposited energy inside of the silicon devices. Burnout condition and charge relation is illustrated in Fig. 4-24.

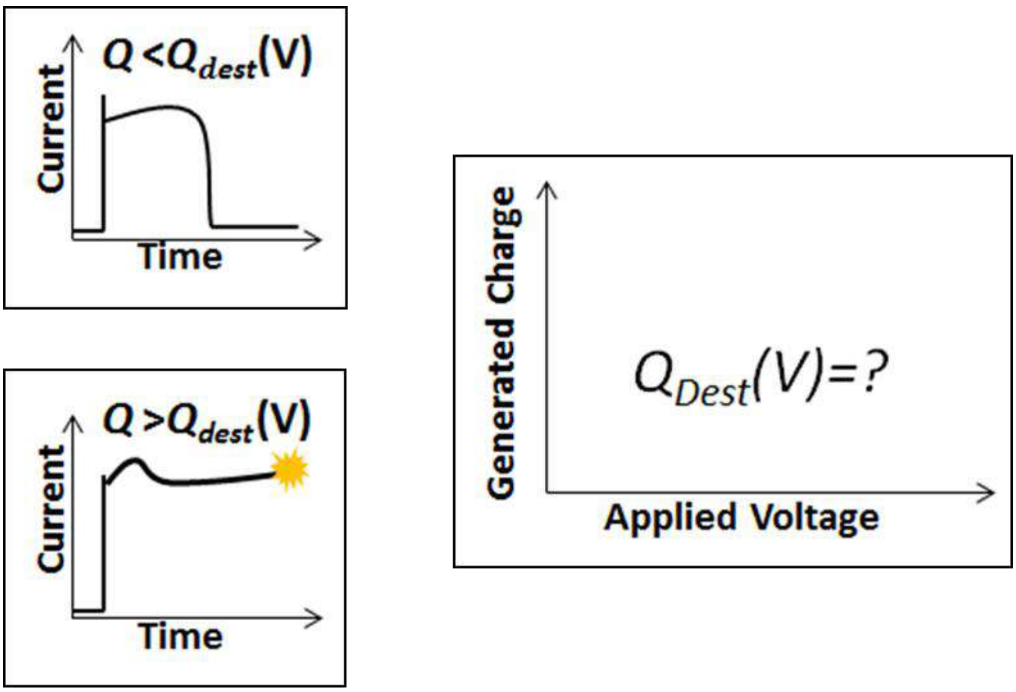


Fig. 4-24 Burnout condition and charge relation

The values of generated charge and applied voltage depending should be obtained from T-CAD transient simulation and then charge generation as a function of applied voltage for different LET by ionization particle in 3.3kV PiN diode should be predicted and it is shown in Fig. 4-25.

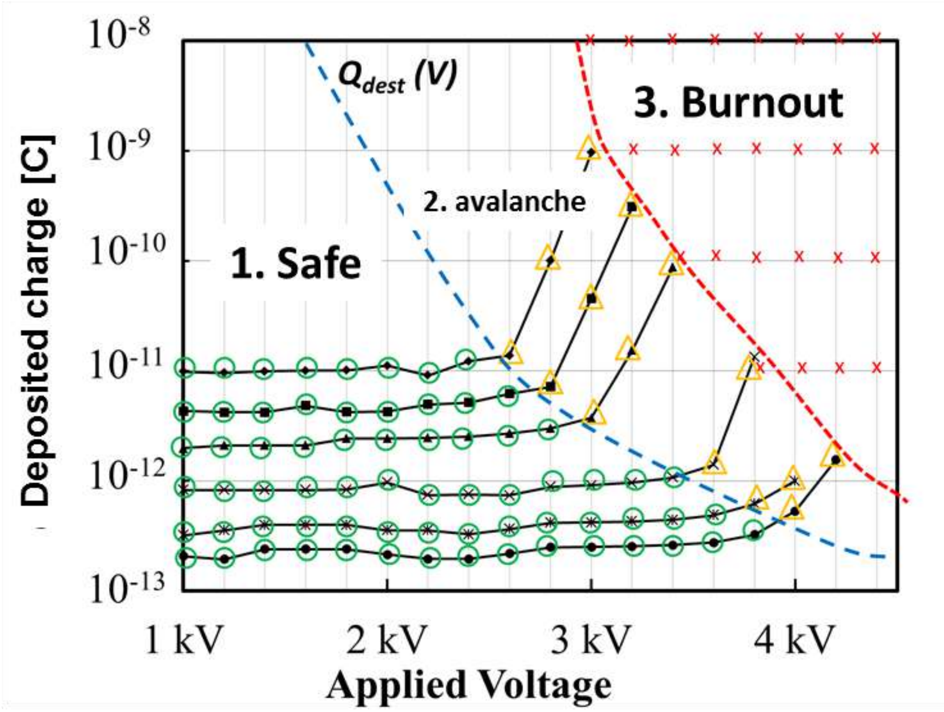


Fig. 4-25 Prediction of charge generation as a function of applied voltage for different LET by ionization particle in 3.3kV PiN diode

On this plotted prediction for destruction charge, 102 points simulation has been made. Green circles represent safe zone of generated charge and applied voltage. When deposited energy increases then generated charge will be increase. As we can see here, generated charge suddenly increases along applied voltage. That means avalanche phenomena occurred there. In this case that certain amount of basic charge at bending point of graph becomes destruction charges. Along the bending points of several curves, several points can be obtained. Those points depend on the applied voltage can be the function of the destruction charge which is shown in the Fig. 4-24 as blue dashed line.

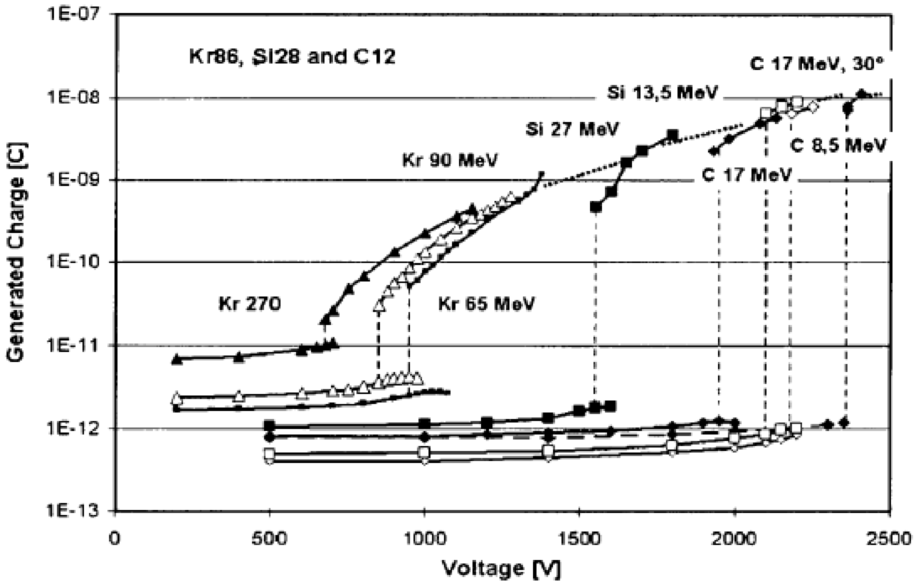


Fig. 4-26 Generated charge versus applied voltage simulations [**33**]

From here we can gather destruction charge values which can be trigger of avalanche phenomena. Based on these results, fitting function for destruction charge and applied voltage dependence were built. Value of this function written as $Q_{dest}(V)$ in main formula. It should be fitted the literature result for instance Fig. 4-26 [**33**]. From the prediction and existing data, we can see that charge multiplication immediately increased when voltage reaches certain values. In this case, charge value of base line of the curve is assumed for the destruction charge value on that corresponded voltage value. For example, on Fig. 21, charge value assumed $10^{-11}$ C, when voltage is corresponded to approximately 2.6kV. As this methodology, destruction charge function of applied voltage can be obtained from TCAD simulation. Result will be shown in the next chapter 5.

## 5. RESULTS

Basically result consists of five sections. First result is probability function fitting result. Second is T-CAD simulation result which was purposed to evaluate charge generation inside device by ionization particle injection. Third result is the fitted proton flux function. Fourth result is the Cross section calculation depended on applied voltage based on formula calculation. Fifth one is failure rate calculated by proposed formula. Using these results we can have conclusion for this particular study.

### 5.1. Probability Function fitting result

From the literature, that says high energetic proton and neutron's energy deposition is almost same [**34**]. At the 300 um silicon case, energy deposition of 20 MeV, 50MeV and 100MeV of flux is shown in the literature as well. Fig. 5-1 shows that plot energy deposition which generated charge inside silicon. Here we can see that from after 300MeV of particle energy deposition saturates

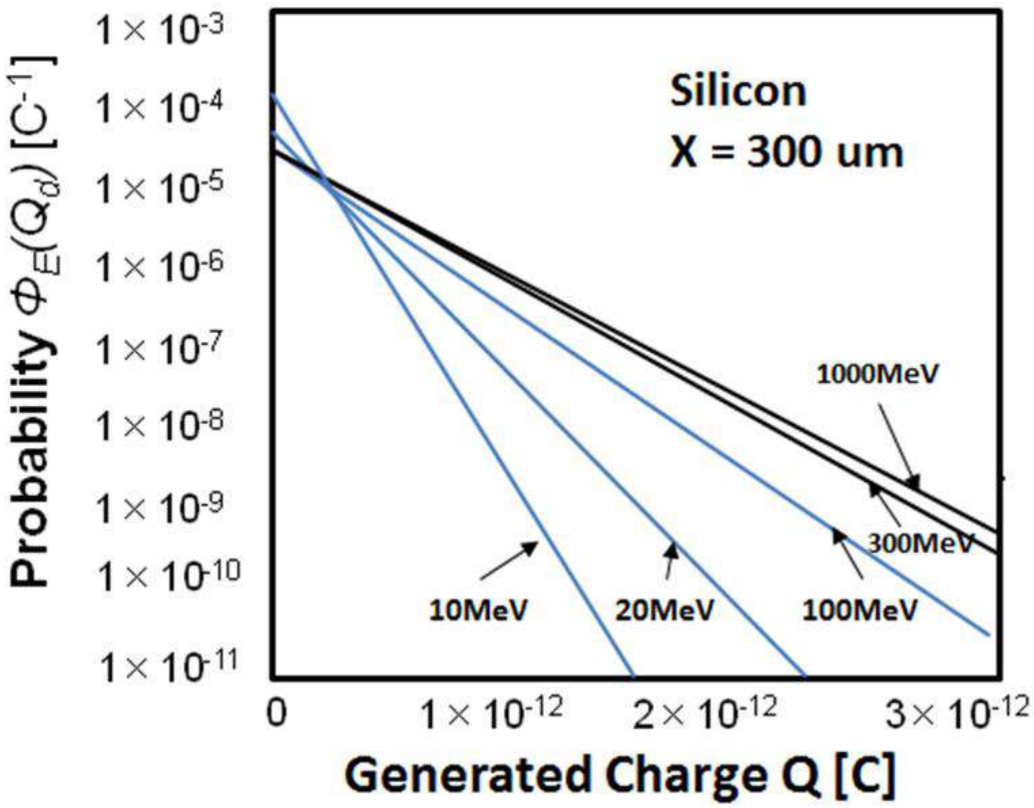


Fig. 5-1 Probability function for deposited charge $\Phi_{Ep}(Q_d)$ for $10^6$ particles.

Then from the plot we can fit the $b_1$ and $b_0$ parameters as shown in Fig. 5-2. After that by fitting dots to continue curve, we can have mathematical expression for the parameters and charge generation function. The expressions are shown in the Eq. 5-1 and Eq. 5-2.

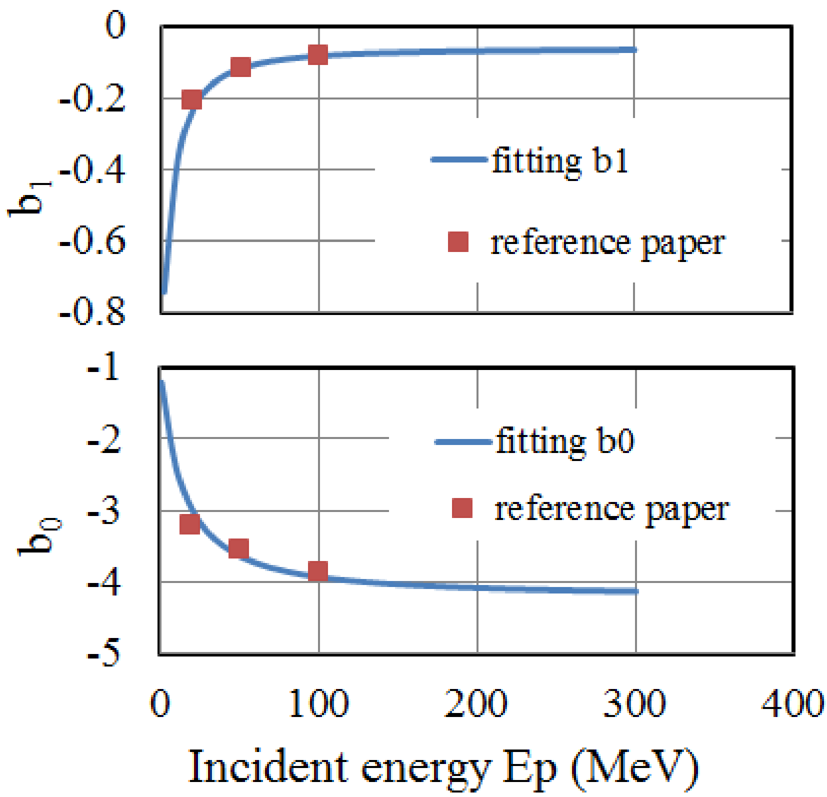


Fig. 5-2 Fitted b1 and b0 parameters

$$b_1(300, E_p) = \frac{-100}{(E_p + 15)^{1.8}} - 0.063$$

Eq. 5-1Fitted function for b1 parameter at 300 um thickness of silicon case

$$b_0(300, E_p) = \frac{200}{(E_p + 20)^{1.38}} - 4.2$$

Eq. 5-2 Fitted function for b1 parameter at 300 um thickness of silicon case

$$\Phi_{E_p}^{300}(Q) = 10^{\frac{-100}{(E_p+15)^{1.8}}-0.063+\frac{200}{(E_p+20)^{1.38}}-4.2}$$

Eq. 5-3 Charge generation probability function which depends on incident energy of the proton

## 5.2. T-CAD simulation result

In the T-CAD simulation, as before mentioned, 3.3 kV of PiN diode model was used for ionization particle injection simulation. The Electron current density distribution was shown in from Fig. 5-3 to Fig. 5-6 after 250ps 100MeV of ionization particle injection when applied voltage was varied. Here we can see that, electron density and amount proportionally increases to the applied voltage. If high voltage applies, more charge carrier is generated. Electron density is higher in the near region to place where ionization particle injected. In our simulation, worst sensitive region, upper side of the diode, was selected to ionization particle injection place. In the electric field simulation, it was observed that ionization particle injection place is at the highest electric field region. It makes to easy simulate worst condition of the operation of diode.

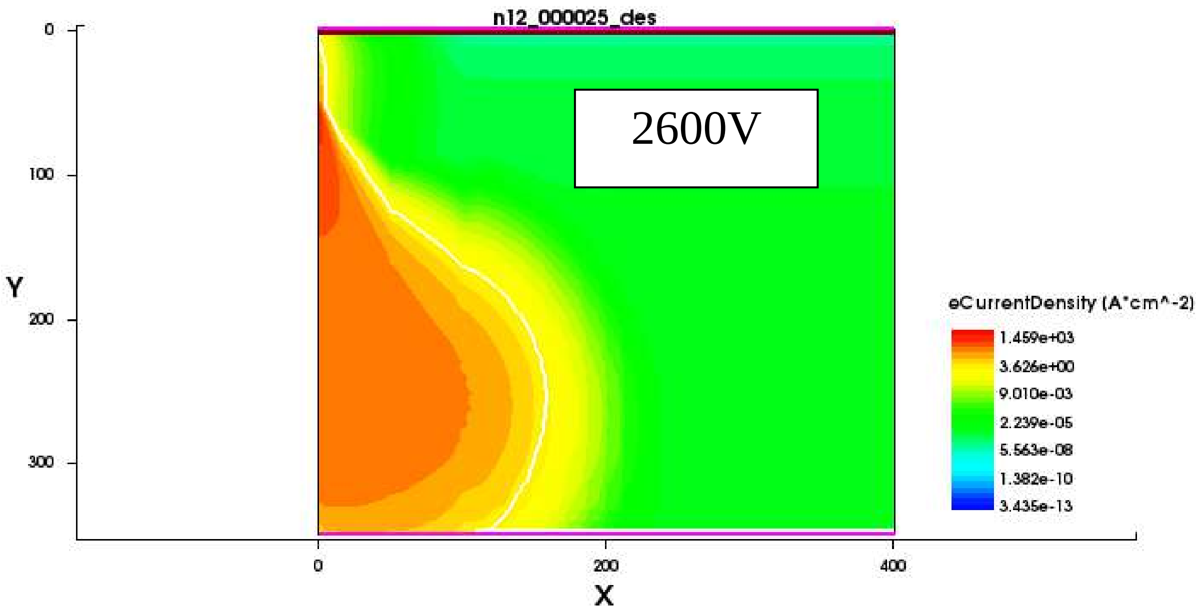


Fig. 5-3 Electron current density distribution after 250ps 100MeV of ionization particle injection when applied voltage was 2600V

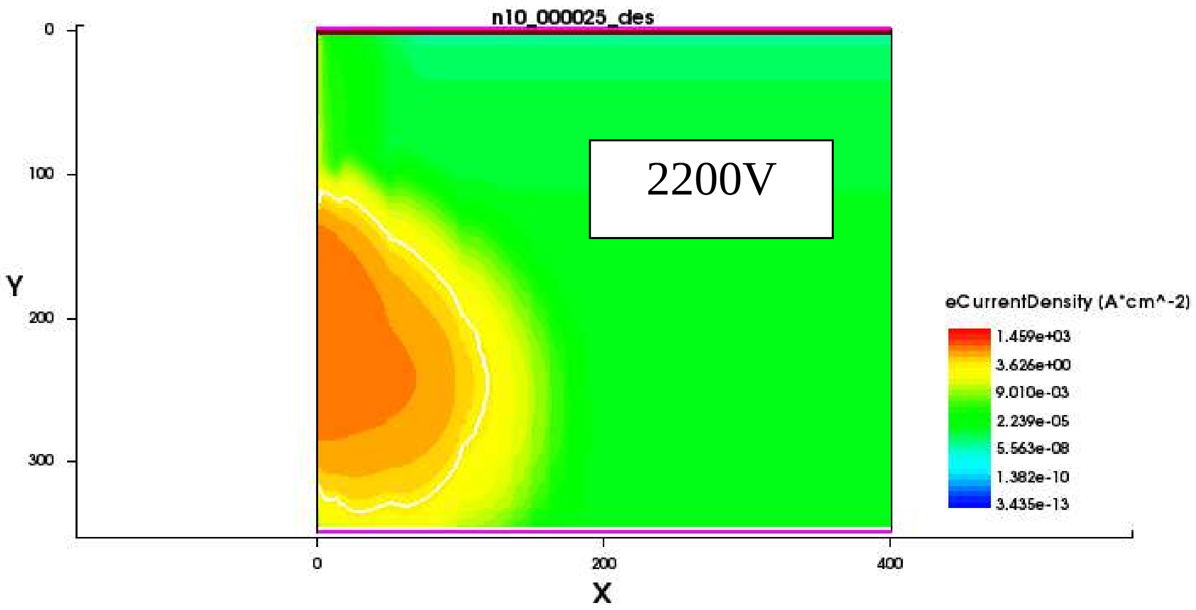


Fig. 5-4 Electron current density distribution after 250ps 100MeV of heavy ion injection when applied voltage was 2200V

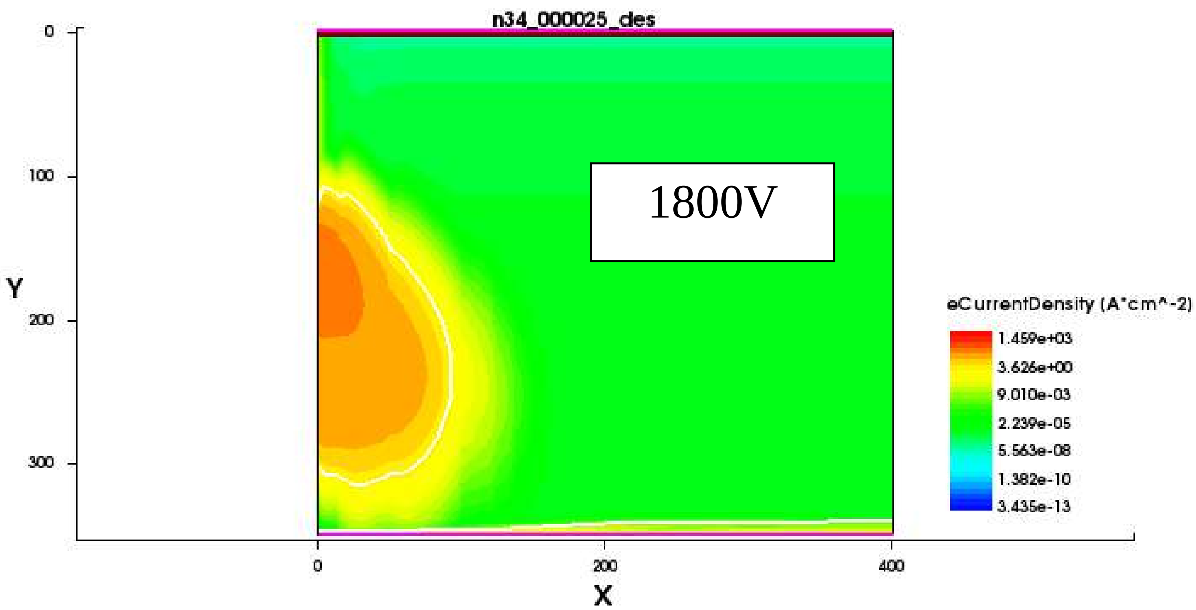


Fig. 5-5 Electron current density distribution after 250ps 100MeV of ionization particle injection when applied voltage was 1800V

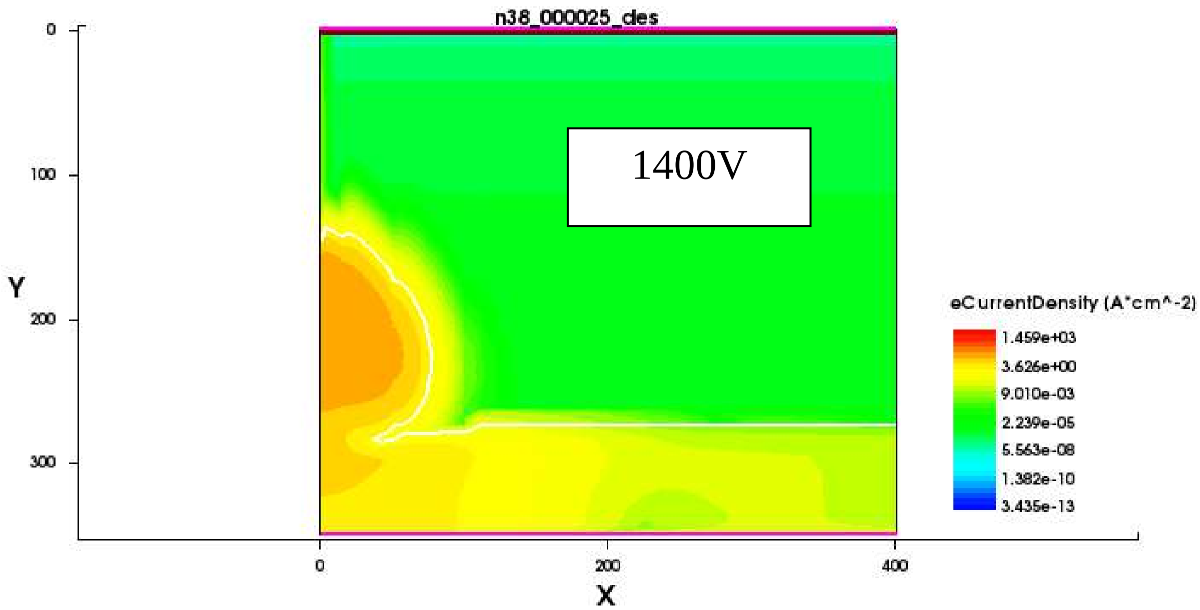


Fig. 5-6 Electron current density distribution after 250ps 100MeV of ionization particle injection when applied voltage was 1400V

After electron density distribution evaluating, Electric filed changes were analyzed under case of 1000V, 2000V and 3000V as shown in from Fig. 5-7 to Fig. 5-9. Here, time moments steady state and after 0ps, 10ps, 20ps of 100MeV energy of ionization particle injection. Red graph represent electric field at the moment of 0ps, green graph represent electric field at the moment of 10 ps, dark blue graph represent electric field at the moment of 20ps and bright blue graph represent electric field at the steady state. In order to understand phenomena inside power device by time step, Table 5-1 to Table 5-4 shows that electron current density dispersiing inside diode at the variation of voltages.

Table 5-1Electron current density inside device after charge injection by time distribution at 1400V of applied voltage case

| Captured Time of Electron current Density | Applied Volatage = 1400V |
|---|---|
| t= 0 ps | 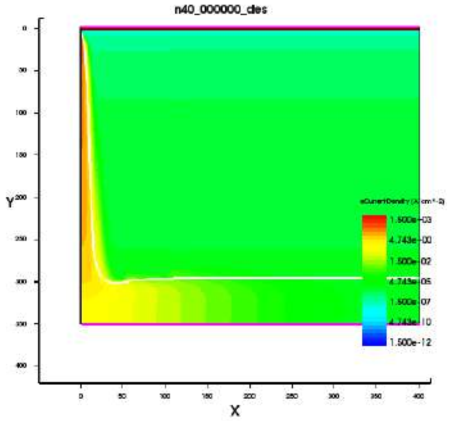 |
| t= 100 ps | 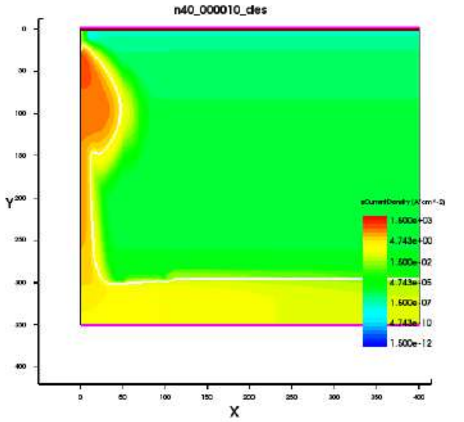 |
| t= 200 ps | 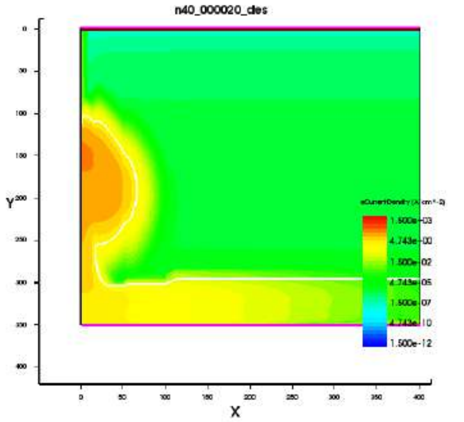 |

| | |
|---|---|
| t= 250 ps | 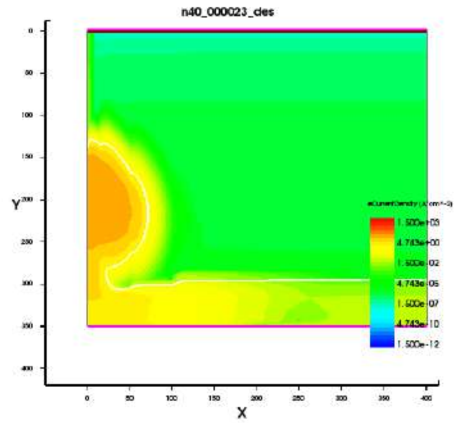 |
| t= 270 ps | 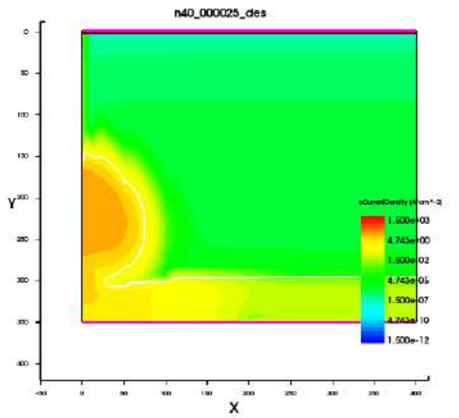 |
| t= 280 ps | 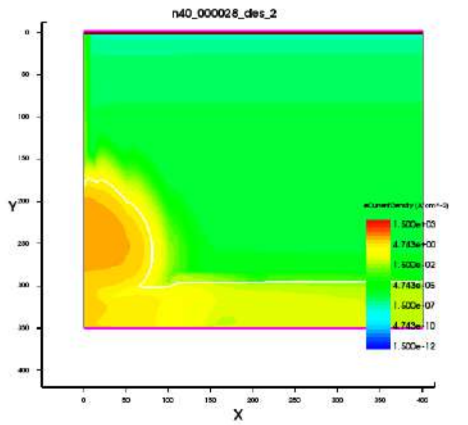 |

Table 5-2 Electron current density inside device after charge injection by time distribution at 1800V of applied voltage case

| Captured Time of Electron current Density | Applied Volatage = 1800V |
|---|---|
| t= 0 ps | 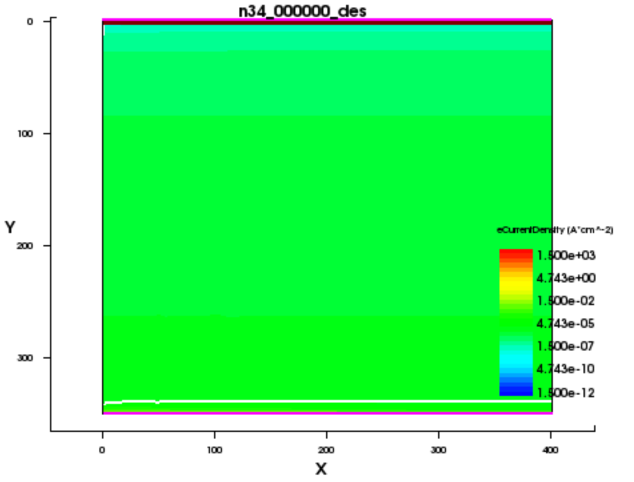 |
| t= 100 ps | 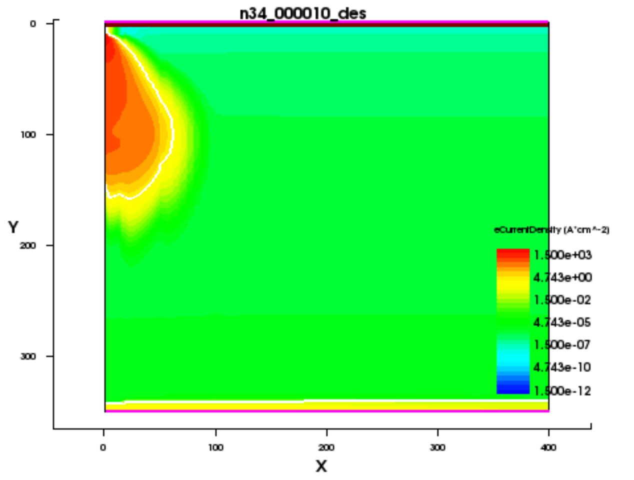 |
| t= 200 ps | 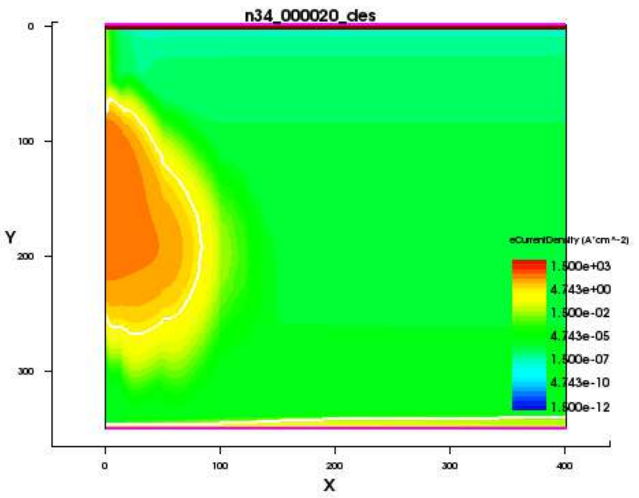 |

| | |
|---|---|
| t= 250 ps | 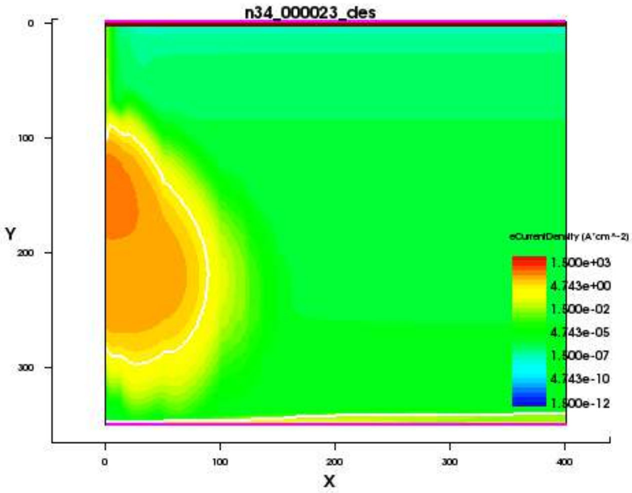 |
| t= 270 ps | 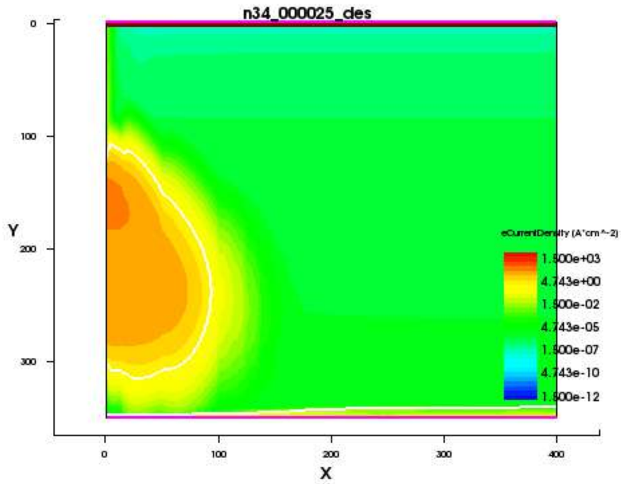 |
| t= 280 ps | 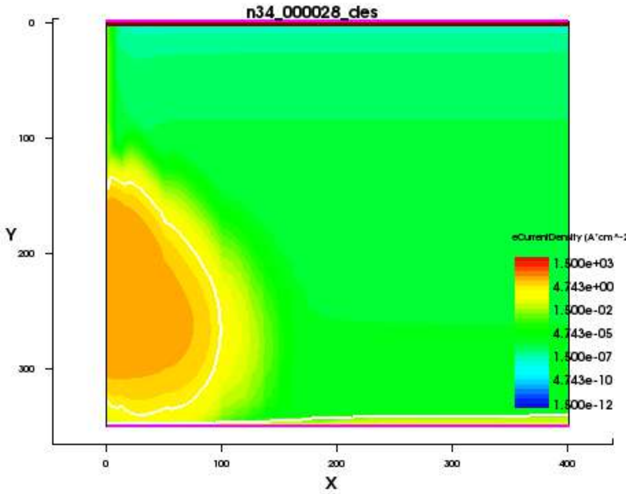 |

Table 5-3 Electron current density inside device after charge injection by time distribution at 2200V of applied voltage case

| Captured Time of Electron current Density | Applied Volatage = 2200V |
| --- | --- |
| t= 0 ps | 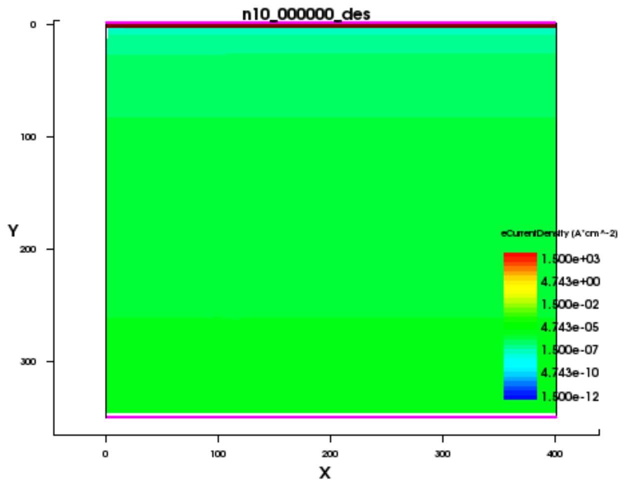 |
| t= 100 ps | 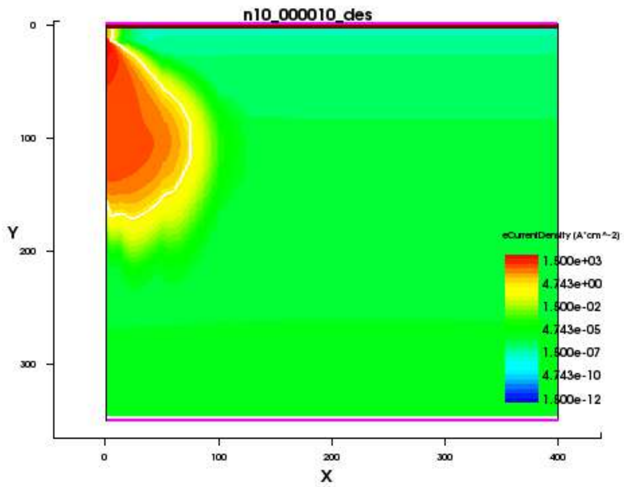 |
| t= 200 ps | 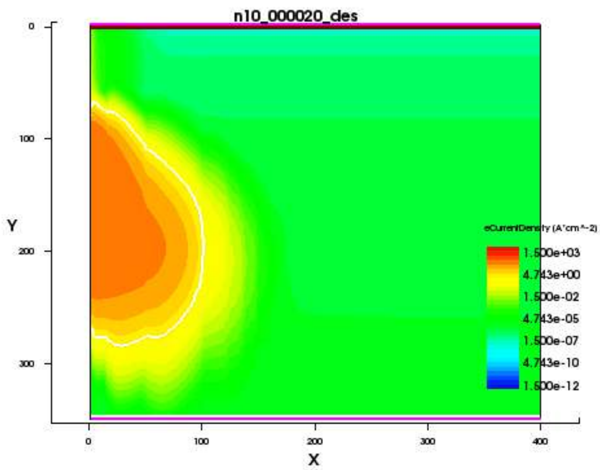 |

<table>
<tr>
<td>t= 250 ps</td>
<td>
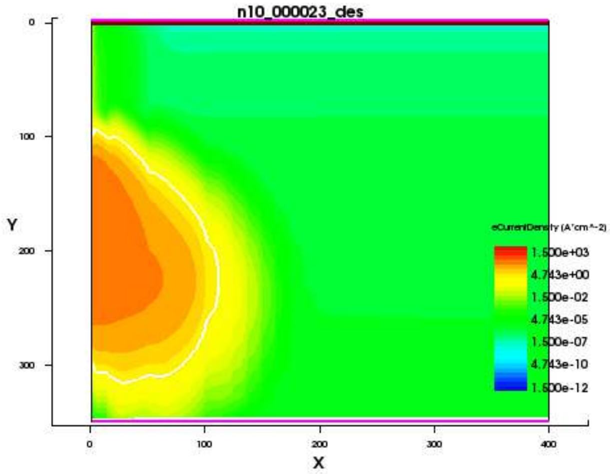

</td>
</tr>
<tr>
<td>t= 270 ps</td>
<td>
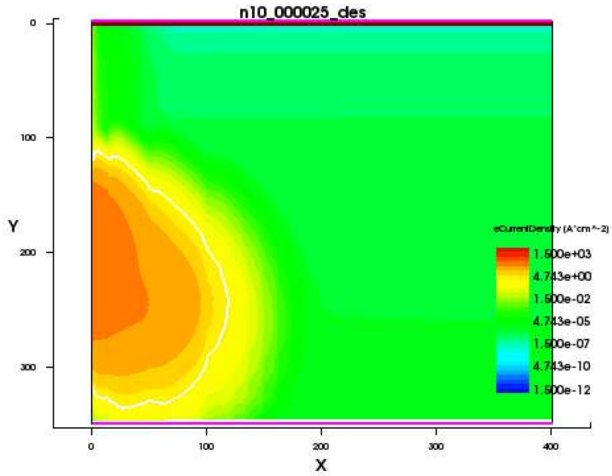

</td>
</tr>
<tr>
<td>t= 280 ps</td>
<td>
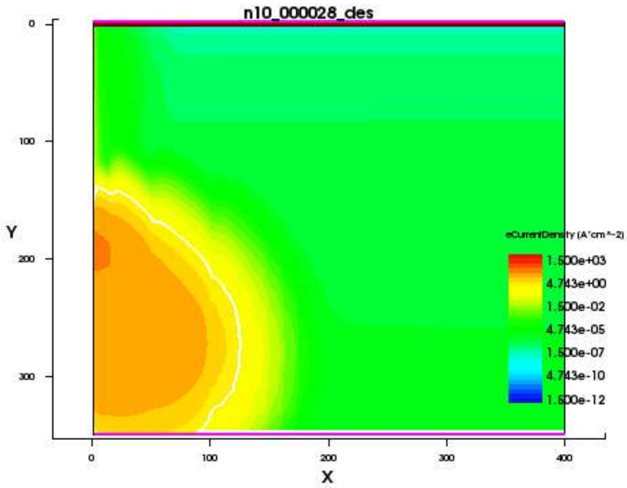

</td>
</tr>
</table>

Table 5-4 Electron current density inside device after charge injection by time distribution at 2600V of applied voltage case

| Captured Time of Electron current Density | Applied Volatage = 2600V |
| --- | --- |
| t= 0 ps | 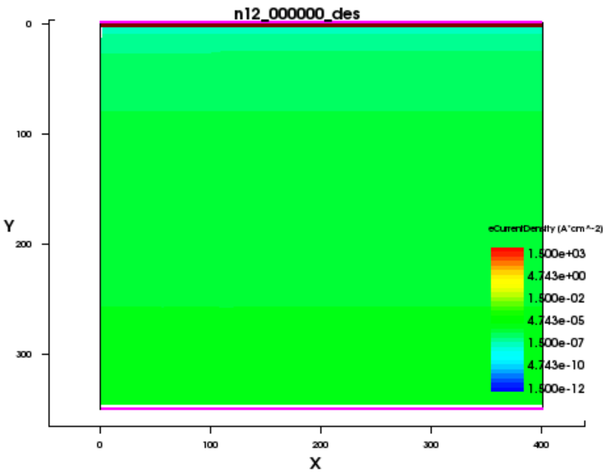 |
| t= 100 ps | 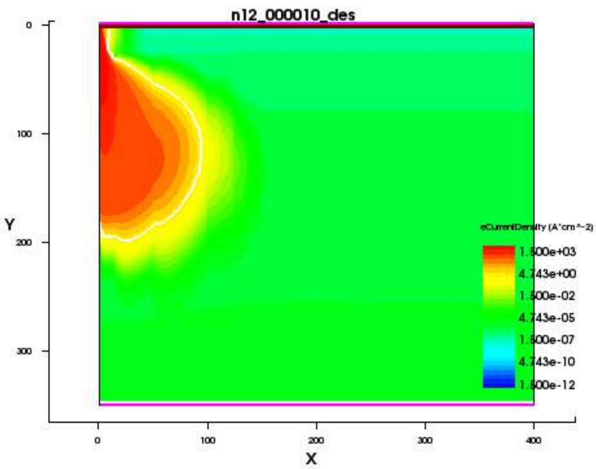 |
| t= 200 ps | 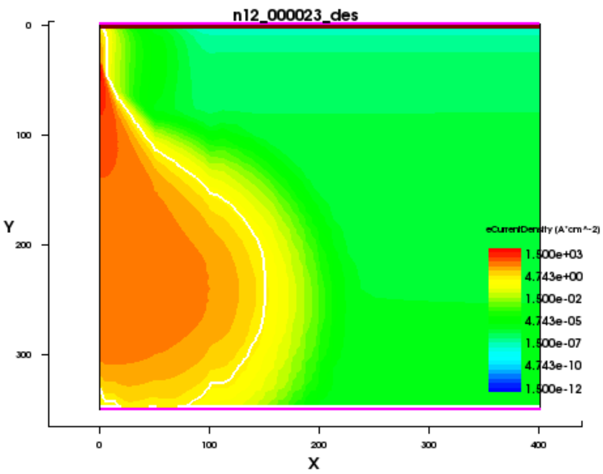 |

<table>
<tr><td>t= 250 ps</td><td>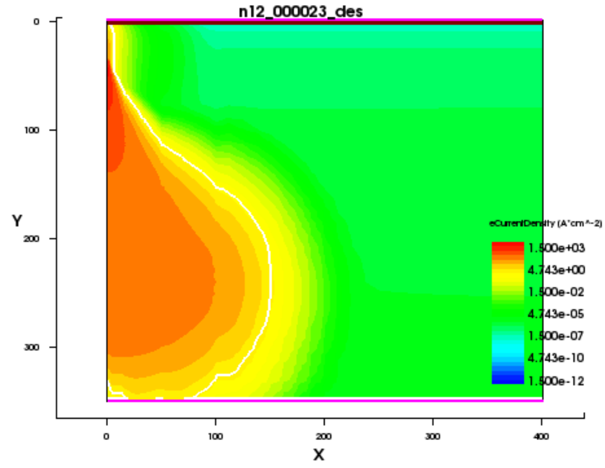
</td></tr>
<tr><td>t= 270 ps</td><td>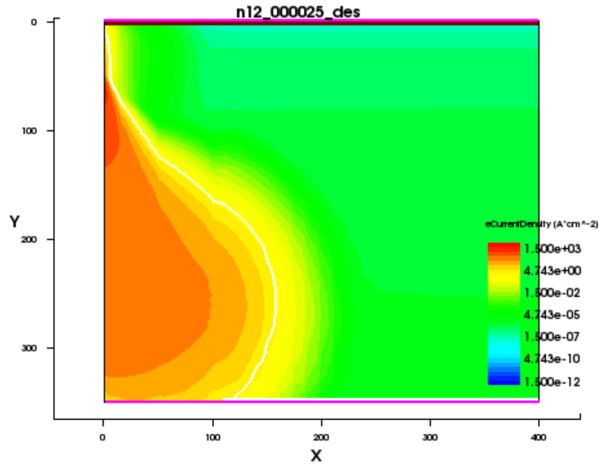
</td></tr>
<tr><td>t= 280 ps</td><td>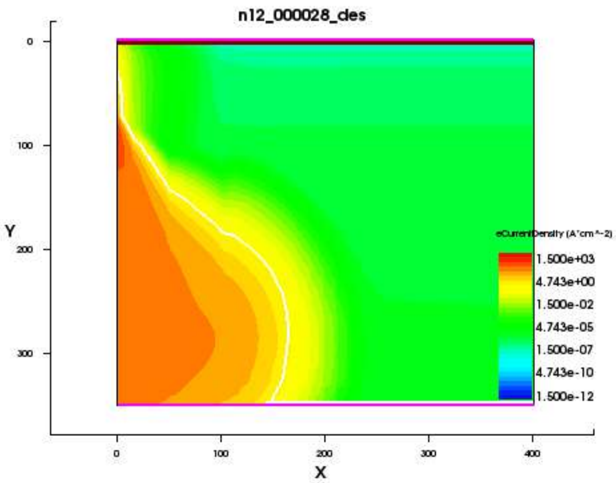
</td></tr>
</table>

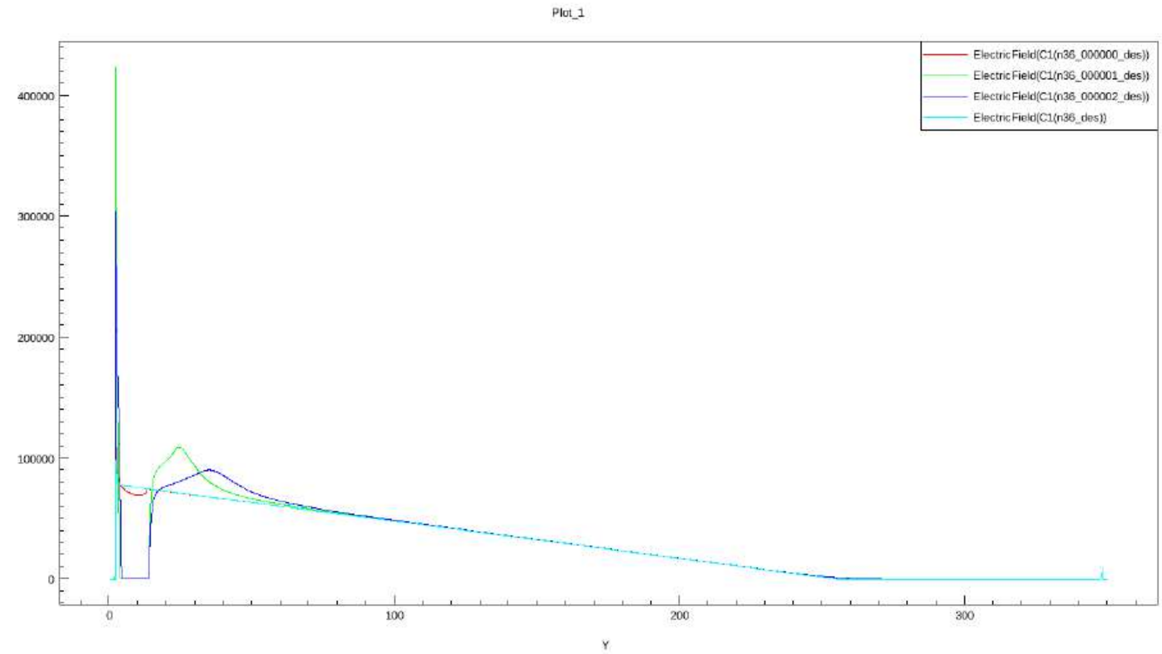


Fig. 5-7 Electric field changes on steady state and after 0ps, 10ps, 20ps of 100MeV energy of ionization particle injection at 1000V of applied voltage case

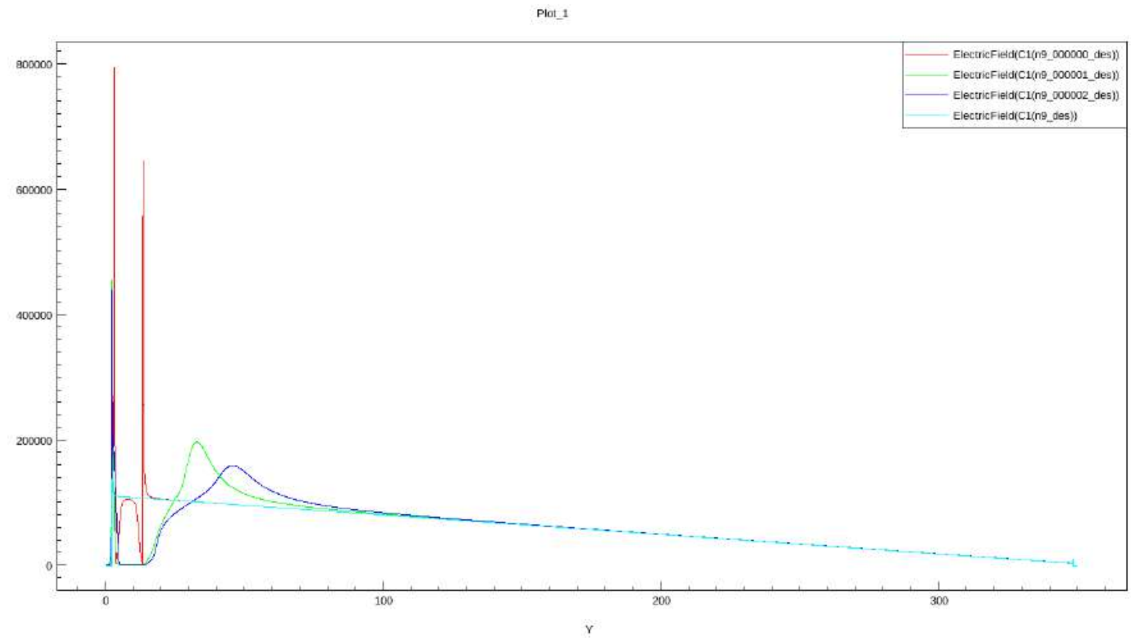


Fig. 5-8 Electric field changes on steady state and after 0ps, 10ps, 20ps of 100MeV energy of ionization particle injection at 2000V of applied voltage case

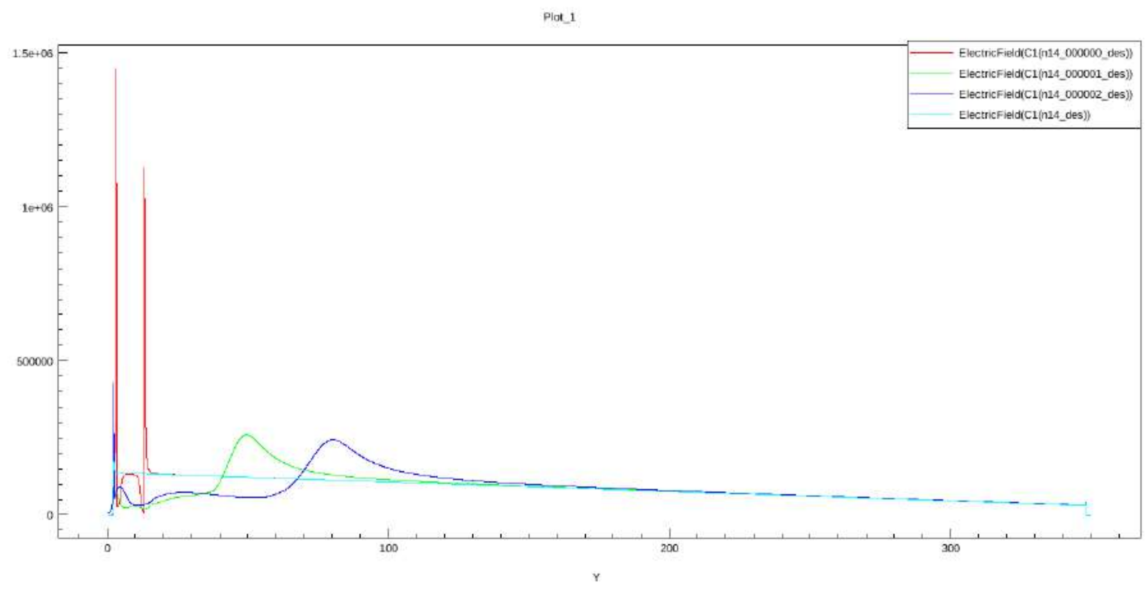


Fig. 5-9 Electric field changes on steady state and after 0ps, 10ps, 20ps of 100MeV energy of ionization particle injection at 3000V of applied voltage case

Here we can see that electric field fluctuation is expanding along its direction. Charge carriers move to along this electric field. At the case of higher applied voltage, widest expanding occurs. The proportional relation between applied voltage and Electric field fluctuating expansion happens due to the avalanche phenomena. The avalanche Phenomena observed at generated charge plotting at energy of 100MeV case which is shown in Fig. 5-10 and it is shown in Fig. 5-11 as a logarithmic scaled.

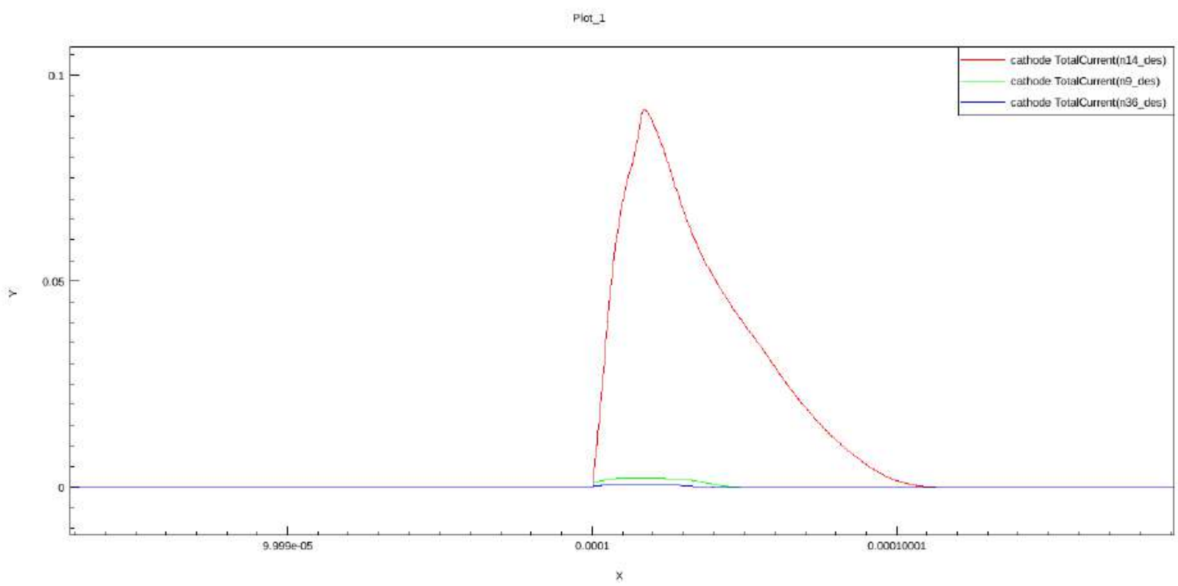


Fig. 5-10 Generated charge inside diode at 1000V, 2000V, 3000V

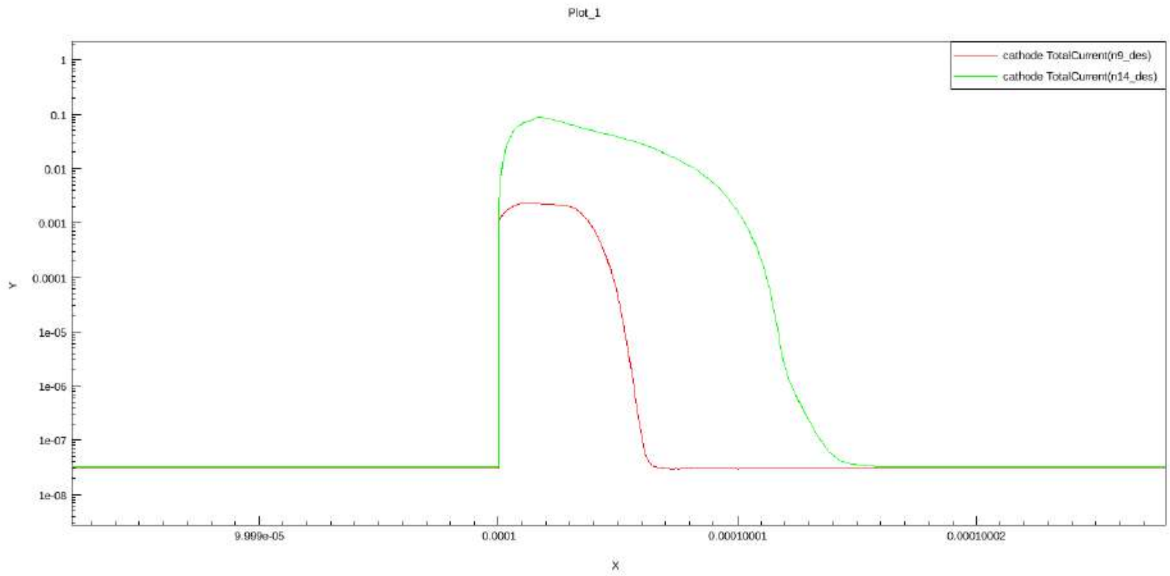


Fig. 5-11 Generated charge inside diode at 1000V, 2000V, 3000V

From here, we can have a generated charge values due to the 100 MeV, 50MeV and 10MeV energy of ionization particle injection. Integral of the graphs give total generated charge *Q*. Then Charge generation as a function applied voltage obtained from T-CAD transient simulation for different deposited charge in 3.3kV PiN diode as shown in Fig. 5-12.

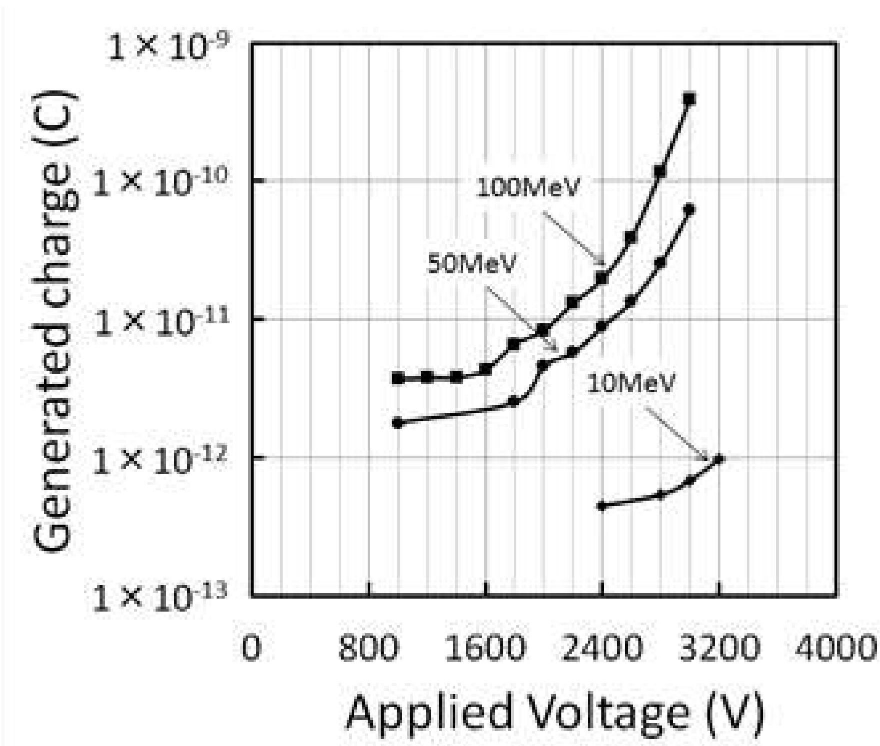


Fig. 5-12 Charge generation as a function applied voltage obtained from T-CAD transient simulation for different deposited charge in 3.3kV PiN diode.

Hence, we can see that generated charge immediately increased at the certain point. In this figure, value of deposited energy is for only related to simulation variation. It means those energy values don't related with particle type. In other word, T-CAD simulation result gives relation between applied voltage dependence respects to the generated charge by any reason. Only important thing is amount of generated charge inside device. If generated charge inside silicon exceeds from certain amount then avalanche phenomena will be starts. This charge called destruction charge as we mentioned before, which is depended on applied voltage to the device. From simulation result as shown in Fig. 5-12, we can have three points to build curve for destruction charge function. After building graph, it should be expanded by mathematical prediction, then from here we have got fitted function and its expression as show in Fig. 5-13 and Eq. 5- 4.

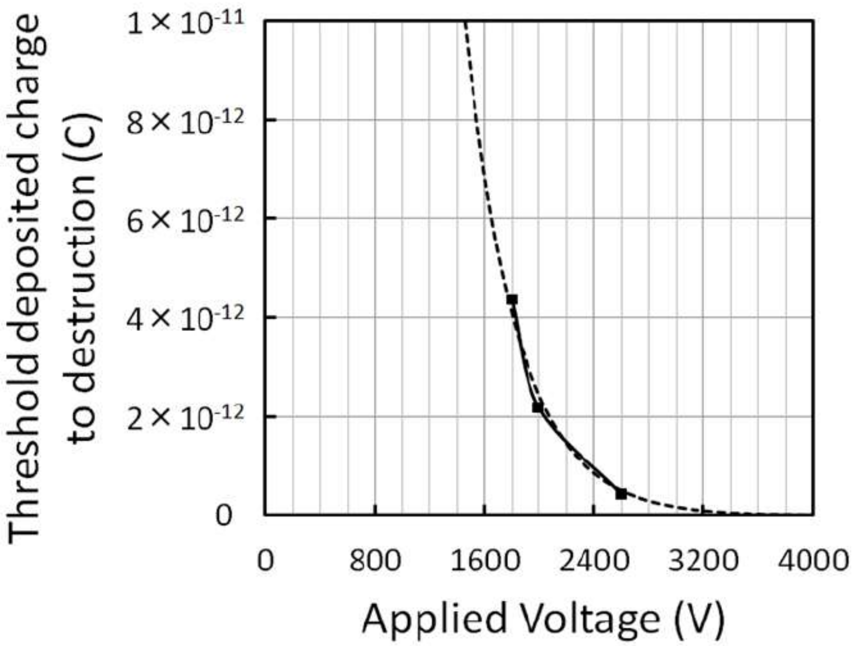


Fig. 5-13 Destruction charge values from penetrated space proton and its fitted function.

$$Q_{dest}(V) = 7 * 10^{-10} e^{-0.003V}$$

Eq. 5-4 Destruction charge function which depends on applied voltage to the device

### 5.3. Proton flux functions fitting results

Proton flux data obtained Most of portion of cosmic ray is proton in Low Earth Orbit. Entire energy range of considered proton flux divided three sections which are in range of 1Mev-200GeV. Firstly, 1MeV-400MeV proton flux data corresponding to 700 km altitude was taken from SPENVIS that data's fitted function is shown in Fig. 5-14, and that accounted sun activation. SPENVIS is the web based software was developed by European Space Agency and is widely used space application studies, here mission period assumed 2018-2019. Second 1GeV-20GeV proton flux data, which measured at around altitude of 350-610km were taken from PAMELA data's fitted function is shown in Fig. 5-15. PAMELA is the spacecraft mission payload for study about possible exotic cosmic ray source and its propagation reasons; mission time was 2006-2008. Proton is top set of data. Helium is the bottom set of data. Thirdly, 20GeV-200GeV proton flux data, which measured at altitude of around 400km, were taken from AMS data's fitted function shown in Fig. 5-16.

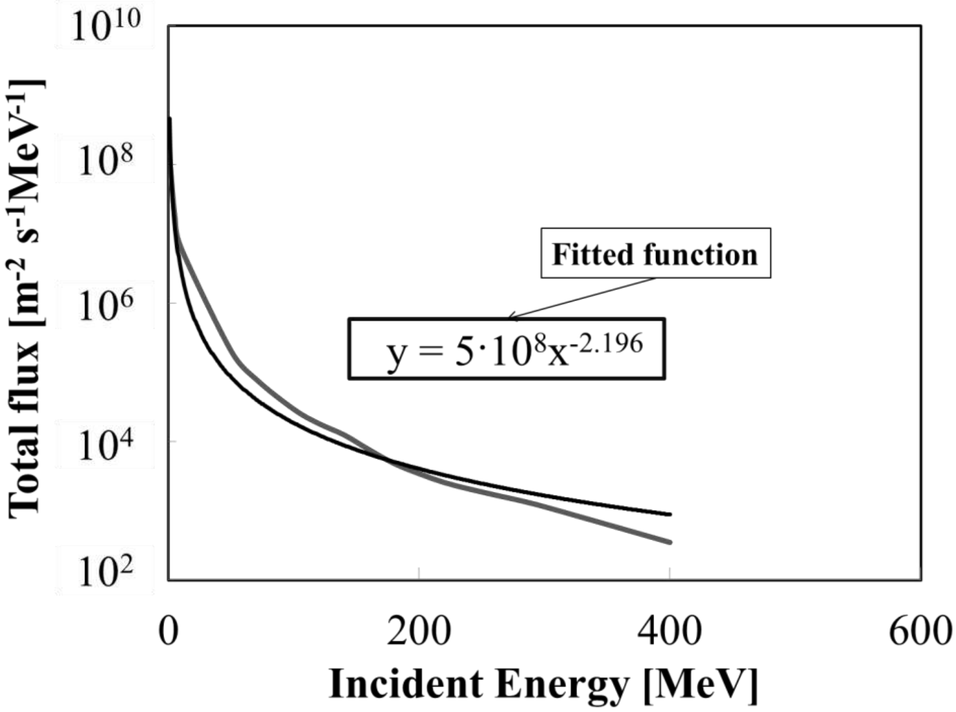


Fig. 5-14 1-400 MeV proton flux data at in LEO /SPENVIS around 700 km altitude/ and its fitted function

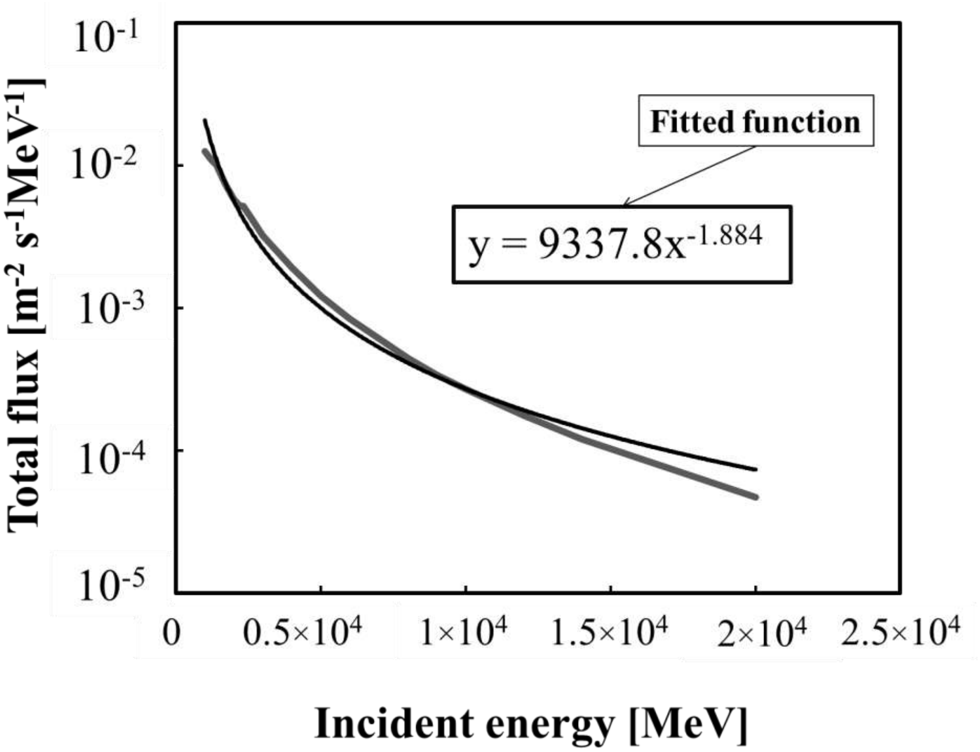


Fig. 5-15 Fitted function has been taken from 1GeV-20GeV proton flux in LEO /PAMELA 350km-610km altitude.

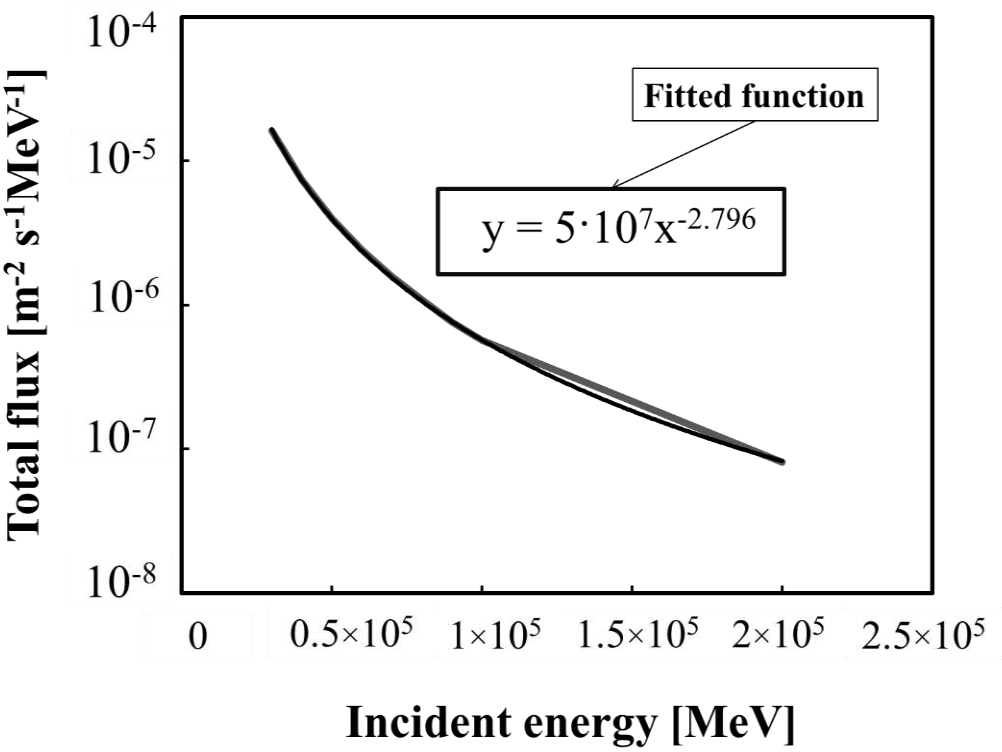


Fig. 5-16 20GeV-200GeV proton flux in LEO/AMS around 400km altitude/ and its fitted function.

From these data fitted functions depending incident proton energy can be written in low, medium and high range of energy levels as shown in Eqs. 5-5, 5-6 and 5-7. Shielding effect was accounted during calculation.

$$E_p^{Low}(E_p) = 5 \cdot 10^8 \cdot (E_p)^{-2.196}$$

Eq. 5-5 1-400 MeV proton flux data at in LEO

$$E_p^{Med}(E_p) = 9337.8 \cdot (E_p)^{-1.884}$$

Eq. 5-6 Fitted function has been taken from 1GeV-20GeV proton flux in LEO /PAMELA

$$E_p^{High}(E_p) = 5 \cdot 10^7 \cdot (E_p)^{-2.796}$$

Eq. 5-7 20GeV-200GeV proton flux in LEO/AMS

### 5.4. Cross section calculation result

By combining data and calculating main formula, as shown in Eq. 5-8, last results were obtained. Result is the 3.3 kV PiN diode's Single Event burnout Cross Section respect varying applied voltages, which can used for any proton flux of environment as shown in Fig. 5-17. This result seems similar to existing data on literature [**35**].

$$\sigma(V) = A * \int_{Q_{dest(V)}}^{Q_{max}} \Phi_{E_p}^{300}(Q)\partial Q$$

Eq. 5-8 Proton induced failure cross section depended on applied voltage

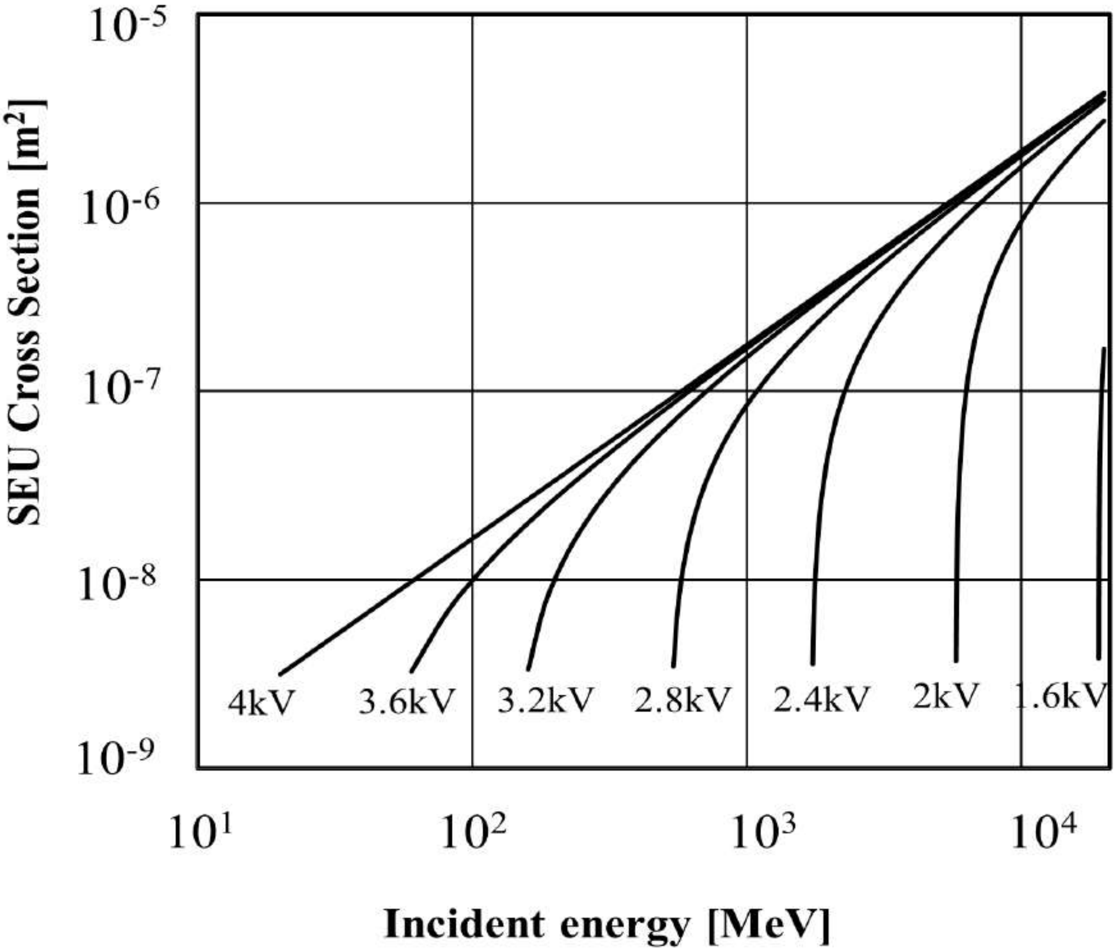


Fig. 5-17 SEU Cross section VS Incident energy of Proton dependence at various applied voltages (3.3kV PiN diode, Area=10-4 m2, 10MeV-20GeV).

## 5.5. Failure rate calculation result

The voltage dependent failure rate prediction calculated by proposed formula, as shown in Eq. 5-9, for 3.3 kV PiN diode in Low Earth Orbit condition is shown as below as shown in Fig. 5-18, Fig. 5-19 and Fig. 5-20. In the Fig. 5-18, we can see that proton flux energy affects to which range of applied voltage. Hence we can see that high failure rate corresponds to higher energy of particle flux. Here it seems that experiment of voltage dependent failure rate against radiation is tough in terrestrial level.

$$FR = \int_{E_p^{min}}^{E_p^{max}} A * \int_{Q_{dest(V)}}^{Q_{max}} \Phi_{E_p}^{300}(Q)\partial Q * F(E_p)\partial E_p$$

Eq. 5-9 Proposed failure rate calculation formula

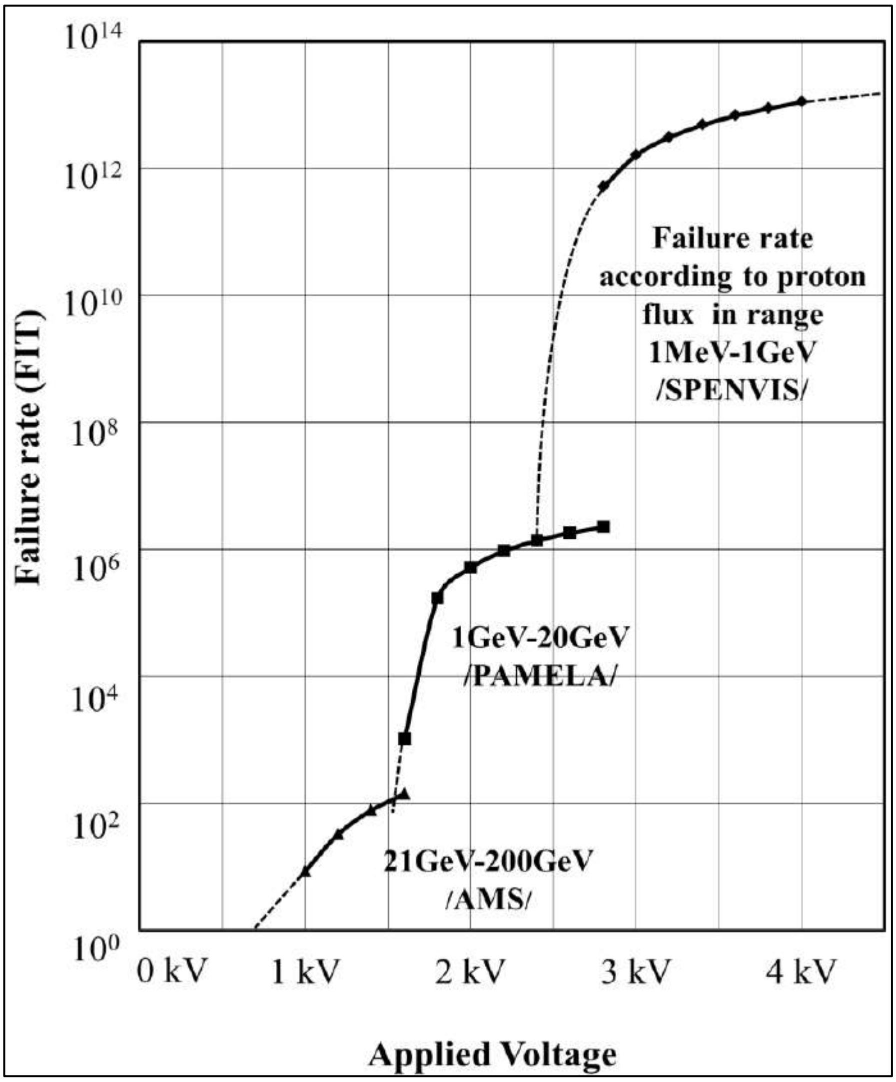


Fig. 5-18 Failure rate VS Applied voltage in Low Earth Orbit (3.3kV PiN diode, Incident energy range 1MeV-200GeV).

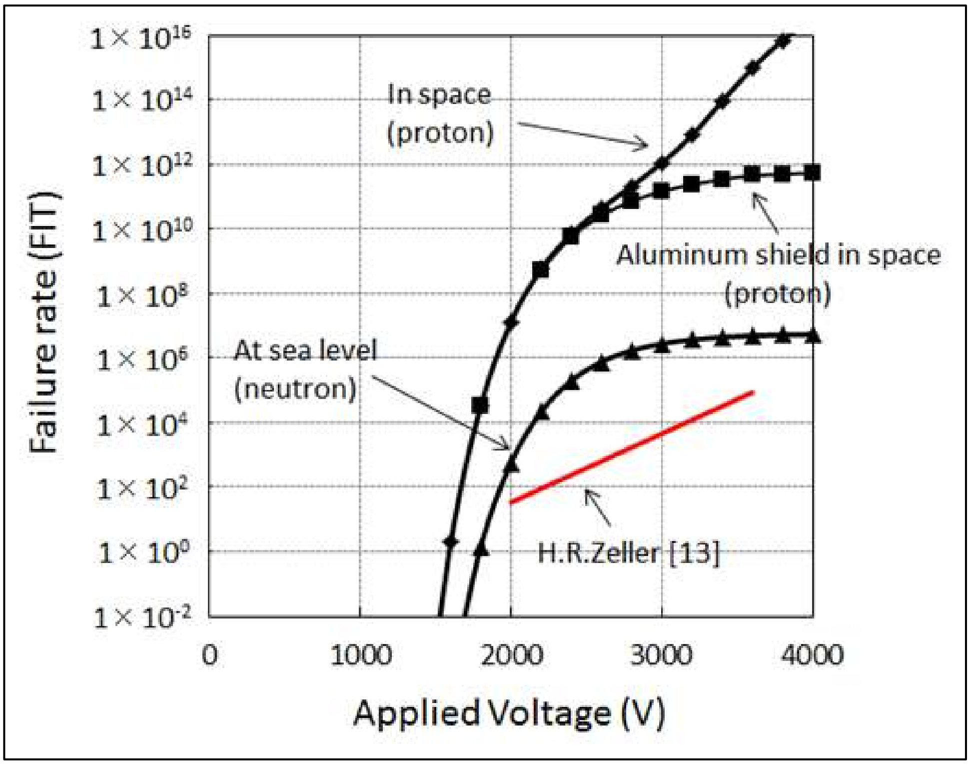


Fig. 5-19 The failure rate of 3.3-kV PiN diode calculated by our proposed calculation method at the sea level and at satellite orbit level.

As before mentioned, majority of the particles compound energetic protons and its percentage is around 90% in space. [**15**] Due to the Earth is protected by geomagnetic field, the proton, which is an electric particle, is bent or confined in the geomagnetism. From them, the protons that fall down to the Earth collide with molecules in atmosphere of the Earth and it makes neutron shower. For that reason, we calculated the failure rate with terrestrial neutron flux at sea level and space proton flux in space.

Fig. 5-19 shows the terrestrial neutron flux and space proton flux induced failures. The terrestrial neutron flux data is analytic model by M. S. Gordon, et al. [**36**]. Space proton flux data have two kinds of data, which is difference altitude and proton energy. One is a STE-QUEST mission data [**37**] and the other is PAMELA data [**26**]. We approximated function of the two space proton flux data. At about 1 MeV - 500 MeV space proton flux data, which measured at around altitude of 800 km - 2400 km and its fitted function were taken from STE-QUEST mission data source. This result also was compared with the terrestrial applications voltage dependent failure rate study [**38**].

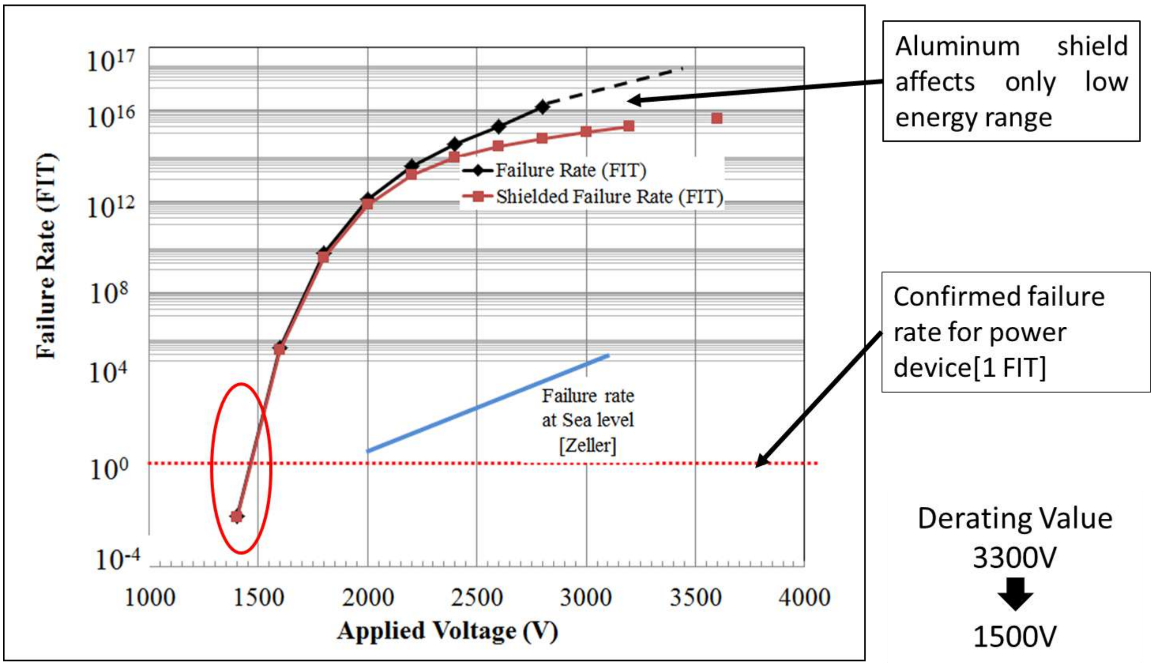


Fig. 5-20 The failure rate of 3.3-kV PiN diode calculated by our proposed calculation method at the sea level and at satellite orbit level.

The failure rate of 3.3-kV PiN Diode was calculated by our proposed calculation method at sea level and in space. As combining three kind of functions, we calculated failure rate of 3.3 kV PiN diode at low earth environment condition was calculated and its result shown in the Fig. 5-21. Here, two types of dotted lines represents failure rate of 3.3kV pin diode, corresponding to case of shielded and unshielded condition. Shielding material is 0.1 in of Aluminum. Shielding function obtained from literature [**39**]. As seeing this result aluminum shielding could not be proper protection against proton flux. The red dashed line represents FIT=1(one failure in $10^9$ hours) that typically used for power device's allowed failure rate for commercial application. In this case, as seeing the result, application voltage of 3.3kV diode should be approximately 1.5kV for space application. The blue line represents power devices failure rate at terrestrial. In space, the failure rate can be expressed as one function, even with multiple flux of particles $Flux(E_p)$. The reason is that the failure rate is the sum of the failure rates for the each particle energy. The failure rate depends strongly on flux of particles $Flux(E_p)$ and threshold charge to destruction $Q_{dest}(V_{DC})$. Below about $V_{DC}$ = 2200V, the failure rate drops suddenly, it is influenced by threshold charge to destruction $Q_{dest}(V_{DC})$. Threshold charge to destruction $Q_{dest}(V_{DC})$ increases exponentially if applied voltage is decreased beyond that point. Therefore, the failure rate is decreased at low applied voltage. From these result, it is possible to ensure the reliability of high voltage devices in satellite electrical power system. Also, we confirmed that there is no effect of aluminum shield because high energy proton does not prevent to penetrate into devices.

In our result, since generated charge $Q$ position is the most electric field, the failure rate is considered to be high. In experience, charge generations positions were in various points. Also, we obtained aluminium shielding space proton flux data at same condition, too. Comparing results, space applications power semiconductor devices failure rate is higher than terrestrial failure rate several magnitude. From one of the existing studies about voltage dependent failure rate, it showed that 50V increase of change makes approximately three magnitudes increasing of FIT.

## 6. CONCLUSION

We established method that consists of Destruction charge values from T-cad simulation, proton flux data and probability of energy deposition due to proton-silicon interaction from literature.  From the result we can see that failure rate is apparently higher than terrestrial region case (assumed terrestrial FIT=1). By using Single Event burnout cross section $\sigma(V)$, that we obtained can be used for any proton flux of environment. PiN diode model can be changed by any other power semiconductor devices. The main formula which used for calculation compounds of three independent parts. Each part can be developed separately and it could be changed by other environment other devices. That means the proposed method for high voltage power devices failure rate calculation is feasible to diversity of any other power devices at any radiation environment. In further, using this flexible aspect of method, software application will be developed for radiation induced failure rate calculation of power devices. Proposed method can contribute to mitigate failure for high power devices' usage and predict space application's MW range of power systems reliability in future. In this study, T-CAD simulation electric field, that can affected by proton hitting position in silicon, was fixed at highest field of position. Crystal degradation due to space radiation was not considered as well.

Furthermore, in order to confirm calculation result by experiment, testing facilities required. But in the reality, feasibility of the equipment of radiation source is limited to simulate real space environment. Then cubesat class of satellite mission could be the solution of the experimental result of this study as developing dedicated model for high power devices radiation testing.

## 7. LIST OF FIGURES

## 8. LIST OF TABLES

# 9. BIBLIOGRAPHY


[1] Organisation for Economic Co-operation and Development, "The Space Economy at a Glance 2007," 2007.

[2] Space Foundation, "Space Report," Washington, 2015.

[3] Carissa Bryce Christensen, Hans Ten Ethan E. Haase, "Global Commercial Space Industry Indicators and Trends," *Acta Astronautica*, vol. 50, pp. 747–757, 2002.

[4] Shohei Harada, Yuji Shiba, Ichiro Omura Erdenebaatar Dashdondog, "Failure rate calculation method for high power devices in space applications at low," *Microelectronics Reliability*, vol. 64, pp. 502–506, September 2016.

[5] Clay S. Mayberry, Dave S. Glaister Kitt C. Reinhardt, "Space Power Technology in Power Management and Distribution Electronics," *Journal of Spacecraft and Rockets*, vol. 35, no. 6, November–December 1998.

[6] J. R. Wertz and W. Larson, *Space Mission Analysis and Design*., 1999.

[7] G. a Gonzalez, and M. G. Houts V. J. Lyons, "DRAFT fuel cell space Power and Energy," 2010.

[8] Kenneth J. Metcalf, "Power Management and Distribution (PMAD) Model Development," November 2011.

[9] Ichiro Omura Masahiro Tanaka, "Novel Structure Oriented Compact Model and Scaling Rule for Next Generation Power Semicunductor Devices," Kitakyushu, 2012.

[10] Satyavrat Peter Wilson, "What's The Difference Between IGBTs And High-Voltage Power MOSFETs?," 2014.

[11] E.L. Petersen W.L. Bendel, "Proton Upsets in Orbit," *IEEE Transactions on Nuclear Science*, vol. NS-30, no. 6, p. 4481, Dec 1983.

[12] G. Sokner, G. Wachutka W. Kaindl, "Analysis of Charge Carrier Multiplication Events in NPT and PT-Diodes Triggered by an Ionazing Particle," *Electron Devices and Solid-State Circuits IEEE*, p. 383, 2003.

[13] Peter Voss, Winfried Kaindl, Gerhard Wachutka, K. H. Maier, H.-W. Becker, Gerald Soelkner, "Charge Carrier Avalanche Multiplication in High-Voltage Diodes Triggered by Ionizing Radiation," *IEEE Transactions on Nuclear Science*, vol. 47, no. 6, December 2000.

[14] A.M. Albadri et al, "Single event burnout in power diodes: Mechanisms and models," *Microelectronics Reliability*, vol. 46, no. 2-4, pp. 317-325, February–April 2006.

[15] J.F.Ziegler, "Terrestrial Cosmic Rays," *IBM*, vol. 40, no. 1, p. 19, 1996.

[16] ESA. (1997-2016) SPENVIS. [Online]. https://www.spenvis.oma.be/models.php

[17] Milton S. Ash George S Messenger, *Single Event Phenomena*.: Springer, 1997.

[18] M. Aguilar et al. (AMSCollaboration), "Precision Measurement of the Proton Flux in Primary Cosmic Rays from Rigidity 1 GV to 1.8 TV with the Alpha Magnetic Spectrometer on the International Space Station," *PHYSICAL REVIEW LETTERS*, vol. 114, no. 17, April 2015.

[19] Marlon Núñez. (2014) Space Weather. [Online]. http://spaceweather.uma.es/solarstorms.html

[20] James D. Kinnison, "Single Event Phenomena: Testing and Prediction," *4th NASA Symposium on VLSI Design*, vol. N94-2169, p. 1.2.1, 1992.

[21] M.J. Bochini et al, "Nuclear and Non-Ionizing Energy-Loss for Coulomb Scattered Particles from Low Energy up to Relativistic Regime in SpaceRadiation Environment," in *12th ICATPP Conference*, Villa Olmo, Como, Italy, 2011, pp. 9-23.

[22] HPAUL. (2007, Feb) Wikiwand.com. [Online]. http://www.wikiwand.com/en/Stopping_power_(particle_radiation)#/overview

[23] IROTECH. (2013) Webinar. [Online]. https://www.slideshare.net/iROCTech/i-roc-webinar-do-i-really-need-to-worry-about-soft-errormay302013

[24] Sebastien Morand Florent Miller, "Method for characterizing the sensitivity of electronic components to destructive mechanisms ," Grant US 9506970 B2, Nov 29, 2016.

[25] Giovanni Busatto, "Cosmic Rays induced," University of Cassino, Presentation 2006.

[26] et al., O. Adriani, "PAMELA Measurements of Cosmic-Ray Proton and Helium Spectra," *Science*, vol. 332, no. 6025, pp. 69-72, Apr 2011.

[27] B. Doucin et al., "Characterization of proton interactions in electronic components," *IEEE Transactions on Nuclear Science* , vol. 41, no. 3, pp. 593-600, Jun 1994.

[28] B., Carriere, T., Poivey, C., Garnier, P., Beaucour, J., Patin, Y. Doucin, "Model of single event upsets induced by space protons in electronic devices," *Proceedings of the European Conference on Radiation and its Effects on Components and Systems, RADECS*, pp. 402-408, Sep 1995.

[29] S. H. Zhou, T. E. Ward, V. E. Viola, Jr., H. Breuer, G. J. Mathews, A. Gökmen, and A. C. Mignerey K. Kwiatkowski, "Energy Deposition in Intermediate-Energy Nucleon-Nucleus Collisions," *PHYSICAL REVIEW LETTERS*, vol. 50, p. 1648, May 1983.

[30] T.A. Gabriel, "The High Energy Transport Code, HETC," in *Proceedings of the LEP Experimenters' Workshop on Shower Simulation*, CERN, Geneva, Switzerland, Jan 1985.

[31] Qun-Feng Chen, Stephan Schiller, Tobias J. Kippenberg, Victor Brasch, "Radiation Hardness of High-Q Silicon Nitride Microresonators for Space Compatible Integrated Optics," *Optics Express*, vol. 22, no. 25, pp. 30786-30794, 2014.

[32] S. Bloom, and C. W. Struck R. C. Alig, "Scattering by ionization and phonon emission in semiconductors," *PHYSICAL REVIEW B*, vol. 22, no. 12, 1980.

[33] W. Kaindl, H.-J. Schulze, G. Wchutka G.Soelkner, "Reliability of power electronic devices against cosmic radiation-induced failure," *Microelectronics Reliability*, vol. 44, no. 9-11, pp. 1399-1406, Sep-Nov 2004.

[34] J.M. Palau', J. Gasiot, J.P. Nadai, M.C. Calvet, S. Fourtine, D. Roth, O. Bersillon C. Vial', "Energy Deposited by High Energy Neutrons and Protons in Silicon (Comparison between HETC and COSMIC codes)," *Radiation and Its Effects on Components and Systems*, September 1997.

[35] J.P. Meyers, J.B. Langworthy, E.L. Petersen W.J. Stapor, "Two parameter Bendel model calculations for predicting proton induced upset (ICs)," *IEEE Transactions on Nuclear Science*, vol. 37, no. 6, pp. 1966 - 1973, Dec 1990.

[36] P. Goldhagen, K. P. Rodbell, T. H. Zabel, H. H. K. Tang, J. M. Clem and P. Bailey, M. S. Gordon, "Measurement of the flux and energy spectrum of cosmic-ray induced neutrons on the ground," *IEEE Trans. Nucl. Sci.*, vol. 51, no. 6, pp. 3427-3434, 2004.

[37] Q. F. Chen, S. Schiller and T. J. Kippenberg V. Brasch, "Radiation hardness of high-Q silicon nitride microresonators for space compatible integrated optics," *Optics Express*, vol. 22, no. 25, pp. 30786-30794, 2014.

[38] H. R. Zeller, "Cosmic ray induced failures in high power semiconductor devices," *Microelectron. Reliab,* vol. 37, no. 10-11, pp. 1711-1718, 1997.

[39] E. C. Smith, "Effects of Realistic Satellite Shielding on SEE Rates," *IEEE Transactions On Nuclear Science,* vol. 41, no. 6, p. 2396, Dec 1994.

[40] M. Aguilar and others, "Precision Measurement of the Proton Flux in Primary Cosmic Rays from Rigidity 1 GV to 1.8 TV with the Alpha Magnetic Spectrometer on the International Space Station," *Physical review letters*, vol. 114, pp. 171103-1, May 2015.

## 10. ACRONYMS

CMOS = Complementary Metal Oxide Semiconductor

MOSFET= Metal Oxide Semiconductor Field Effect Transistor

IGBT= Insulated Gate Bipolar Transistor

LET = Linear Energy Transfer

SEU = Single-Event Upset

SOI = Silicon-On-Insulator

SRAM = Static Random Access Memory

EPS = Electrical Power System

## 11. PUBLICATION LIST

- Screening Process And In-Orbit Performance Of Horyu-IV Battery Proceeding The 35th Space Energy Symposium, 2016,3, Mohamed Yahia Edries, Erdenebaatar Dashdondog, Ichiro Omura, Mengu Cho;
- Failure Rate Calculation Method For High Power Devices in Space Applications at Low Earth Orbit, Microelectronics Reliability 64 pp. 502–506,20169, Erdenebaatar Dashdondog, Shohei Harada, Yuji Shiba, Ichiro Omura;
- Formulation of Single Event Burnout Failure Rate for High Voltage Devices in Satellite Electrical Power System, Proceedings of ISPSD 29th,2017,6, Yuji Shiba, Erdenebaatar Dashdondog, Masaki Sudo, Ichiro Omura;
- The Failure Rate Calculation Method for High Power Devices in Low Earth Orbit, Proceedings of ISTS 31st, 2017,6, Erdenebaatar Dashdondog, Shohei Harada, Yuji Shiba,Masaki Sudo, Ichiro Omura;
- Method for the synthesis of semiconductor structures n-InSb1-xBix-i-GaAs, n-InSb1-xBix-i-GaAs/Te, looking for the manufacture of highly element hall. “Physics”, 2011, National University of Mongolia; Golimensee Shilagardi, Erdenebaatar Dashdondog
- Electrical properties of semiconductor structures n-InSb1-xBix-i-GaAs, and n-InSb1-xBix-i-GaAs/Te. Published in “Physics”, 2011, National University of Mongolia; Golimensee Shilagardi, Erdenebaatar Dashdondog
- Features para magnetism samples of brown coal in their thermal degradation, “Physics” , 2012, National University of Mongolia; Golimensee Shilagardi, Erdenebaatar Dashdondog
- Effect of neutron irradiation on para magnetism coals, “Physics” , 2012, National University of Mongolia; Golimensee Shilagardi, Erdenebaatar Dashdondog

## 12. ABOUT AUTHOR

Erdenebaatar Dashdondog was born in Erdenet city, Mongolia on June 30, 1987. He received Bachelor degree in Physics and Electronics from the National University of Mongolia in 2009 and Master's degree in Physics and Electronics from the National University of Mongolia in 2011. He was electrical and electronics researcher and assistant teacher at National University of Mongolia until 2014. He has been a doctoral student in Graduate School of Engineering, Kyushu Institute of Technology in Japan. During that time he was member of engineering team of Mongolian first satellite project and participated to other two satellites projects, HORYU-4 and SPATIUM as Electrical Power System engineer. His interest is power system, system engineering and to study for possibility of developing countries space technology ownership and its indirect benefit to technological field development of home country.

Email address: erdenebtr@gmail.com